TIME-TEMPERATURE SUPERPOSITION FOR BLOCK COPOLYMERS

Thesis by

Donald George Fesko

In Partial Fulfillment of the Requirements

for the Degree of

Doctor of Philosophy

California Institute of Technology

Pasadena, California

1971

(Submitted May 24, 1971)

to Betty

ACKNOWLEDGEMENTS

Most of all, I would like to thank Dr. Nicholas Tschoegl, whose guidance went far beyond the science to which I was exposed at Caltech. His encouragement to apply an analytical approach to every area of activity will certainly affect the continuing development of my personal life as well as my scientific career. I would also like to thank the faculty, students, and institute employees of the polymer science research group for their friendship and for the knowledge and time they have shared with me. In particular, I want to thank Keikichi "Kay" Yagii, for many valuable discussions, and Robert Cohen for his assistance in acquiring experimental data. Indeed, I want to thank the people of the Chemical Engineering Department for contributing their support and their skills. This gratitude is extended to the members of Caltech community as a whole for making my stay most pleasant as well as educational.

Deep thanks go also to the National Science Foundation for supporting four years of my residence at Caltech by way of a graduate fellowship and to Caltech and the Chemical Engineering Department for extending this period to allow me to continue my work. I thank also the United States Air Force for financing much of the research, the Shell Oil Company for providing samples of block copolymers, and the Ford Motor Company for permitting the use of some of their facilities in the preparation of this manuscript.

ABSTRACT

The proposition is made that simple time-temperature superposition should not be valid for block copolymers exhibiting multiple mechanical transitions; and an explanation of the time-temperature behavior, which is more consistent with the behavior of the individual phases, is presented in terms of an equivalent mechanical model. Based on this model, a method for generating time-temperature shifts, which depend on the experimental time as well as temperature, is developed. This method can easily be extended to any mechanical model and should be valid for polymer composites in general.

The storage and loss compliances of three benzene cast polystyrene/1,4-polybutadiene/polystyrene triblock copolymers with different compositions were measured between -85 and 90°C over a frequency range from 0.1 to 1000 Hz. The measurements suggest the presence of four relaxation processes. Two, the polystyrene and polybutadiene glass transitions, are treated according to the method of time-temperature superposition referred to above. Anomalous behavior appearing between the two glass transitions is attributed primarily to a temperature dependent interlayer between the two phases and can be treated as a compositional change in the composite.

Entanglement slippage in the rubbery matrix also contributes to the total relaxation.

The apparatus used for these experiments is an extensively modified model of the Miles shear generator. This improved version offers large experimental frequency and temperature operating ranges.

TABLE OF CONTENTS

		Page
I.	Introduction	1
II.	Time-Temperature Superposition for Block Copolymers	8
III.	Experimental Results and Discussion	30
	A. Shell 16/78/16	30
	The Interlayer	43
	B. NBS 10/30/10	57
	C. Kraton 102	64
IV.	Apparatus - The Modified Melabs Rheometer and Tests on Galcit I	76
	References	92
V.	Appendix	
	A. A Derivation of a General Expression for the Temperature Variation of log a_T	96
	B. Part of the Operation Manual for the Modified Melabs Dynamic Rheometer	98
	C. The Measurement of Small Phase Angles in the Subaudio Frequency Range - by N. W. Tschoegl and J. R. Smith	122
	D. Characterization of Shell Research-Grade Block Copolymers	140
	E. Data	143
	1. Storage and Loss Compliance Data of Low Molecular Weight Polystyrene Used to Calculate the Polystyrene Contribution to the Time-Temperature Shifts of Block Copolymers	144
	2. Storage Compliance Data of Shell 16/78/16 (unannealed) used to Calculate the Polybutadiene Contribution to the Time-Temperature Shifts of Block Copolymers	145
	3. Raw Dynamic Compliance in Simple Compression Data for Shell 16/78/16 (annealed) as Determined with the Modified Melabs Rheometer	146

Page

4. Raw Dynamic Shear Compliance Data for NBS 10/30/10 as Determined with the Modified Melabs Rheometer..... 153

Proposition I: Instability of the Z-Form Numerical Method of Inverse Laplace Transformation for Large Time Increments 158

Proposition II: Choosing an Approximation for Calculating the Relaxation Spectrum from Storage Modulus Data 168

Proposition III: The Role of Computational Errors in the Computer Simulated Packing of Circles 182

I. INTRODUCTION

Block Copolymers

The discovery of "living" polymers by means of anionic polymerization reported by Szwarc, Levy, and Milkovich (1) in 1956 offered to rheologists an opportunity to make polymer molecules much more precisely than ever before. Certainly the capability of producing polymers with very narrow molecular weight distributions is a valuable asset. Much more exciting from both a fundamental and practical standpoint, however, is the ability to produce block copolymers. Block copolymers are macromolecules having large homopolymer segments. This is illustrated for a diblock (A/B) and a linear triblock in Fig. 1.

A/B A/B/A or A/B/C

Figure 1. Block Copolymers

Typically the blocks consist of polybutadiene or polystyrene, although combinations of most monomers which will polymerize anionically can be used. A short list was compiled by Fetters (2) in 1966 and this has been extended considerably since then. Two very helpful guides to the anionic synthesis of block copolymers are those by Fetters (3) and Morton et al. (4).

One polymer is generally insoluble in another. This is because the large size of the molecules involved in mixing reduces the number of configurations available and hence a small entropy of mixing results. Barring strong interaction between the molecules, the heat of

mixing is predicted to be positive, and since this now dominates the free energy of mixing, resulting in a positive free energy, mixing does not take place. Thermodynamics has been used to predict domain sizes and other morphological characteristics in A/B type block copolymers in fairly good agreement with electron microscope observations (5-8). Thermodynamics has also been used for triblock materials (9,10) and for copolymers with any number of blocks (11). When more than two blocks are present, however, it is impossible to attain an equilibrium state (12) (except in certain cases when the domains assume a lamellar geometry) and so any close agreement with the real situation is probably fortuitous.

The closely related graft copolymers have been of commercial and scientific interest for some time (13,14), particularly in the area of high impact plastics (15). These have usually involved emulsion or polymer-monomer solution polymerization schemes. Block and graft copolymers have been synthesized by various other methods such as by making use of the free radicals produced in mechanical processing (16) and by joining prepolymers through reactive end groups (17). The latter technique has found considerable application recently particularly in the field of urethane resins. None of these methods, however, have as much precision, uniformity, and flexibility as the living polymer technique.

Mechanical Properties

The introduction of anionically produced block copolymers commercially has been surprisingly slow. The synthesis technology

is readily available for a wide variety of monomers and microstructures. A wealth of literature exists describing the reaction kinetics since the clean nature of the anionic polymerization has made it an ideal subject for investigation. Economics has perhaps inhibited development through patents, the high purity required for the reactants, trends in the national economy, etc. However, the specialized nature of the block copolymers should more than compensate for this. Very likely the lack of understanding of the viscoelastic phenomena that take place in multiple phase polymer blends, specifically in those two-phase systems formed by two-constituent block copolymers, is the principle factor that keeps research and development efforts from taking full advantage of and selling the special characteristics of block copolymers. One application that has achieved some success is the use of polystyrene-polybutadiene-polystyrene block copolymers (cf. Fig. 1) to form "thermoplastic elastomers." The Shell Chemical Company is the chief supplier of these. In these systems, the polystyrene forms a rigid separate phase from the rubbery polybutadiene and mechanically crosslinks the rubbery matrix. At room temperature, the material acts like a rubber, but at high temperatures, it can be made to flow. This rubber can, therefore, be molded with no vulcanization step.

Thus there is a great deal of interest in studying the mechanical properties of block copolymers from a commercial standpoint. In addition, the special qualities of block copolymers offer to the rheologist a valuable opportunity to study viscoelastic behavior in composite systems and in well-defined rubbery networks, and to investigate specific molecular mechanisms of mechanical relaxation, such as free ends,

which can be built into the system. A good introduction to the areas of investigation being pursued in block copolymers are the papers presented at the Block Copolymer Symposium held at the California Institute of Technology in 1967 and collected in the volume edited by Moacanin, Holden, and Tschoegl (18). The various reports are concerned primarily with triblock copolymers of the polystyrene-polybutadiene-polystyrene type which form the rubbery networks discussed above. This is because of their ready availability and the current commercial interest in them.

The mechanical properties of these polymers can be described basically as having two (or more) glass transitions and a broad plateau region between the transitions. The problem of mechanically characterizing these materials is essentially one of discovering how the mechanical properties of the various phases interact. The plateau region is the transition between the two glass transitions and therefore holds much of this information; but the changes there are very subtle since they are very small and take place over very large spans of time or temperature.

Considerable work has been carried out on determining the mechanical properties of these polymers, a large percentage of which has been on Shell's Kraton and Thermolastic materials. Again reference 18 gives much of this. Other works are by Canter (19), Shen and coworkers (20,21), and that of Lim, Cohen, and Tschoegl (22) in this laboratory. Because the microstructures of these materials are not well characterized, however, they are not very good research materials, and they have been studied extensively primarily because of their ready availability. Recently, the Shell Chemical Company has made available research grade

triblock copolymers which are much more suitable. This thesis is largely the result of investigating one of these research grade materials. Other recent contributions to the understanding of block copolymers and polymer blends are those of Angelo, Ikeda, and Wallach (23), Miyata and Hata (24), and Arnold and Meier (25), and Kraus, Rollmann, and Gruver (26).

Time-Temperature Superposition

A key to the understanding of the mechanical behavior of polymeric materials is the description of the time-temperature superposition behavior. Tests carried out on a laboratory apparatus are necessarily limited to a small time scale, typically one to four logarithmic decades of time. Time-temperature superposition presumes that a temperature change is related to a shift in time, so that data accumulated at different temperatures can be used to extend the time scale. This has numerous applications. Obviously, with an apparatus of fixed time scale, one can predict, by changing temperature, the response of that material in a different time regine. Also, in order to correlate data from two different experiments, e.g. stress relaxation and creep, it is necessary to have a knowledge of the viscoelastic functions over a wide time range. Once the time-temperature behavior is known, one needs only this knowledge and one isothermal "master curve" or one isochronal curve to predict that function at other temperatures or times. Time-temperature superposition is very useful for characterizing "thermorheologically simple" (27) materials for which all relaxation mechanisms have one temperature dependence. This is usually the case

for a single relaxation phenomenon such as the glass transition. Application has been extended for homogeneous polymers to include a second relaxation phenomenon, entanglement slippage (28) or terminal flow viscosity (29), which takes place at long times in the rubbery state. To do this, the compliances of the two relaxation (retardation) phenomena are assumed to be additive and are separated. The separated data are then shifted to determine the time-temperature superposition behavior of each. The fact that the material has one phase is a notable point as one does not have to worry about weighting the various contributions.

Simple time-temperature superposition has often been used for multiple phase systems although there has been little justification for this. Crystalline polymers are one example and difficulties understandably arise when the degree of crystallinity (the composition) changes with temperature. It has also been applied to block copolymers (19,20, 21), although the apparent success obtained with the method is very likely due to the short time scale available in any one experiment as will be explained later.

Most of the mechanical characterization work that has been presented in the literature is isochronal dynamic data, and while the presence of two transitions is clearly indicated, nothing is revealed about the time dependence. Further, these dynamic data reveal higher mechanical loss than one would predict in the plateau region at intermediate temperatures which is presumably due to an additional relaxation mechanism.

In this work, the dynamic compliances of various triblock

copolymers were determined in an apparatus originally built by Melabs, Inc., on the model of the Miles shear generator (30) but which was extensively modified in this laboratory. Measurements were made either in shear or simple compression at temperatures generally between -85°C and 87°C over a frequency range from about 0.1 to 1000 Hz. Three polystyrene-polybutadiene-polystyrene samples were investigated: Kraton 102 with molecular weights estimated to be 12,000/48,000/12,000 for the S/B/S segments; Shell TR-1648, a research grade material which is designated Shell 16/78/16 to describe the molecular weights of 16,000/78,000/16,000; and a similarly designated sample, NBS 10/30/10. A technique is developed for the prediction of time-temperature superposition behavior based on a mechanical model. This treatment is applied to experimental data using an additive compliance model to describe the thermoplastic elastomer-type system. The characterization of these materials necessitates the inclusion of four viscoelastic retardation mechanisms. Two mechanisms correspond to the glass transitions of the two polymer phases. The other two mechanisms are attributed to the slippage of trapped entanglements and the presence of an interlayer between the two polymer phases. The scheme can easily be extended to homogeneous and composite systems other than block copolymers which exhibit multiple transitions. The scheme can also be extended to additive modulus or more complex mechanical interaction models.

II. TIME-TEMPERATURE SUPERPOSITION FOR BLOCK COPOLYMERS

Experimental investigations of the mechanical properties of block copolymers have in the past indicated that data taken at different temperatures can be superposed (21,22). In the experiments reported here, there are indications that the data do not superpose. One other investigator has reported lack of superposition (31), and another has given some indication of this (25).

Intuitively, one feels that if two relaxation mechanisms which shift differently with respect to temperature are present, simple superposition should be prohibited. This is clearly seen if one considers the case of a styrene-butadiene two phase system. If each phase acts as a pure homopolymer, one can predict at what time each phase will go through its transition at a given temperature. For instance, suppose one chooses a reference temperature of 90°C. The polystyrene would exhibit a transition at a time of the order of 10^2 seconds. If the polybutadiene followed WLF behavior, one might expect to see its transition at a time about 10^{-9} seconds, resulting in about 11 decades between the two transitions. Now choose a reference temperature of 0°C. For this temperature change, polybutadiene exhibits little temperature dependence and the transition would shift two or three decades in time. Time-temperature superposition in the glassy state is not well understood, but the shifts encountered are generally much higher. The polystyrene transition would probably shift about 10 decades in time. Thus the transitions would appear at about 10^{-7}

and 10^{12} seconds for the polybutadiene and polystyrene respectively - a separation of about 19 decades. A master curve assembled at a reference temperature of 0°C should therefore be much wider than one at 90°C in order to show the two transitions, contrary to the concept of superposition.

In attempting to synthesize a master curve of a viscoelastic function from data taken at different temperatures, then, this problem would manifest itself as a lack of superposition when one tries to shift the data. In other words, isothermal data taken at different times would require different shifts for superposition as illustrated in Fig. 2.

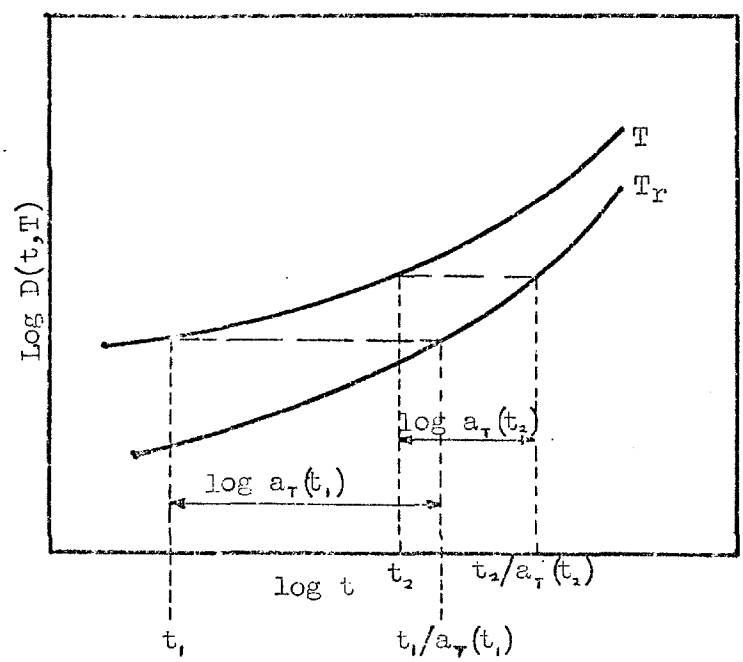

Figure 2. Lack of Time-Temperature Superposition for Materials With More Than One Relaxation Mechanism.

Since electron photomicrographs of S/B/S block copolymers show two different polymer phases, one must expect that the superposition previously seen for these materials must be due to a lack of resolution in experimental measurements, probably in the shortness of the experimentally accessible time scale.

Additive Compliance Model

If one knows how different mechanical response mechanisms in a composite combine to give the overall response, perhaps one can formulate the time-temperature behavior. Compliances or moduli are usually assumed to be additive in some way depending on whether stresses or strains, respectively, are uniform (28). Thus a hard phase dispersed in a soft matrix is better characterized by additive compliances while additive moduli better describe soft domains in a hard matrix. Many models have been proposed to describe this coupling; and the distinction of whether compliances or moduli are additive disappears as the complexity of the model increases.

Additive compliances for block copolymers having a rigid polystyrene phase dispersed in a rubbery polybutadiene matrix (these will be referred to as Kraton-type block copolymers) have been postulated previously (21). The simplest way compliances can add to represent the mechanical response of this two phase system is in series as shown in Fig. 3, where S represents the compliance of

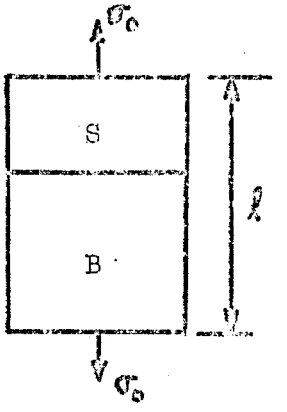

Fig. 3. Additive Compliances

the polystyrene phase and B represents that of the polybutadiene phase. Applying a stress σ_o to the model results in additive strains.

$$\varepsilon = \frac{\Delta \ell}{\ell} = \frac{\Delta \ell_B + \Delta \ell_S}{\ell_B + \ell_S} = \frac{\Delta \ell_B}{\ell_B} \cdot \frac{\ell_B}{\ell_B + \ell_S} + \frac{\Delta \ell_S}{\ell_S} \cdot \frac{\ell_S}{\ell_B + \ell_S} = w_B \varepsilon_B + w_S \varepsilon_S$$

Of course the weighting factors w_B and w_S must sum to 1. For a single phase system with two retardation mechanisms, $w_B = w_S = 1$; and each epsilon represents the contribution of each mechanism to the strain. The corresponding compliance is

$$D = \frac{\varepsilon}{\sigma_o} = w_B D_B + w_S D_S \qquad (1)$$

If w_B and w_S are assumed to be proportional to the amount of each phase present (either volume or perhaps a linear counterpart), the model has no arbitrary parameters. This can be an advantage over more complex models. In addition, the simplicity of Eq. (1) allows one to derive the relationships below.

The temperature shift behavior must be known for a material in order to represent its viscoelastic response as a function of time and temperature with only one response-time or response-temperature curve. The temperature shift behavior is also necessary in order to assemble a meaningful master curve from experimental data at different temperatures. Time-temperature reduction of compliance is delineated in Fig. 4. Because one now expects the shift factor to depend on time as well as temperature as discussed above, $a_T(t)$ is written instead of the conventional a_T. One would like to constrain one of the variables in order to write a differential relationship. Generally one is looking for the temperature dependence of the shift behavior from the

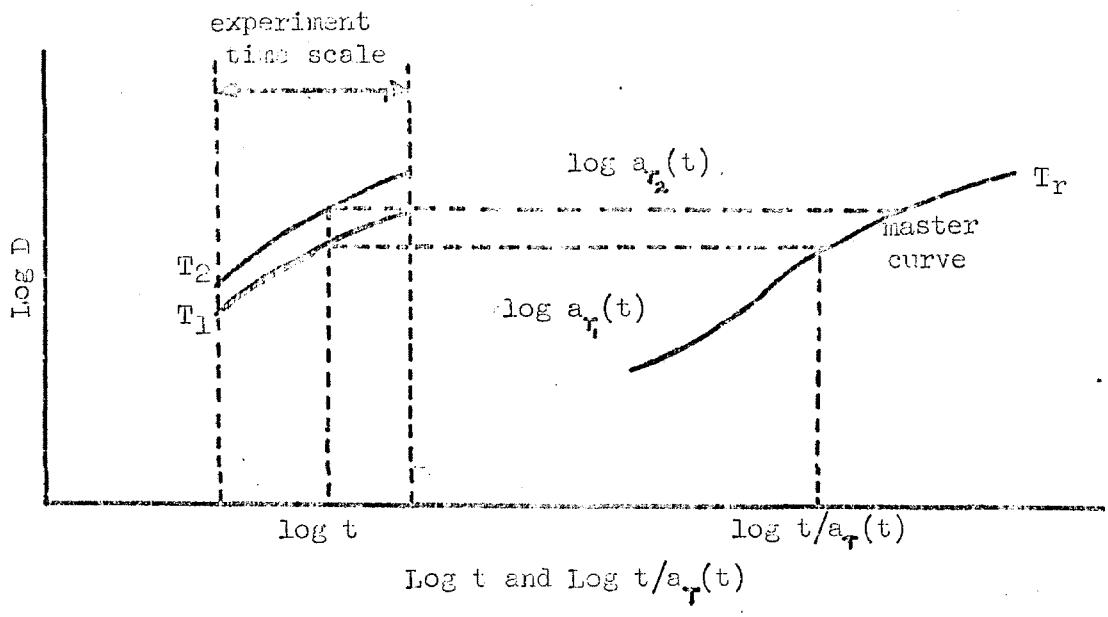

Figure 4. General Case of Time-Temperature Superposition

reference temperature to the experimental test temperature, and so time is constrained. Also, if temperature is constrained, one can forsee an integral over time which is undesirable because of the lack of knowledge of the compliance curves involved. Holding time constant, one can see that the slope of the compliance at the reference temperature and the shifted time, $\left(\frac{\partial \ln D(t/a_T(t), T_r)}{\partial \ln t/a_T(t)}\right)_{T_r}$, is equal to the differential change in compliance with respect to temperature at the test temperature, $\left(\frac{\partial \ln D(t,T)}{\partial T}\right)_t$, divided by the change in the shift factor with respect to temperature, or

$$\left(\frac{\partial \ln a_T(t)}{\partial T}\right)_t = -\left(\frac{\partial \ln D(t,T)}{\partial T}\right)_t \Big/ \left(\frac{\partial \ln D(t/a_T(t), T_r)}{\partial \ln t/a_T(t)}\right)_{T_r} \qquad (2)$$

A derivation of Eq. (2) using Taylor series expansions about a point is given in Appendix A. This is a discouraging relationship from the

standpoint of practical application because the derivatives are evaluated at different places and $a_T(t)$ appears on both sides of the equation. Direct application to an experimental problem is therefore prohibited, but the relationship can be developed to provide some insight into the viscoelasticity of polymeric composites.

In the case of a thermorheologically simple polymer a_T is only a function of temperature; and the slope, $\left(\frac{\partial \ln D(t/a_T, T_r)}{\partial \ln t}\right)_{T_r}$, appearing in the denominator of Eq. (2) is independent of temperature. Eq. (2) thus reduces to

$$\left(\frac{d \ln a_T}{dT}\right) = -\left(\frac{\partial \ln D(t,T)}{\partial T}\right)_t \Big/ \left(\frac{\partial \ln D(t,T)}{\partial \ln t}\right)_T \tag{3}$$

Since $\frac{\partial \ln y}{\partial x}$ can be written as $\frac{1}{y}\frac{\partial y}{\partial x}$, and since $D(t,T)$ is equal to $D(t/a_T(t), T_r)$, and incorporating the additive compliance model via Eq. (1), Eq. (2) can be written for the model in Fig. 3 as

$$\left(\frac{\partial \ln a_T(t)}{\partial T}\right)_t = -\frac{w_B\left(\frac{\partial D_B(t,T)}{\partial T}\right) + w_S\left(\frac{\partial D_S(t,T)}{\partial T}\right)}{w_B\left(\frac{\partial D_B(t/a_T(t), T_r)}{\partial \ln t/a_T(t)}\right)_{T_r} + w_S\left(\frac{\partial D_S(t/a_T(t), T_r)}{\partial \ln t/a_T(t)}\right)} \tag{4}$$

Utilizing Eq. (3) and letting $m_i(t,T) = \left(\frac{\partial \ln D_i(t,T)}{\partial \ln t}\right)_T$, where i identifies the compliance mechanism--in this case one of the polymer phases, one obtains

$$\left(\frac{\partial \ln a_T(t)}{\partial T}\right)_t = \left(\frac{d \ln a_T}{dT}\right)_B \cdot \left(\frac{w_B m_B(t,T) D_B(t,T)}{A(t/a_T(t), T_r)}\right) + \left(\frac{d \ln a_T}{dT}\right)_S \cdot \left(\frac{w_s m_s(t,T) D_s(t,T)}{A(t/a_T(t), T_r)}\right) \quad (5)$$

where

$$A(t/a_T(t), T_r) = w_B m_B(t/a_T(t), T_r) D_B(t/a_T(t), T_r) + w_s m_s(t/a_T(t), T_r) D_s(t/a_T(t), T_r) \quad (6)$$

This is intuitively gratifying because one would expect that the contribution of the compliance of a component to the total shift should be proportional to the amount of that material, the compliance of that phase, and some rate of change of that compliance with time.

One can see from Eq. (5) that time dependence enters the relationship through coefficients. The time scale of the experiment will determine at which temperature the polystyrene of a polystyrene-polybutadiene composite will go through its transition thereby shifting the major weight from the first term to the second. A consequence of the polystyrene shift term becoming important at different temperatures is that it appears with different activation energies since the slope of the shift of pure polystyrene $\left(\frac{d \ln a_T}{dT}\right)_S$ changes.

Since $\left(\frac{\partial D_B}{\partial \ln t}\right)_T$ is the zeroth approximation to the retardation spectrum, L(t), (30), Eq. (5) can be approximated as

$$\left(\frac{\partial \ln a_T(t)}{\partial T}\right)_t \cong \left(\frac{d \ln a_T}{dT}\right)_B \cdot \frac{w_B L_B(T)}{w_B L_B(T_r) + w_s L_s(T_r)} + \left(\frac{d \ln a_T}{dT}\right)_S \cdot \frac{w_s L_s(T)}{w_B L_B(T_r) + w_s L_s(T_r)} \quad (7)$$

where $L_i(T)$ is an abbreviation of $L_i(t,T)$ and $L_i(T_r)$ is short for $L_i(t/a_T(t),T_r)$ (the retardation spectrum is actually a function of retardation times, τ, which are set equal to t in this approximation). This then suggests that the contribution of each phase alone to the differential shift is proportional to the number of retardation times seen in the experiment at temperature T contributed by that phase to the total number of retardation times seen on the reference master curve at temperature T_r at the same overall compliance. Thus, this interpretation of Eq. (5) might be written as

$$\left(\frac{\partial \ln a_T(t)}{\partial T}\right)_t = \left(\frac{d \ln a_T}{dT}\right)_B \cdot \frac{n_B(t,T)}{N\left(t/a_T(t), T_r\right)} + \left(\frac{d \ln a_T}{dT}\right)_S \cdot \frac{n_S(t,T)}{N\left(t/a_T(t), T_r\right)} \qquad (8)$$

where n_i is the number of retardation contributed by species i and is evaluated at (t,T) and N is the total number of retardation times one would see in an experiment at $(t/a_T(t),T_r)$ where the overall compliance for the composite is the same. It seems unlikely that the coefficients in Eq. (8) must necessarily add up to one although one coefficient must go to one as the other approaches zero when a single phase dominates the shift behavior. Thus, one would expect the coefficients to change as indicated in Fig. 5. A qualitative expression similar in form to Eq. (8) with coefficients like those shown in Fig. 4 based on intuitive grounds was suggested by Mancke (33).

The very large changes in magnitude of the compliance that take place in the glass transition region have two effects. One is to make the change from one term predominating to the other take place over a relatively short temperature span. Thus, a step function

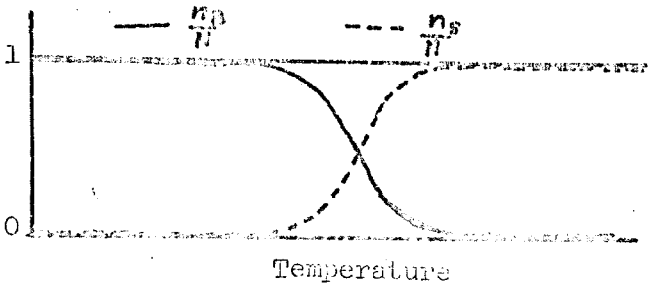

Figure 5. The Weighting of Different Contributions to the Retardation Spectrum of a [Styrene (S)]/[Butadiene (B)] Composite.

approximation would often be accurate. The rapid change in coefficients over a short range of temperature effectively isolates the shifts due to the different mechanisms above and below that range. This is indeed fortunate for it aids the identification and characterization of the mechanisms. For instance, the polystyrene phase in these block copolymers apparently has a slightly lower T_g than one would expect, possibly due to a small concentration of dissolved polybutadiene or a lower effective polystyrene molecular weight than is calculated. This means that if log a_T and compliance data for homopolystyrene are used, they will be at the wrong glass transition temperature. Very likely, the homopolymer compliance data are little affected by this modification; and one can correct for this solely by shifting the homopolymer log a_T curve to fit the composite shift factors in the region where the shift behavior is dominated by the glass transition of the polystyrene. Secondly, the large changes tend to make Eq. (5) insensitive to the homopolymer compliance data chosen for the different phases, to the choices for w_B and w_S, and probably even, to a large extent, to the model. This last point is very

significant; for, although more complex models may be desirable for a description of the actual mechanical response of a composite, the simple model of compliances adding in series should generally be adequate to describe the time-temperature behavior. If the morphology is such that a model with additive moduli is more appropriate, relationships for the shift behavior in terms of this model could similarly be derived. This generality of course supposes that the relaxation mechanisms present and their respective shift behaviors are properly identified and accounted for--a factor which certainly needs more investigation for polymer composites.

Another informative relationship lies in applying the above derivation to dynamic response functions. One can write an expression similar to Eq. (4) with $D'(\omega)$, ω, and $\omega a_T(\omega)$ replacing $D(t)$, t, and $t/a_T(t)$ respectively and omitting the negative sign. Eq. (5) is modified by similarly changing the variables. Eq. (7) again follows as an approximation with $t = 1/\omega$. Another zeroeth order approximation for the retardation spectrum $L(\tau)$ is $\frac{2}{\pi} D''(\omega)\Big|_{\omega = 1/\tau}$. Each $L(t)$ in Eq. (7) can therefore be replaced by $D''(\omega)$, with the corresponding arguments. Since Eq. (5) can be derived for any viscoelastic function, including $D''(\omega)$, one sees immediately that the coefficients in the expression for $\left(\frac{\partial \ln a_T(t)}{\partial T}\right)_t$ as in Eq. (5) must differ for $D'(\omega)$ and $D''(\omega)$ when two retardation mechanisms are present, although both functions have the same shift when one mechanism predominates. This is expected since the loss function tends to weight longer retardation times. Evaluating the coefficients for $D''(\omega)$ is bound to be more

ambiguous and sensitive, however, since the function is not monotonic as are the other functions considered and is often difficult to measure precisely.

Previous investigations on Kraton 102 (21,32) have indicated that the temperatures where the activation energy with which a second compliance adds to the compliance of the polybutadiene network may depend on the time scale of the experiment. Shift data from those experiments--creep at long times and dynamic shear at short times--are shown in Fig. 6A. As discussed in the introductory paragraphs of this part, this model predicts qualitative behavior like that shown in Fig. 6B, where the log a_T values approach the values that would be seen for each invididual contribution taken alone.

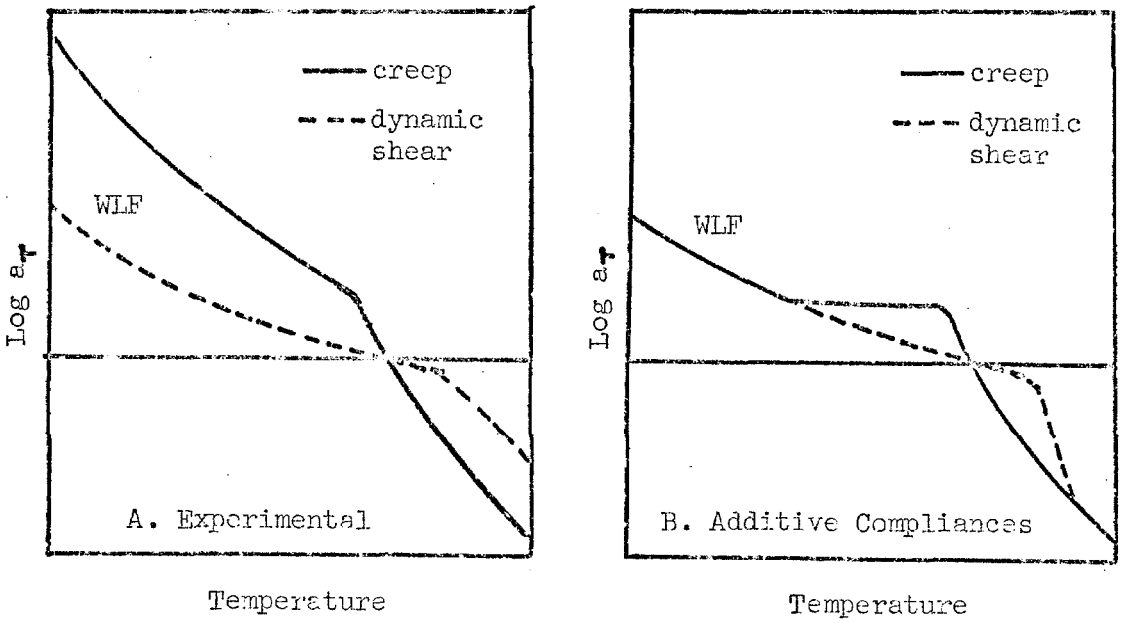

Figure 6. Time-Temperature Shifts of Block Copolymers: A. Experimentally Observed, B. According to Mechanical Model

The primary difference between the experimental curves and the theoretical ones is that the experimental curves diverge while the theoretical curves must converge to a single line when one mechanism dominates.

The difference between the two graphs in Fig. 6 can be related to Eq. (5) when one considers the experimental shifting procedure. Isothermal segments of the compliance curve covering a few decades of time are brought together. Then they are shifted to one another until all the data are assembled into one "master curve." This process will be referred to as "empirical" shifting. Thus, the actual reference temperature for each set of data is the temperature of the set preceding it. For a thermorheologically simple material this results in a valid master curve. For materials with more than one relaxation mechanism, however, this has a serious effect. The shifting can be regarded approximately as one at constant time since the "window" one looks through in an experiment reveals only a small part of the logarithmic time scale. Then instead of evaluating the denominator of the coefficients in Eq. (5) at the chosen reference temperature, the evaluation is done at the previous temperature or at that temperature. Essentially the reference temperature is continuously changing and is approximately the same as the experimental test temperature. The result then is more closely related to an integration over a relationship similar to Eq. (5) only with all the coefficients evaluated at t and T. This is an easy integration to carry out numerically, using tabulated compliance data, and it does indeed lead to results qualitatively the same as those seen in experiments.

The shift behavior as predicted by the model will be quantitatively discussed later.

Another relationship that naturally arises from Fig. 4 has perhaps more practical significance, although its interpretation is a bit more difficult when assigning individual contributions. This is the change of the shift factor with temperature at constant compliance (35). From Fig. 4, one can write

$$\left(\frac{\partial \ln a_T(t)}{\partial T}\right)_D = -\left(\frac{\partial \ln D(t,T)}{\partial T}\right)_t \Big/ \left(\frac{\partial \ln D(t,T)}{\partial \ln t}\right)_T \tag{9}$$

Bringing in the additive compliance model, Eq. (1), and following the steps in the derivation of Eq. (5) leads to

$$\left(\frac{\partial \ln a_T(t)}{\partial T}\right)_D = \left(\frac{d \ln a_T}{d T}\right)_B \cdot \frac{w_B m_B D_B}{w_B m_B D_B + w_S m_S D_S} + \left(\frac{d \ln a_T}{d T}\right)_S \cdot \frac{w_S m_S D_S}{w_B m_B D_B + w_S m_S D_S} \tag{10}$$

where m_i and D_i are the same as in Eq. (5) except that they are evaluated here at (t,T) throughout. Eq. (10) is now subject to the additional constraint on the coefficients that

$$w_B D_B(t,T) + w_S D_S(t,T) = D \tag{11}$$

where D is a constant. Of course, now the coefficients in Eq. (10) add to one. If the restriction, at constant D, is omitted, one would have the same relationship which qualitatively generates the experimental results in Fig. 6A discussed above.

Application of the Additive Compliance Model

The integral of Eq. (10) can be indirectly evaluated exactly for a discrete time and temperature once the compliances in the model are described. To do this, one takes the compliance data for each mechanism (this is easily extended to more than two contributions) along with the time-temperature shift description of each and constructs a master curve of the compliance at the reference temperature according to Eq. (1). At the temperatures and times of interest, similar short master curves are generated. Then, by comparing the time t at which a given compliance appears at temperature T to the time $t/a_T(t)$ at which the same compliance appears on the reference master curve, and taking the difference, one generates the shift $\log a_T(t)$ for that time and temperature. The monotonic nature of $D(t)$ and $D'(\omega)$ allows very rapid computational procedures to be constructed and results in a very efficient computer routine. These shifts, so generated, are then applied to experimental data. For reasons previously mentioned, lack of agreement probably lies not so much in the additive compliance model as in the individual shift descriptions that one puts into the model. However, unlike the equations that have been derived, this method of generating the time-temperature shift data can accomodate a more complicated model of mechanical coupling if increased sophistication is desired.

The shift for the loss compliance is determined in the same way as the shift for the storage compliance. Since $D''(\omega)$ is not a monotonic function as was the case with $D'(\omega)$, however, special precautions must be taken. In certain cases, this one included, the loss

compliance data themselves can be modified in the following way. Data for low molecular weight polystyrene present no problem since no maximum appears. For the matrix, a representative compliance of constant slope is chosen as shown in Fig. 7 by the solid line.

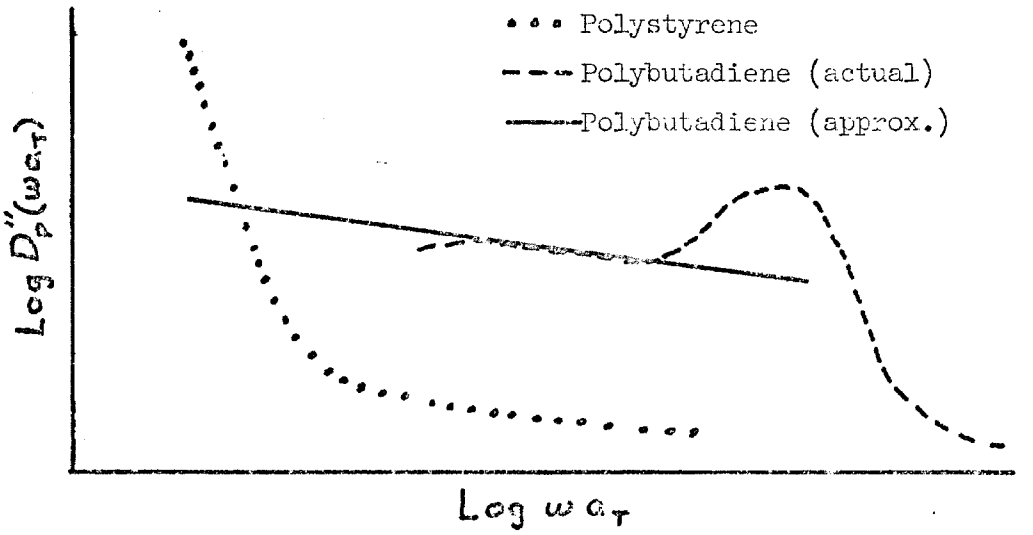

Figure 7. Representation of Loss Compliance Data

The slope was chosen to be parallel to the storage compliance so that the loss tangent would be constant. Thus, when the polystyrene is in the glassy state, it makes little contribution to the shift and log a_T is essentially the shift due to the matrix. Since polystyrene is already in the glassy state at high frequencies, no difficulty is encountered when the loss compliance of the matrix deviates from the straight line representation since the shift is already representative of the matrix alone.

From these data, master curves are synthesized via the additive compliance model at the reference temperature and at the test temperature. Then, as in the case of $D'(\omega)$, the shift factor,

log $a_T(\omega)$, is determined as that shift necessary to superpose a point on the test temperature curve, $D''(\omega,T)$, with the same loss compliance on the reference curve, $D(\omega a_T, T_r)$.

In order to illustrate the time dependence of the shift behavior, log a_T vs. temperature curves for the storage modulus of a polystyrene-polybutadiene-polystyrene triblock copolymer were constructed at two frequencies, 10^{-6} and 10^{5} sec^{-1}. Most common laboratory methods for measuring mechanical response fall within this range, with dynamic tests falling roughly in the high frequency half and transient experiments taking place in the low frequency half of this spectrum. For the polystyrene phase, Plazek and O'Rourke's shear creep compliance data (29) for a polystyrene with a molecular weight of 16,400 were converted to the extensional storage compliance using the Maekawa-Yagii technique (36) and assuming a constant Poisson's ratio of 0.5. To keep the representation simple, the Plazek unshifted data were shifted empirically to obtain a master curve which included both the glass transition and the terminal flow viscosity contributions. Superposition was fairly good as it was not necessary to be concerned with the great precision necessary to separate the two mechanisms. The converted data are shown in Fig. 8. Beyond the range of the data in the glassy region, the relationship $\log D'(\omega) = -3.46 - 0.014\cdot(\log\omega - 3.8)$ was used. The slope was taken from glassy polymethylmethacrylate data (37). The calculated loss compliance is also shown as this will be used later. The Plazek shift curve for the glass transition was corrected from a T_g of 92°C to one of 85°C to correspond to the polystyrene phase in Shell 16/78/16 to be

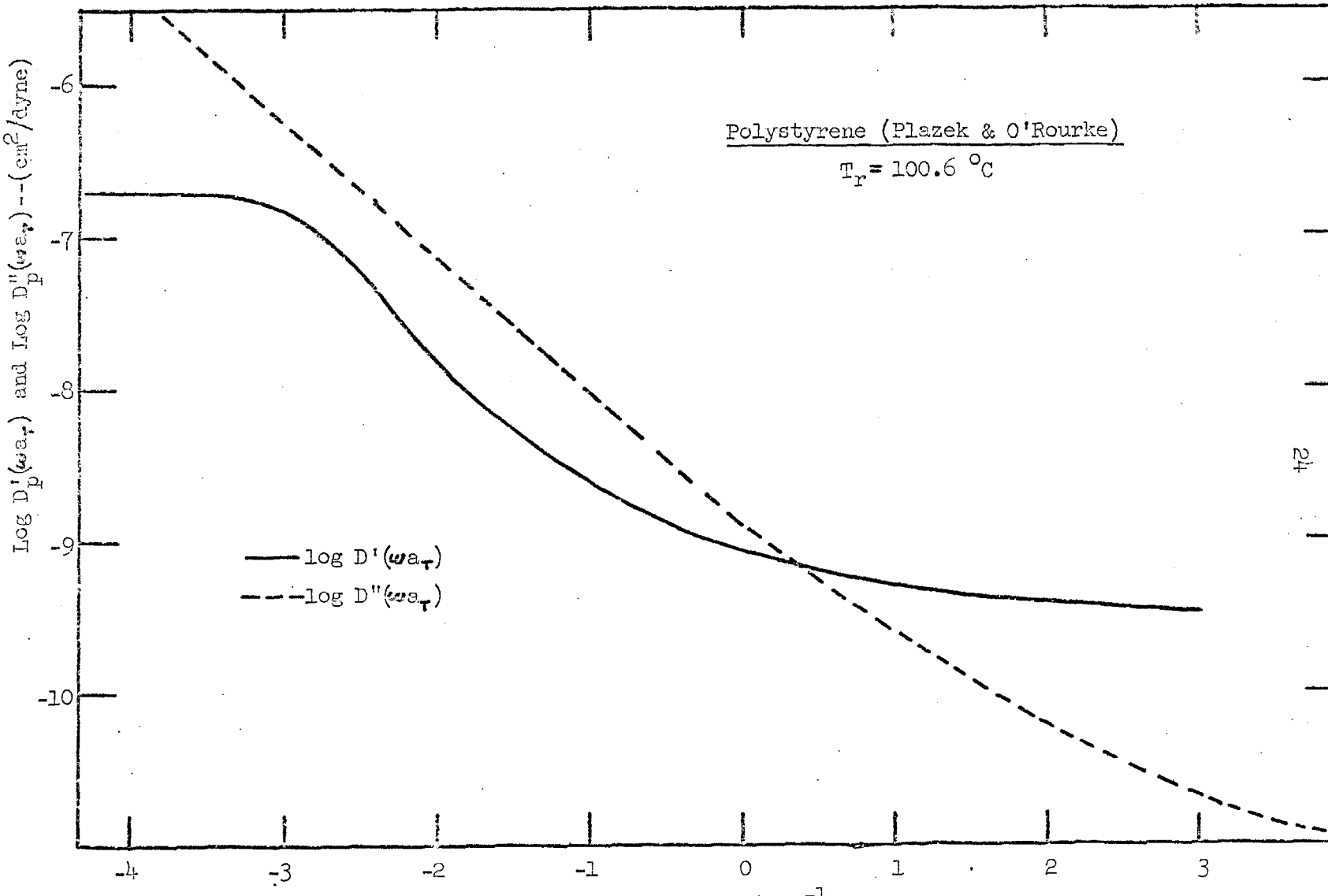

Figure 8. Converted Polystyrene Data.

discussed later. The shift behavior was extended into the glassy state using a linear dependence on temperature based on the data of Lohr (38) and Hideshima (39) as summarized by Rusch (37). Smith and Dickie (35) also felt that a linear shift with temperature was representative of the glassy state in their investigation of block copolymers, although the phenomena they observed in Kraton 101 and Thermolastic 125 probably reflected entanglement slippage and/or an interlayer effect rather than glassy behavior of the polystyrene directly. Thus, the shift behavior of the polystyrene phase was taken to be

$$(\log a_T)_S = \begin{cases} -13.46 + 389./(T-85.0 + 28.9) & T > 85.0°C \\ -0.208\cdot(T - 85.0) & T \leq 85.0°C \end{cases}$$

For the polybutadiene matrix, the Shell 16/78/16 data for the polybutadiene transition and plateau region were used. This will be discussed further with the Shell material experimental results. The shift behavior could be divided into a WLF portion and an Arrhenius portion, but only the WLF part was used here in order to keep the picture as clear as possible. The shift behavior will also be fully described later.

The shift behavior for the individual phases is shown in Fig. 9 for a reference temperature of 85°C. Using the method constructing compliance curves for the composite ($w_B = 0.7$, $w_S = 0.3$) at the reference temperature and at the test temperature and subsequently finding the shift factors between them for the frequencies of interest, the shift curve for the additive compliance model in Fig. 3 is shown in Fig. 10, again at a reference temperature of 85°C.

To show how the behavior now varies with reference temperature, Figs. 11 and 12 show the result at reference temperatures of 60 and 30°C respectively.

From their empirical shifting of Kraton 102 data, Lim, et al. (22) defined a characteristic temperature T_o, below which the shift behavior is dominated by one mechanism and above which it is dominated by a second mechanism. To the extent that the changes from one mechanism to another takes place over a short temperature range, as discussed above, this is true. From Figs. 10-12, however, one sees that T_o must be a function of frequency, being about 60°C for $\log \omega = -6$ and about 110°C for $\log \omega = 5$. What empirical shifting cannot show is the large jump to get from one polymer log a_T curve to the other. In Fig. 10, for instance, the $\log \omega = 5$ curve contains a large vertical jump to get from the polybutadiene curve to the polystyrene curve and the $\log \omega = -6$ curve has a very flat region where essentially no shifting takes place over a broad span of temperature in order to connect the polybutadiene and polystyrene regions. Interestingly, this indicates that the empirical shifting of long time experiment data may give more valid results since the large vertical shift, which represents a degeneracy of sorts, can be avoided. Further, one can see that if T_o corresponds to T_r, as it does approximately for the $\log \omega = -6$ curve in Fig. 11, empirical shifting should result in a fairly accurate log a_T curve when only two mechanisms are present.

Shen and Kaelble (20) observed a straight line dependence of log a_T at intermediate temperatures, and this line intersected the low

temperature WLF curve from above, in a similar fashion to the flat region seen in Fig. 10 for the $\log\omega = -6$ curve. The slope of this line, however, is probably too steep to be the same phenomena, although the data are so scant that one cannot determine the fine structure of the line. It could also conceivably be the effect of entanglement slippage, which will be discussed in the experimental results section, since these experiments were carried out at very long times. The whole observation is somewhat suspect, however, since they used the universal form of the WLF equation which gives a steeper curve than that determined in the experiments reported here. More will be said about Shen's data in the section on Kraton 102.

There are several advantages of this approach to the treatment of polymer composite properties over the decomposition schemes used previously to separate the contributions of various mechanisms. One is that the shift factors are not critically dependent on the accuracy of the experimental data. Decomposing compliance data, for instance, into various components usually requires taking very small differences. In conjunction with this is the problem of accurately shifting the data empirically according to one mechanism or extrapolating the mechanical contribution of one mechanism before the compliances can be decomposed, necessarily involving some guesswork. As will be seen in Part III, prescribing the shift according to theory and applying it to experimental data has the further advantage that deviatoric behavior stands out. Thus it is possible to account for known behavior and, in the process, exhibit behavior that arises from unexpected mechanisms. Thus, the technique offers a

methodical way of separating and identifying components of complex viscoelastic data. A further advantage, from an engineering point of view, is that one obtains, in the end, a master curve for the actual composite material and not master curves of the separate contributions which must then be combined to produce the true master curve.

Among the difficulties in applying this approach to the study of complex viscoelastic phenomena, the large number of calculations involved almost necessitate the use of a computer. However, the calculations are straightforward and efficient, and this cannot be considered a disadvantage with the general availability of computers. There exists the problem of determining the time-temperature shifts of the individual mechanism as would be the case in any attempt to characterize these composite materials. For example, in SBS block copolymers, the shifts for polystyrene in the glassy state must be assumed, and the understanding of glassy behavior is as yet very primitive. Another example is that not much is known about the shifts a glass transition undergoes at temperatures more than 100 ^{o}C above the glass transition temperature, i.e. whether or not it continues to follow WLF behavior. These questions concerning the properties of the homopolymers in polymer composites are, of course, fundamental to understanding the composites themselves, as the interest in them lies to a great extent in their properties over very large ranges of time and temperature.

This approach to the investigation of polymer composite viscoelastic behavior by using a mechanical model to generate the time-temperature shifts gives an intuitively satisfying picture since

the shifts of independent transitions are made largely independent of one another. Experimental data presented in Part III lend support to the consistency of the technique as well as illustrating its strengths.

III. EXPERIMENTAL RESULTS AND DISCUSSION

A. Shell 16/78/16

Material and procedure

This material was provided by the Shell Chemical Company (Experimental Block Polymer TR-41-1648). The styrene/butediene/styrene block segments were determined at Shell to have respective molecular weights of 16,000/78,000/16,000. The polybutadiene microstructure was determined at Shell to be 41% cis, 49% trans, and 10% 1,2 addition. A fact sheet describing the synthesis and characterization is included in Appendix D. DTA in this laboratory showed a glass transition at -91 °C but could not resolve any transition at higher temperatures.

A sample was prepared by casting on mercury a degassed solution of 17.0 g polymer and 0.04 g N-phenyl 2 naphthylamine antioxidant dissolved in 200 ml benzene. After drying for one week, the sample was carefully detached from the dish, lifted off the mercury, dried in vacuum at room temperature for twenty-three hours, and stored at -18 °C. The resultant film was 1.02 mm thick. Viewing the film under polarized light revealed no stress patterns. The modified Melabs Rheometer was used to examine the dynamic mechanical properties of two specimens in simple compression. Each specimen was composed of three laminations, each lamination being cut from the cast film, such that the imposed strain was perpendicular to the laminations. The laminations were put together by washing the surfaces with methanol, placing them together while still wet, and allowing the laminated sample to dry first at atmospheric pressure and then

in vacuum for a few hours. A trapezoidal section was cut out with a razor blade, washed with methanol, and dried for twenty-four hours in vacuum before installation in the Melabs apparatus. The lamination process was carried out independently for each specimen. The trapezoidal shape was dictated by the structure of the Melabs Rheometer, which was not originally designed to work in compression, and the desire to obtain as small a shape factor (thickness/area) as possible. The first specimen was 0.308 cm thick with a cross-sectional area of 0.200 cm^2. When annealing was observed at high temperatures during the Melabs tests and subsequent investigation showed that annealing could change the thickness by as much as 30%, the second specimen was prepared. The only difference in preparation between the two specimens was that the second laminated sample was annealed at 100 ^{o}C for six hours in a small evacuated dessicator before the trapezoidal specimen was cut. The thickness of this specimen was 0.404 cm., an increase of 31%, with a cross-sectional area of 0.176 cm^2. Adhesion between laminations and between the specimens and the rheometer in both the annealed and unannealed specimens was very good; and once the specimens were cut, it was very difficult to visually determine the precise location of the interfaces. Most of the ensuing discussion will be concerned with the data obtained on the annealed specimen.

When a specimen was installed in the compression mode of the Melabs apparatus, the force monitor plate was allowed to drop and rest on the specimen. The monitor plate was then pushed by finger pressure to apply a small compressive strain to the specimen and was secured in place by tightening a screw against the upper part of the

monitor plate. The applied strain was estimated to be of the order of 5%. The apparatus was then heated to 50 °C for twenty-four hours which allowed some annealing to take place and resulted in good contact between the specimen and the driver and force monitor plates. While in the rheometer, a nitrogen blanket was kept over the specimen except at the lowest temperatures when a liquid nitrogen cooled heat sink surrounded the apparatus. The first data were taken at 50 °C followed by the low temperature measurements. The 50 °C measurements were then repeated before and after the high temperature series. The 50 °C data were reproducible except for the final set for the unannealed specimen which, as mentioned, had annealed at the high temperatures.

Mechanical Properties

The storage compliance for the annealed specimen is shown in Figure 13 for 9 temperatures. Data at 16 other temperatures, primarily in the 0 - 80°C range, have not been included in order to simplify the picture. Compliances appearing below the value of -3.5 in Fig. 13 are beyond the calibrated hardness range of the Melabs apparatus, though this will not disturb the time-temperature superposition results as discussed in the section dealing with the apparatus (Part IV). The reduced data below 40°C could be shifted, together with the loss compliance, into very good superposition.

The usual $T_\rho/T_o\rho_o$ factor (28) was used to reduce data falling in the plateau region above the polybutadiene glass transition; and in the transition region, the shift was allowed to vary between zero and

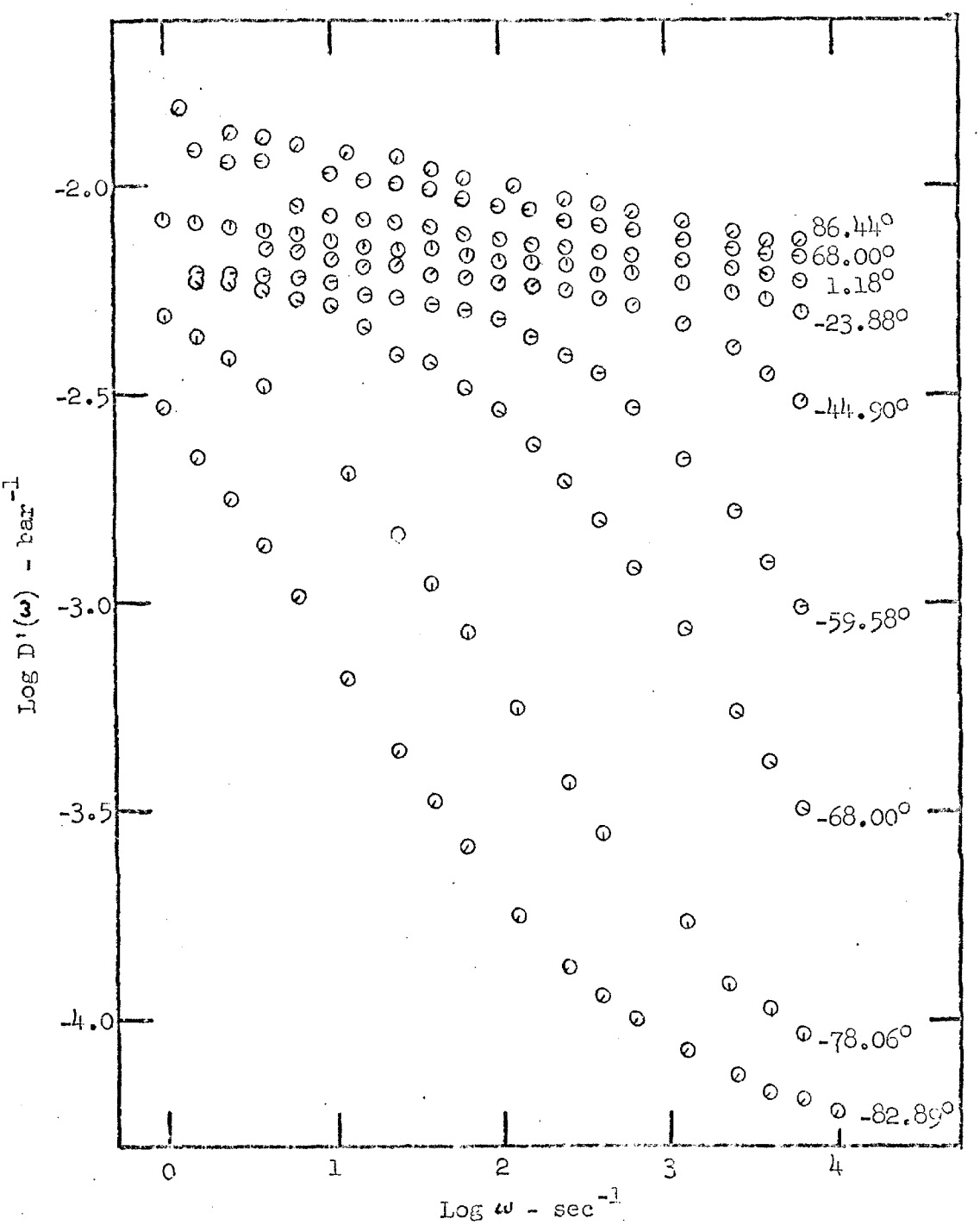

Figure 13. Storage Compliance of Shell 16/78/16.

$T_\rho/T_o\rho_o$ (28) in order to obtain the best superposition. In reality, just the T/T_o shift is applied to the data since the rheometer, in confining the specimen to a constant thickness, measures the density reduced compliance if it is assumed that no bulging takes place. No estimate of the amount of bulging in the specimen can be given and this has been neglected.

The shift factors, together with the shift factors for the unannealed specimen are shown in Fig. 14 based on a reference temperature of -78°C. The WLF equation, also shown in Fig. 14 by the solid line, is determined from the plot of $T-T_r/\log a_T$ vs. $T-T_r$, as shown in Fig. 15, to be

$$\log a_T = - \frac{7.76\cdot(T+78.0)}{51.1+(T+78.0)} \qquad (13)$$

In Fig. 15, the shift data deviate from the WLF equation at about 0°C for the annealed material and at about -40°C for the unannealed specimen. However, in the intermediate temperature range, the shift behaviors appear to be the same as they are parallel in Fig. 14.

Time-temperature superposition shifts deviating from the WLF expression at temperatures above the polybutadiene glass transition imply that another mechanism, other than the glass transition, is contributing to the compliance. Smith and Dickie (35) speculate that this is due to glassy behavior of polystyrene domains in their investigation of Kraton 101 and Thermolastic 226. However, the idea of glassy polystyrene contributing to the mechanical properties was prompted by the steep slope of the $\log a_T$ curve. The slope observed here is much smaller making it more likely that relaxation is taking

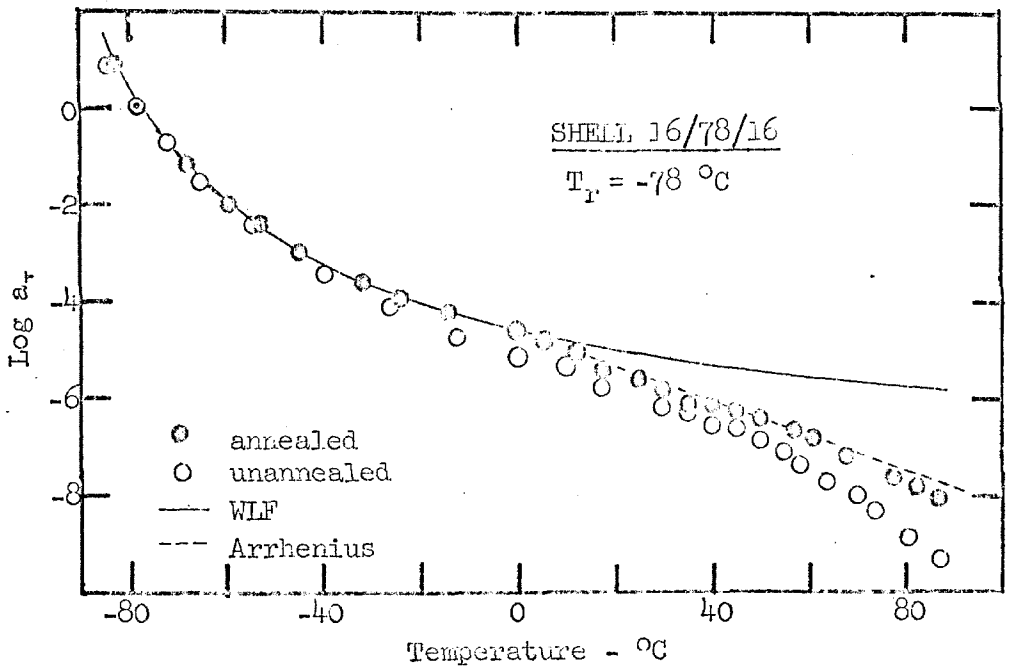

Figure 14. Empirical Shift Factors of Shell 16/78/16.

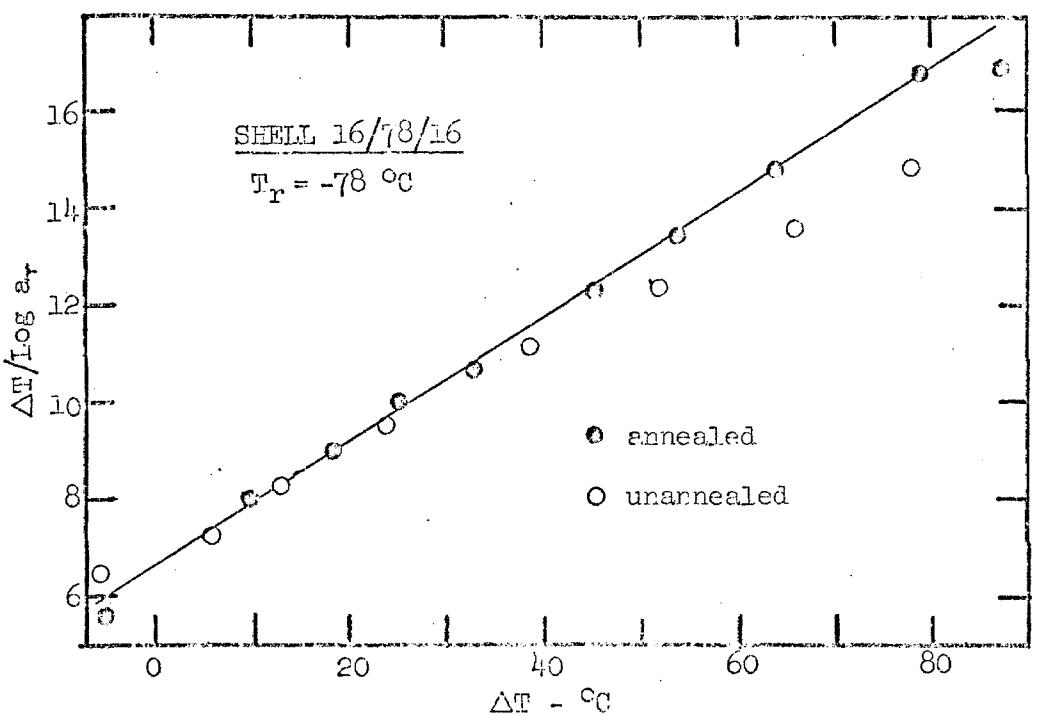

Figure 15. WLF Plot of Data in Fig. 12.

place in the rubbery network or perhaps in the interlayer between the polystyrene and polybutadiene phases. Of course, a decided advantage here is that the Shell 16/78/16 is well characterized whereas the commercial Kraton 101 and Thermolastic are not.

An approximate decomposition of the shift factors can be obtained by subtracting the WLF curve from the experimental shift data. The actual decomposition of the compliance data into the various components to determine the decomposed shift factors is very sensitive to the accuracy of the data and assumptions regarding the polybutadiene equilibrium compliance. One obtains an activation energy of about 8 kcal/mole for this secondary relaxation--about twice the value quoted by Ferry (28) for entanglement slippage. From the additive compliance model presented earlier, however, one would predict that the WLF shift should not be subtracted, but rather that the activation should be calculated from the data directly. This is because a decomposition of the compliance into the polybutadiene transition, governed by the WLF equation, and entanglement slippage, governed by an Arrhenius equation, assumes an equilibrium compliance on the rubbery end of the transition. As one approaches this equilibrium compliance with its zero slope, the contribution of the WLF portion to the total shift goes to zero and the total shift is determined by the entanglement slippage part alone. This analysis results in an activation energy of 13 kcal/mole. The slope of the log a_T curve in this region is small enough, however, that, as far as representation of the data is concerned, it does not matter which scheme one uses, or even if a proportionality with temperature rather

than inverse temperature is used. Long time tests should result in this deviation from WLF behavior occuring at lower temperatures so that the deviation could be above the WLF curve rather than below. Then the distinction would be important as subtracting a WLF shift would produce a negative and changing activation energy.

Langley and Ferry (40) suggest that very long entanglement relaxation times are a result of the slipping of large branched structures which are only very lightly linked to the gel and thus have low mobilities. If the relaxation seen here is indeed entanglement slippage, it can only involve trapped entanglements with very little branching. Thus the long relaxation times seen apparently support the concept of very long range entanglements and that trapped entanglements in a uniformly crosslinked network involve long relaxation times in their own right.

As mentioned above, the dynamic compliance data below 40°C superpose very well. If empirical shifting is attempted at higher temperatures, however, one can observe that superposition is not obeyed. The effect is very small in $D'(\omega)$, and at first one may tend to think of this as experimental error. A typical example where $D'(\omega)$ data, determined at 68.00°C, have been shifted in an attempt to superpose them with data at 60.98°C is shown in Fig. 16 with an expanded ordinate. This is a real discrepency, though, and it has been observed in numerous investigations of a similar block copolymer, Kraton 102, which will be discussed later. Thus one tends to suspect the applicability of simple time-temperature superposition. Further, the anomaly seems more pronounced in the loss compliance so that

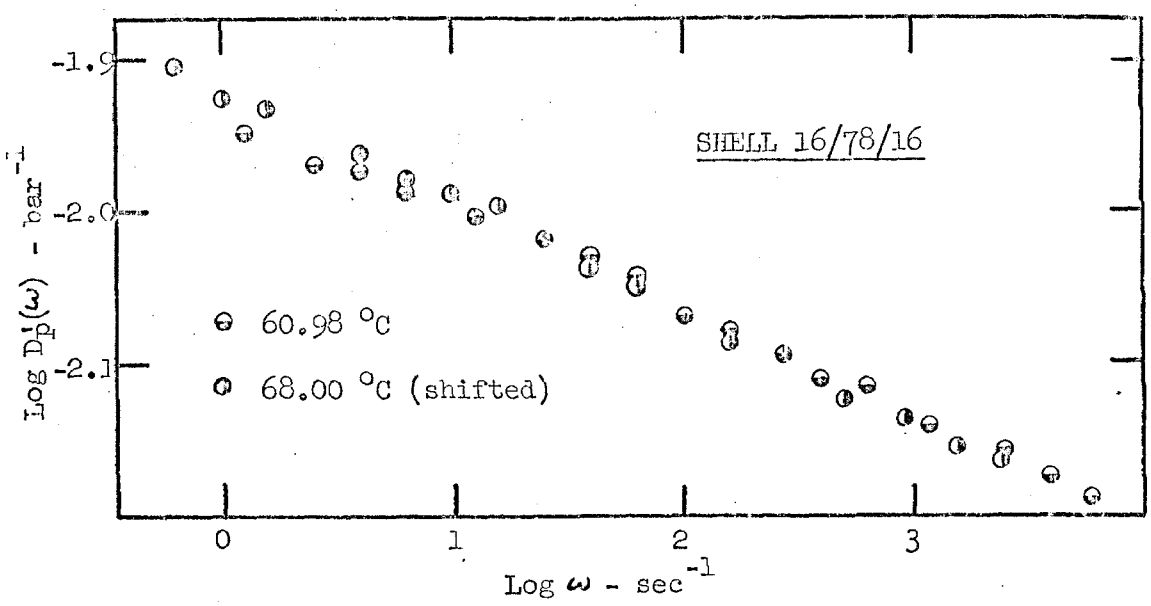

Figure 16. Lack of Superposition in Shell 16/78/16.

shifts different from those for $D'(\omega)$ appear to be necessary. Therefore, one is motivated to apply the time-temperature superposition scheme derived earlier for materials with multiple transitions. For this one needs a representation for compliance and log a_T data for each phase involved.

For the matrix, it was felt that that data which superposed well at intermediate and low temperatures down through the polybutadiene glass transition would be most representative. The master curve of the storage compliance of the unannealed specimen was adopted by tabulating points read off the master curve at 0.2 decade intervals up to a region of constant slope (-0.039 decades of compliance/decade of time). To go further into the rubbery region, the data were extended by extrapolation along a line of this slope. There was no need to represent the glassy compliance of the matrix as the experimental data do not go beyond the transition region. The loss

compliance data require an approximation to be made in order to avoid problems of nonuniqueness and sensitivity to error in the data. This was discussed earlier in Part II along with the representation adopted. The shift behavior of the matrix has been described above. The relationship adopted was

$$(\log a_T)_{WLF} = -4.51\cdot(T-0.08)/(T+146.3) \qquad (14)$$

and for temperatures above 0°C an Arrhenius expression was added so that

$$\log a_T = \begin{cases} (\log a_T)_{WLF} & T\leq 0°C \\ (\log a_T)_{WLF} + 1760\cdot\left[1/(273+T) - 1/273\right] & T>0°C \end{cases} \qquad (15)$$

These relationships were derived from the data obtained for the unannealed specimen, so the WLF coefficients differ from those appearing in Eq. (13) which result from the analysis of data from both the annealed and unannealed specimens and which were derived much later in this investigation. The difference between Eq. (13) and (14) was not sufficient to invalidate the use of Eq.(14) in the computer program.

Equations (14) and (15) state that the polybutadiene transition shifts with WLF behavior at low temperatures and then has a small added shift at temperatures above 0 °C. If the polybutadiene transition actually follows the prescribed WLF behavior at the higher temperatures, this adds an incorrect shift if the transition is referred to those higher temperatures. This is exactly the error that the decomposition of the shifts of the various mechanisms via the additive compliance

model presented earlier attempts to avoid. However, the relationship shown in Eq. (14) and (15) has been used rather than the decomposition scheme for a number of reasons. First, two assumptions are necessary in order to decompose the data: (1) An equilibrium compliance must be assumed in order to separate that portion due to entanglement slippage and (2) intrinsic to the decomposition is the assumption that the low frequency relaxation is really due to entanglement slippage and entanglement slippage alone. If another mechanism, e.g. the presence of a finite interlayer between the phases, which is discussed below, contributes in this region (it would tend to raise the apparent activation energy above Ferry's value of 4 kcal/mole), this decomposition would be misleading. Secondly, the decomposition would be very sensitive to the accuracy of the experimental data as well as to the equilibrium compliance assumed. In addition, the WLF equation is generally proposed for use in the temperature span from T_g to T_g + 100°C and one cannot say whether or not the same equation should be valid at higher temperatures. Thus, in light of present knowledge, it seems wisest to treat the problem in this simple, if somewhat empirical, fashion. If WLF behavior is assumed to be correct at high temperatures, the error in the location of the polybutadiene transition would be only about 1.8 decades at a reference temperature of 85°C and this error would decrease almost linearly to zero at 0°C.

The data used to describe the polystyrene phase were described previously in Part II. A glass transition temperature of

85°C is assumed.

With these data, then, shifts were determined and applied to the experimental compliance data obtained on the Melabs Rheometer. The master curve so generated is shown in the bottom of Fig. 17. Obviously there is still a lack of superposition. One's first reaction would be to say that the polystyrene is affecting the data at higher frequencies (or lower temperatures) and a T_g lower than 85°C should be adopted. This is judged to be unlikely on the basis of three observations. First, although $D'(\omega)$ and $D''(\omega)$ shift differently when two mechanisms are present, they cannot be made to shift that differently by simply changing the polystyrene T_g so that the lack of superposition in both curves will be resolved. Secondly, by lowering the T_g of the polystyrene, the general appearance of $D_p'(\omega a_T)$ and $D_p''(\omega a_T)$ can be improved, but the fine structure shows superposition as bad as that obtained by empirical superposition alone. For instance, the model discussed in Part II suggests that the superposition should get better as the higher temperatures are approached, and the opposite is seen if the T_g is lowered. Although not many data have been obtained at low frequencies at the highest temperatures, their superposition is very sensitive to the selection of the glass transition temperature used to generate the shifts. At 85°C, they superpose fairly well, but a choice of 87 or 83°C shows obvious lack of superposition. Unfortunately a malfunction of the apparatus prohibited measurements at higher temperatures. Thirdly, this value of 85°C is also consistent with DTA measurements on Kraton

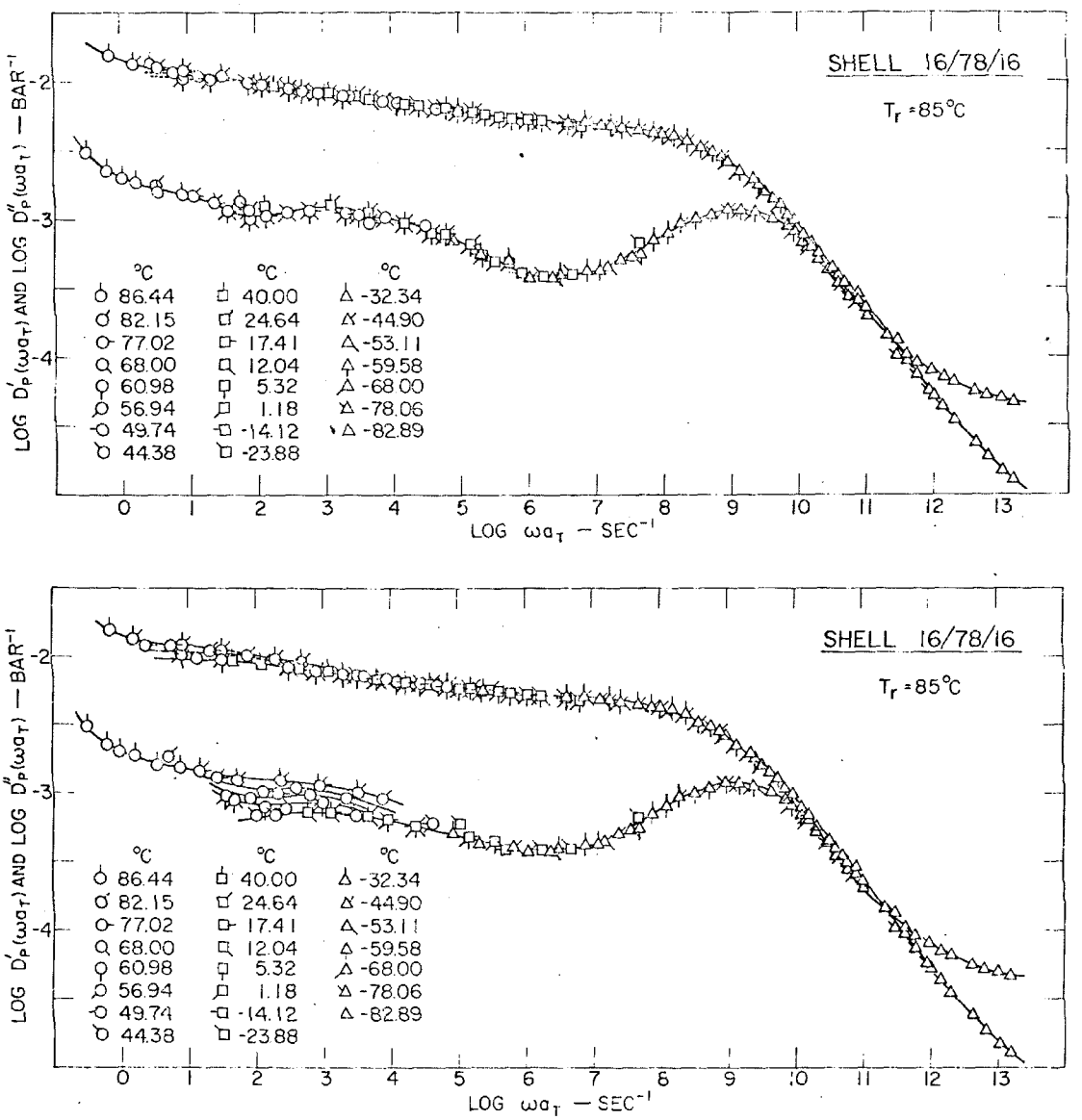

Figure 17. The Storage and Loss Compliance of Shell 16/78/16 Shifted According to the Method Developed in Part II: Without the Interlayer Correction (lower) and with The Interlayer Correction (upper).

102 which give some indication of a glass transition at 83°C (usually in the form of what appears to be stress relaxation as the sample is warmed).

Indeed, $D''(\omega)$ contains indications that the lack of superposition is due to another added compliance which does not affect the horizontal shift. In particular, the horizontal shift of the small maximum that appears at low frequencies seems to be fairly well described, but the value of the maximum and the surrounding data increases as the temperature increased. This could be the case if the composition of the system was changing to make it more compliant, but leaving the horizontal shift behavior unchanged. The presence of an interlayer between the polystyrene and polybutadiene phases in which the two components are mixed would be consistent with these observations.*

The Interlayer

From Eq. (5) in the discussion of time-temperature superposition of block copolymers, one sees that the contribution a mechanism makes to the shift is proportional to the amount of that phase, the compliance of that phase, and the rate of change of that compliance. If an interlayer is present between essentially homogeneous phases, it must have a changing composition subject to the condition that the composition must change smoothly

*The presence of an interlayer has been postulated previously by Kaelble (21,41).

to the compositions of the homogeneous phases at the boundaries. Since the composition of the interlayer, and thus the T_g is continually varying (a function of the radius for spherical domains in a continuous matrix), some of the interlayer will be rubbery, some glassy, and some will be in transition. This is shown in Fig. 18 where the different conditions are shown for discrete spherical

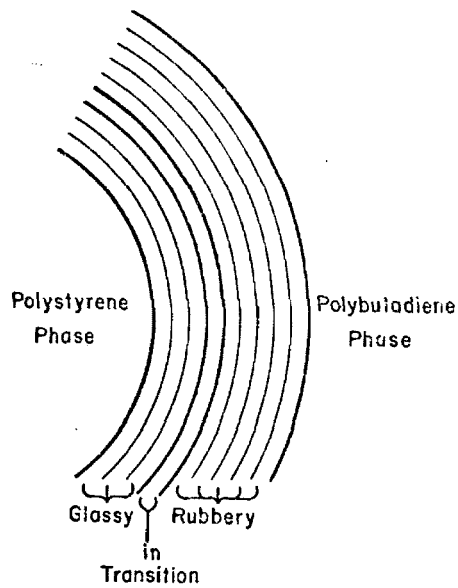

Figure 18. Morphology of the Interlayer.

shells, although the variation is, of course, continuous.

To simplify the description one assumes that the interlayer does not contribute to the horizontal shift behavior because the compliances of those regions in the glassy and rubbery states are not changing rapidly enough, and that portion in transition is such a small fraction that it can be neglected. There is some justification for this assumption in the behavior of the small maximum which appears in the loss compliance and which was ascribed earlier to the

relaxation of entanglements. The fact that the location of this peak changes very little as the compliance changes with temperature strongly supports the contention that the interlayer has little effect on the horizontal shift. The small shift in this region also makes it possible to determine Fig. 19 (discussed below) at constant frequency (100 sec^{-1}). (Even if the horizontal shift was affected, this would be of little consequence since the compliance master curve must still be dominated by the polybutadiene and polystyrene glass transitions and any contribution of an interlayer must lie in between where the changes are relatively small. However, the superposition of fine details, such as the small maximum in $D''(\omega)$, would be lost).

The effect of the interlayer on the total compliance of a polymer composite cannot be neglected, however, and is probably the major cause of the lack of superposition that we've seen in previous master curves. Extending the additive compliance model to include the interlayer, one obtains

$$D(t) = w_B D_B(t) + w_S D_S(t) + w_I D_I(t) \qquad (16)$$

where w_I is the fraction of interlayer present and $J_I(t)$ is an average compliance of the interlayer. We break the interlayer contribution down further into a rubbery portion $w_{IR}D_{IR}$ and a glassy portion $w_{IG}D_{IG}$ so that

$$w_I D_I(t) = w_{IR}D_{IR} + w_{IG}D_{IG} \sim w_{IR}D_{IR} \qquad (17)$$

where the region in transition is regarded as being negligible or effectively factored into the two terms. Since the glassy compliance

would be much less than the rubbery compliance, the contribution that the interlayer makes to the total compliance is approximately that of the rubbery portion. w_{IR} and w_{IG} (which must add to w_I) are functions of the test temperature and the time scale of the experiment since these parameters determine where the transition lies in Fig. 18. This argument will also apply to the dynamic functions $D'(\omega)$ and $D''(\omega)$ as well.

As test temperature increases, therefore, one should see an increase in the experimentally determined storage and loss compliances. This is indeed the case with Shell 16/78/16 for temperatures between 45° and 80°C. It is seen to be most significant for the loss compliance and by determining the differences in the loss compliance at different temperatures, one can determine the fraction of the interlayer in the rubbery state w_{IR}/w_I as a function of temperature assuming that

$$D''_I(\omega) \sim D''_{IR}(\omega) \tag{18}$$

and that at high temperatures,

$$w_{IR} = w_I \qquad T > 80°C \tag{19}$$

The result of this analysis is shown in Fig. 19. We can estimate the product of the fraction of material in the interlayer times the effective rubbery compliances (storage and loss) of the interlayer as $\log w_i D'_{IR} \sim -3.0$ and $\log w_I D''_{IR} \sim -3.1$. With two equations and three unknowns, one cannot determine the individual quantities without further assumptions. The fact that $w_I D'_{IR}$ and $w_I D''_{IR}$ are close

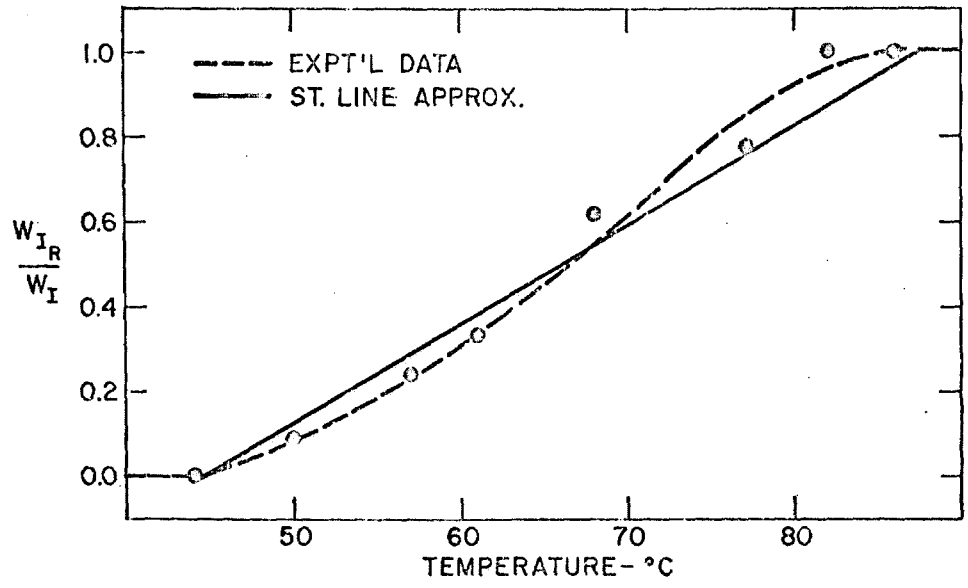

Figure 19. Rubber Fracture of the Interlayer.

together, and hence that D'_{IR} and D''_{IR} are similar points out that this is purely a phenomenological equivalent model that we are supposing, and that the actual values assigned do not have precise physical meanings.

If one can now determine the time dependence of w_{IR} in addition to the temperature dependence, one will be able to include the effect of the interlayer into the shifted curves to obtain a true master curve. We know the temperature dependence of w_{IR}. Essentially the interlayer is described by dividing it into a glassy region and a rubbery region with a step change in between. We say that the material at this step change is at its glass transition. A change in time scale must move the point at which this transition occurs, just as does a change in temperature. Thus a change in the time scale can

be incorporated as a corresponding changing temperature. The relationship is as follows. At a given temperature, a polymer goes through its glass transition at a certain time, and that time has a specific slope of the log a_T vs. temperature curve associated with it. Different polymers have different temperatures where this transition takes place, but within the "universal" nature (28) of polymeric mechanical behavior, this slope would tend to be the same for various polymers. Assuming this to be true for the various polymers in the interlayer (varying polybutadiene/polystyrene ratio) for the range of temperatures involved, one can estimate this slope for a constant time. This slope will then be time dependent, but the assumption of a constant value should be fairly good over the experimental time scale involved. Since this slope is the change in log a_T (or -log t on the master curve) with respect to temperature, in actuality it is the reciprocal of this value that we want. For the polybutadiene transition in Shell 16/78/16, for example, which occurs at approximately -78°C for a frequency of 100 sec^{-1}, the slope of the log a_T curve is about 0.13 decades/°C; and the reciprocal gives about 7.5°C/decade. Plazek and O'Rourke's data for polystyrene with a molecular weight of about 16,000 give about 4°C/decade. These are very approximate figures since it is difficult to assign a specific frequency to the transition and considerable latitude must be allowed. Also we are forcing the model, with the step change in compliance, to the interlayer in order to choose a point on the log a_T curve whereas the smooth transition which should be present must weight the

log a_T curve differently.

A simple way of describing this time dependence as presented in the preceding paragraph is provided by considering isochronal data. For a given time, the polymer goes through its glass transition at a certain temperature, T_g. This T_g changes with the time scale, and the usual variation at long times is generally quoted to be about 3°C/decade (28). This figure would be a lower bound as shorter times would produce somewhat larger values.

Thus, the contribution that the interlayer makes to the mechanical response of a block copolymer is a vertical shift that depends on the test temperature and the test time. Essentially, it is interpreted as a change in the ratio of glassy polymer to rubbery polymer in the composite. A glassy domain consists primarily of homopolystyrene (with perhaps a small concentration of polybutadiene) at the center with the polybutadiene content increasing with the radius. When enough polybutadiene is present to lower the T_g to the test temperature, the material becomes rubbery. Or, at a given test time and temperature, the radius of the glassy domain is determined by the point at which the interlayer material is at its glass transition.

Application of the Interlayer Model

By this method, then, the isothermal compliance data for Shell 16/78/16 are shifted vertically point by point by taking the anti-logarithm, subtracting out a compliance for the interlayer at the experimental temperature and frequency and adding in the

interlayer compliance for the reference temperature and shifted frequency, and taking the logarithm again. The part of the process most likely to strain the validity of the model and the assumption of constant parameters is in determining the time dependence when adding in the interlayer compliance for the reference temperature. The same constant value for $\partial T/\partial \log t$ is used here over a large frequency span. With values of $\log w_I D'_{IR} = -3.0$ and $\log w_I D''_{IR} = -3.1$, using the temperature dependence of w_{IR} shown by the straight line in Fig. 19, and correcting the temperature for each frequency by

$$T_{corr} = T_{exp} - A\cdot(B - 2.0) \qquad (20)$$

where T_{corr} is the corrected temperature, T_{exp} is the experimental temperature, B is the logarithm of the frequency (2.0 is the point at which Fig. 19 was evaluated), and A is taken to be 10.0 degrees/decade, one produces the master curve shown in the top of Fig. 17.

The interlayer is apparently the principal cause of the lack of good superposition that was seen in Fig. 16. Thus direct proof of the breakdown of time-temperature superposition due to the two glass transitions is still lacking. It would require data covering considerably more time or the investigation of a composite with glass transitions much closer together to successfully show this over and above the other relaxation phenomena present.

Some spread is still evident in the region of interlayer contribution at low frequencies in both $D'_p(\omega a_T)$ and $D''(\omega a_T)$ in the final master curve. A possible explanation is that the softening interlayer, particularly as the whole polystyrene domain begins to

soften, may allow added entanglement slippage in the polybutadiene phase by allowing the ends of the block copolymer to rearrange slightly. The difference is very small, but it is unlikely that this is due to a breakdown of the interlayer model because of the approximations made since the behavior is actually in a region that should be best described with the parameters held constant.

Other than this small discrepancy, the experimental data, shifted according to the additive compliance model and corrected for the interlayer, superpose very well. A further test of the consistency of the analysis is to synthesize the master curve as it would appear at a different reference temperature. The upper plot in Fig. 20 presents the same experimental data obtained for Shell 16/78/16 shifted by the same methods to a reference temperature of 25°C. The master curve referred to 85°C that was seen in the upper portion of Fig. 17 is reproduced directly below the 25°C curve. This illustrates the dramatic effect of the reference temperature on the master curve that was discussed with the derivation of the time-temperature superposition scheme. It might be possible to further optimize the values chosen for $w_I D'_{IR}$, $w_I D''_{IR}$, and A in Eq. (20) by examining the superposition at different reference temperatures, but this was not warranted for the data available.

Having described the effect of the interlayer, at least phenomenologically, one must now question the conclusions made regarding entanglement slippage. One must expect the interlayer to be changing over the entire compliance plateau region between the two

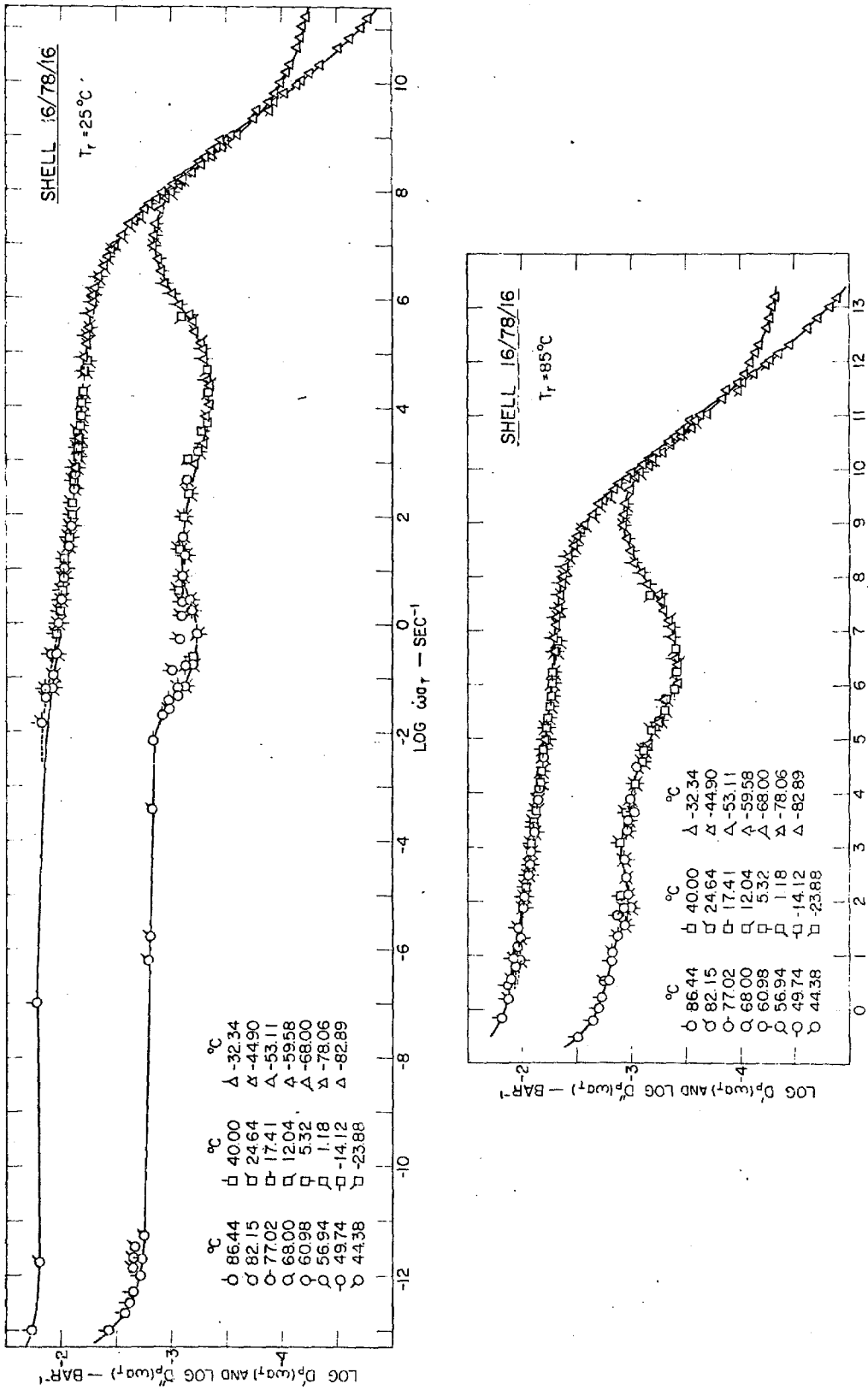

Figure 20. Storage and Loss Compliance Master Curves of Shell 16/78/16: at 85 °C (lower) and at 25 °C (upper).

glass transitions, not just in the high temperature region near the polystyrene transition. In addition, the activation energy that was observed for entanglement slippage was higher than values determined in studies on pure polybutadiene. On the other hand, there is a clear difference in the behavior of the compliance above and below 40°C. This observation was prompted by the behavior of the small maximum in $D''(\omega)$ for which the horizontal shift was consistent, but which experienced vertical shifts at the higher temperatures. Most likely, both relaxation mechanisms are present simultaneously with the small peak arising due to entanglement slippage and the interlayer contributing a small additional compliance. The contributions of both mechanisms are very small and essentially indistinguishable at low and intermediate temperatures.

Some scatter of the data occurred in the area of the minimum in $D''_p(\omega a_T)$. It is attributed to experimental error and those points have been excluded in Figures 17 and 20. The phase angles measured there are very small and close to the limits of the accuracy of the Melabs apparatus. Previous to the investigation of the annealed specimen, the unannealed specimen, with a more favorable shape factor, exhibited remarkably good superposition in this region; and these data superpose very well with the majority of the data points for the annealed specimen. A master curve for this specimen is shown in Fig. 21 at a reference temperature of 0°C and incorporating data for temperatures up to 50°C. The shifts for this curve were determined purely empirically; but observations made on the

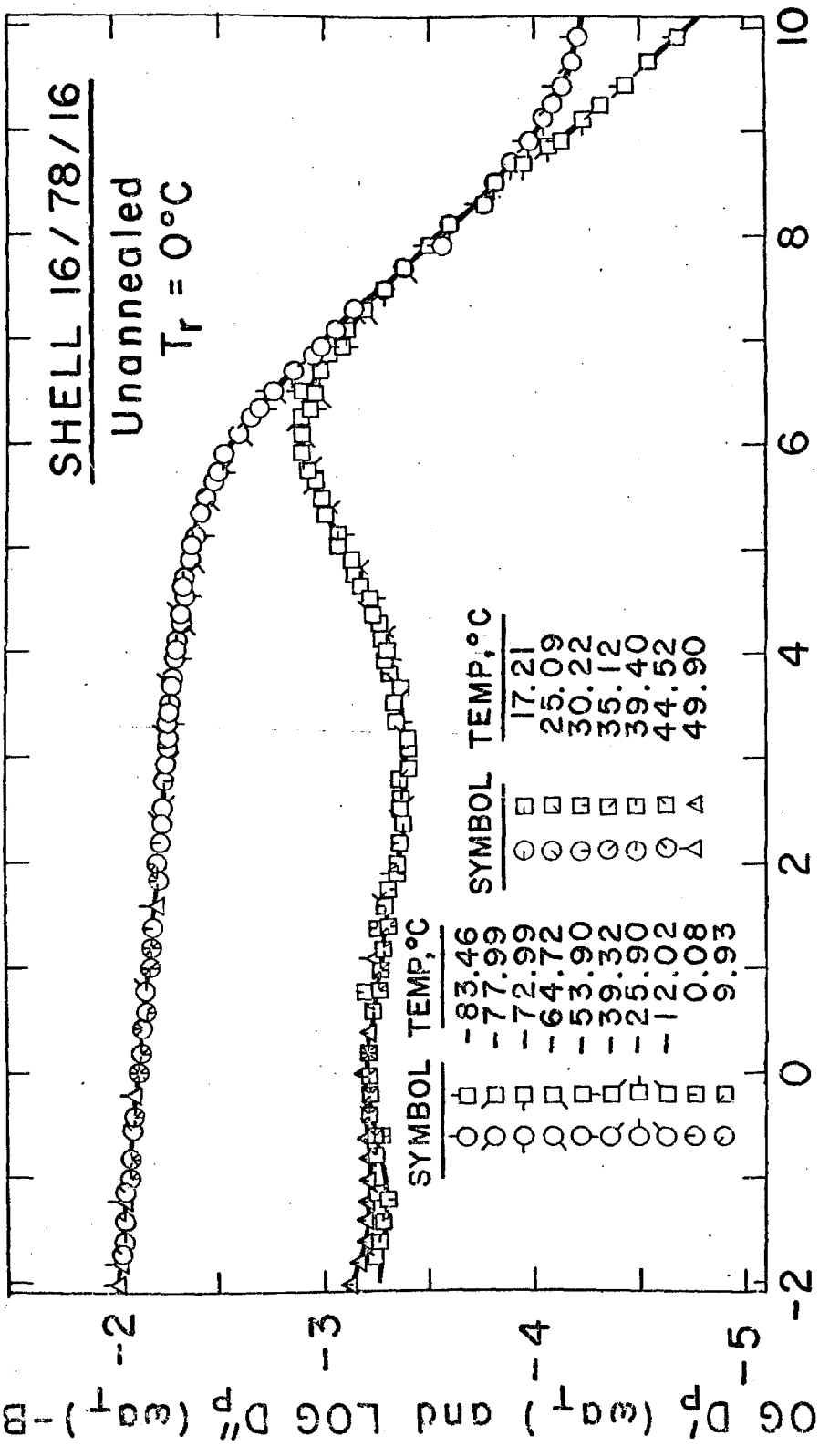

Figure 21. Storage and Loss Compliance Master Curves for Shell 16/78/16 (unannealed).

annealed specimen data indicate that only data taken at higher temperatures than those presented should be affected by a polystyrene contribution. Polystyrene behavior is only important above about 80°C and the interlayer correction is only significant above about 45°C. One sees what is apparently the interlayer effect in log $D''(\omega)$ at the very lowest frequencies in the 50°C data. Annealing during the tests was not a factor since the data taken at 50°C before and after these tests were very reproducible. Data taken at higher temperatures, however, have not been included because annealing occurred simultaneous to the measurements making the results ambiguous.

A point should be made at this time concerning a vertical shift that can arise due to an apparatus malfunction. This will be further discussed in the section describing the apparatus and there it will largely be concerned with the problem as it is seen when the shearing mode of the apparatus is used. Fortunately, the effect arises rarely in tests in simple compression. A result of this error is seen in the room temperature region of the original shift data for the unannealed specimen in Fig. 22. In this region, the compliance data are very flat, and a slight vertical shift can severely affect the horizontal shift. Further, the loss compliance is at a broad maximum at this temperature, so that shifting has to be carried out using the storage compliance alone. The $\rho T/\rho_o T_o$ factor was applied and the reduced data were shifted to obtain the shifts in Fig. 22. The anomaly is obviously an artifact and it is felt that

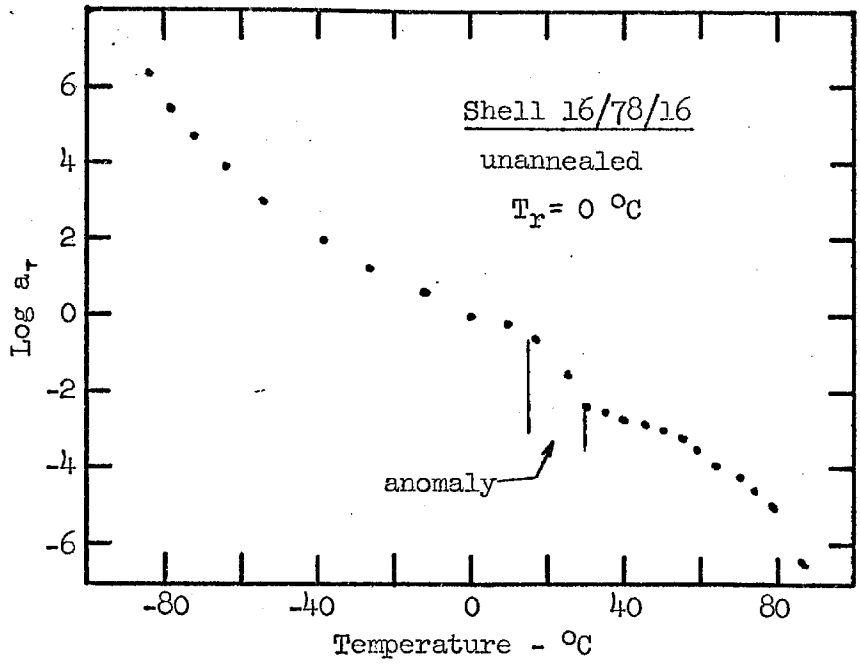

Figure 22. Uncorrected Empirical Shift Factors of Shell 16/78/16 (unannealed) Showing Anomaly.

the shift data can be smoothed. Thus all the high temperature data are shifted up 1.35 decades to be consistent. This action requires that the corresponding compliances have to be shifted 0.075 decades vertically to be consistent with the low temperature data, exactly as if there had been a mistake in the calculation of the shape factor. Interestingly, a recheck of the measurements at 50°C yielded precisely the same results as were seen before the low temperatures were investigated, so that the vertical shift observed was apparently reversible. No anomalies of this sort were observed in the shifts derived from the measurements on the annealed specimen.

B. NBS 10/30/10

Material

This S/B/S triblock copolymer was prepared by Dr. L. Fetters at the National Bureau of Standards and supplied to this laboratory courtesy of Dr. F. N. Kelley of the Air Force Rocket Propulsion Laboratory. The block lengths of molecular weights 10,000/30,000/10,000 were determined stoichiometrically by Dr. Fetters. DTA showed a polybutadiene glass transition at -93°C, but again gave no indication of a polystyrene transition. The material had been subjected to some thermal history previous to this investigation, having been compression molded once, and so it was dissolved in benzene and filtered to remove any impurities and gel that might have formed. The solution filtered easily indicating that very little, if any, gel had formed. In all, 31.3 g of polymer were dissolved in 115 ml of reagent grade benzene to which 0.03 g N-phenyl 2 naphthylamine antioxidant was added. The solution was cast on mercury and allowed to dry for four days. The resulting film had a very slight yellowish hue which may have been due to degradation suffered in the compression molding. The film was much stiffer than other films obtained, being similar in feel to the corrugated cardboard used in boxes. Indeed, a plot of force vs. length in a constant strain rate experiment at room temperature, shown in Fig. 23, revealed a yield point intrinsic to a continuous polystyrene phase. Because of the high polybutadiene content, though, probably both phases are continuous. Also shown is the tracing for the second pull illustrating typical stress softening

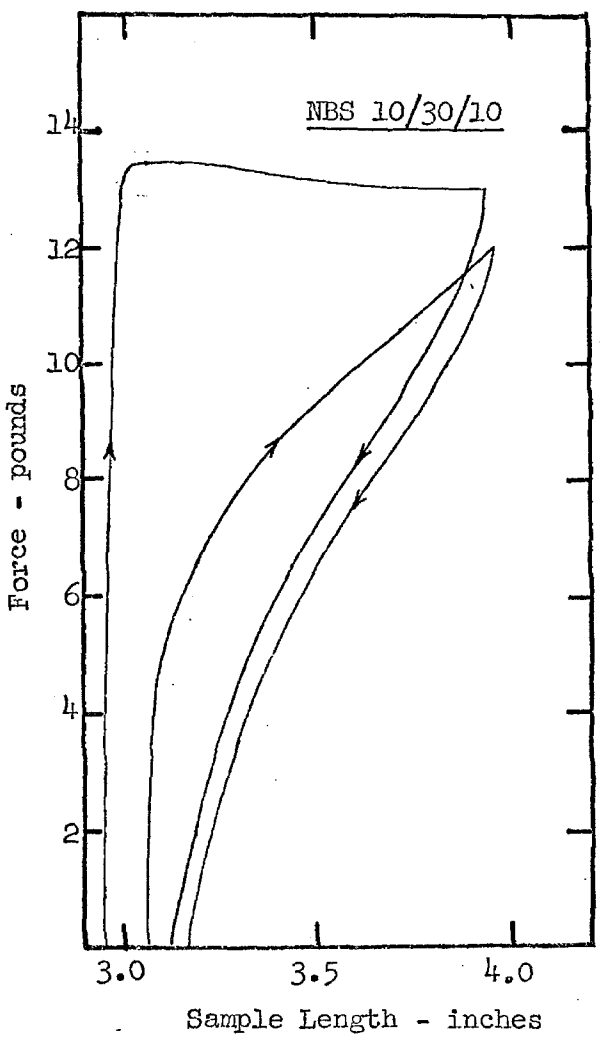

Figure 23. Constant Strain Rate Experiment Showing Yielding in NBS 10/30/10.

of block copolymers (42,43) resulting from the disruption of the continuous polystyrene phase at the yield point so that the composite thereafter acts as an elastomer. Annealing allowed one to reproduce the yield curve repeatedly. This annealing phenomenon and its relation to morphology has been discussed elsewhere (42). Annealing did not result in a dimension change as was seen with the Shell 16/78/16 material.

Mechanical Properties

A specimen 0.55 cm x 0.87 cm in lateral dimensions x 0.188 cm thick was cut from the film with a razor blade and dried in a high vacuum (10^{-5} Torr) for 27 hours at room temperature. Dynamic measurements were carried out in a simple shear on the Melabs apparatus at 15 temperatures between -80 and 90°C. Above room temperature, the apparatus and specimen were blanketed with dry nitrogen. Since the measurements were in shear, arbitrary vertical shifts were often required in order to make the data superpose (cf. Part IV concerning the apparatus). Because the modulus of this material is quite high, though, measurements were very easy and the resulting accuracy in both $J'(\omega)$ and $J''(\omega)$ lended considerable confidence to the shifting. Shifting log tan δ, which removes any vertical shift effect, including the shift factor, $T\rho/T_o\rho_o$, as well as the apparatus error, resulted in log a_T values identical to those obtained by shifting $J^*(\omega)$. At most, the vertical shifts were less than 0.2 decades and the empirically determined superposition was excellent.

The assembled master curves are shown in Fig. 24. The

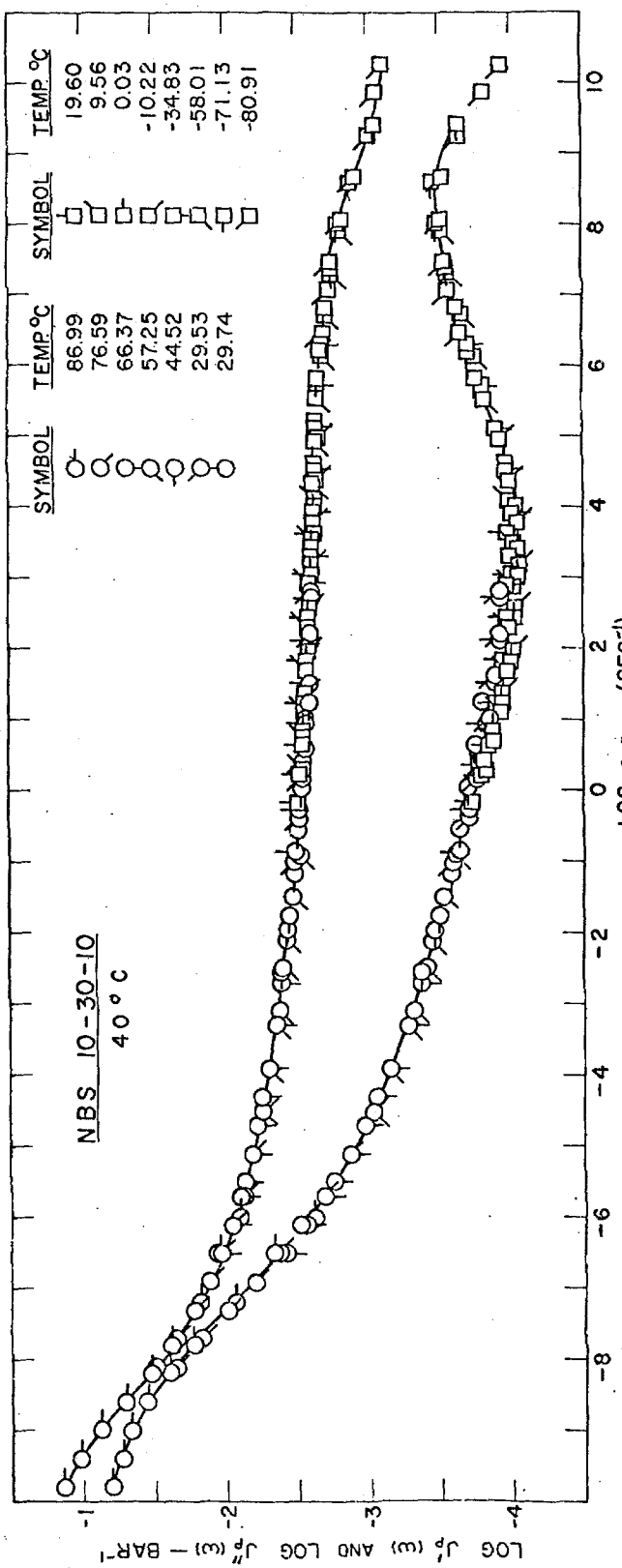

Figure 24. Storage and Loss Compliance Master Curves for NBS 10/30/10.

subscript p on $J'_p(\omega)$ and $J''_p(\omega)$ in this case represents reduction involving the vertical shifts necessary for superposition rather than simply the $T\rho/T_o\rho_o$ factor. Indeed, in this case where the compliance is dominated by the glassy polystyrene, the $T\rho/T_o\rho_o$ factor probably should not be used. Vertical shifts were made relative to the 0°C data, which is an arbitrary choice, but the frequency scale has been referred to 40°C, the reason for which is explained below. The plateau region has a much lower compliance than was seen for the Shell 16/78/16 material as a result of the continuous polystyrene phase. A small polybutadiene transition is seen at high frequencies (low temperatures); and interestingly, the glassy compliance here is higher than that seen in the glassy region of the Shell material. Whether this is a result of the morphology can only be speculated at this point. At low frequencies (high temperatures), the compliance increases as the polystyrene softens and is apparently entering another plateau region.

The shift factors, referred to 0°C, are very revealing and are shown in Fig. 25. Although the polybutadiene transition is very small, as seen in the master curve, the shift behavior is purely polybutadiene in nature and is the same as that seen in Shell 16/78/16. The WLF parameters describing the low temperature data are $C_1 = 13.36$ and $C_2 = 109.2°C$ at a reference temperature of -80.91°C. At high temperatures, the mechanical behavior is dominated by polystyrene, apparently in the glassy state. In fact, the linear relationship used to describe the shifts of glassy polystyrene for Shell 16/78/16

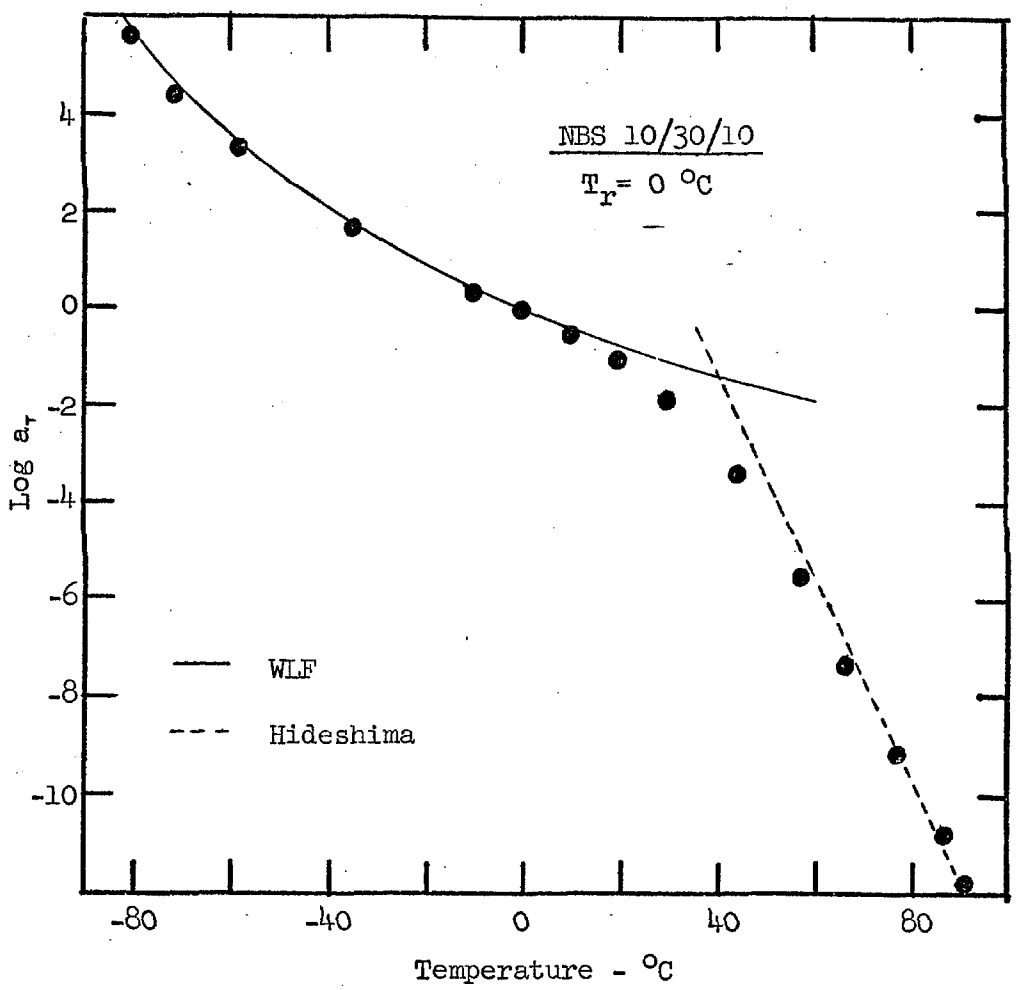

Figure 25. Empirical Shift Factors of NBS 10/30/10.

based on Hideshima's data (39) shows remarkable agreement and is incorporated as a dashed line in Fig. 25. This intersects the WLF curve determined for the polybutadiene transition at 40°C. Thus, the master curve in Fig. 24 should be fairly valid at 40°C according to the theory discussed in Part II. A complete analysis of the time-temperature superposition should be carried out in a similar fashion to the Shell 16/78/16 data, though probably using an additive modulus model. Data without the arbitrary vertical shift are necessary for a meaningful analysis, however. There is evidence that the mechanical

properties in dynamic extension are drastically different from the shear properties because the polystyrene forms a continuous network within the polybutadiene matrix (44,31). This would probably preclude a simple comparison between shear and compression data that could be gotten on the Melabs Rheometer.

Since the data are over a fairly small temperature range, the high temperature shifts also appear to be linear when plotted against the reciprocal of the temperature. The calculated activation energy, however, is about 91 kcal/mole, which is much higher than activation energies observed previously for Kraton 102 (22) in a similar temperature region. Since the NBS material seems to be genuinely representative of polystyrene glassy behavior, it seems likely that the intermediate temperature shifts observed previously in Kraton 102 are due to mechanisms other than simple relaxation in the glassy polystyrene phase.

Investigations into the finite deformation properties of NBS 10/30/10 may shed more light on the theory of the polystyrene-polybutadiene interlayer. Specifically, if the polystyrene network can be assumed to be composed of overlapping polystyrene domains, connected primarily by the interlayer, the yield curve seen in Fig. 23 should be very sensitive to higher temperatures. If no interlayer is involved, the yield curve should remain essentially unchanged until temperatures close to the glass transition of polystyrene are encountered.

C. Kraton 102

Material

Kraton 102 was supplied by the Shell Chemical Co. Samples were prepared by solution casting as in the cases of Shell 16/78/16 and NBS 10/30/10. In addition, one sample was prepared by compression molding in vacuum and at minimal pressures to minimize internal stresses. The compression molding process has been described elsewhere (34). Molecular weights determined in this laboratory have been reported (22) as 37,000 for the polybutadiene center block and 9,500 for each polystyrene endblock, although these figures could be higher if some diblock and/or low molecular weight polystyrene are also present. The polybutadiene transition temperature was determined by DTA to be -88 °C. No high temperature transition could be observed directly with DTA, but often a small endothermic peak, generally ascribed to stress release, could be observed indicating a transition at 83 °C. Free oscillation experiments have also shown the low temperature side of a loss peak at about 80 °C (the entire peak could not be mapped because of flow in the specimen). Creep and stress relaxation tests (22) and dynamic compliance measurements (34) made in this laboratory have been reported. Mechanical testing on a related material, Kraton 101; similar to Kraton 102 but with a higher molecular weight, has also been reported (20,21,35,42).

Mechanical Properties

Dynamic experiments reported here were carried out both in simple shear, specimen dimensions of about 0.9 x 0.6 x 0.15 cm thick,

and in simple compression, dimensions of about 0.2 cm^2 of cross-sectional area and 0.3 cm thick in the direction of the strain. Empirical shifting of the dynamic compliance data yielded well-defined WLF behavior for the polybutadiene matrix glass transition (apparatus error in the shear investigations again limited the validity of the log a_T values to temperatures below 0 °C where the shifting could be pegged on the polybutadiene transition). The WLF behavior observed, however, was markedly different from that observed previously for Kraton 102 in creep and stress relaxation experiments (22); although the agreement was fairly close to those shifts obtained from dynamic experiments with the Fitzgerald transducer (34). The dynamic compliance of a compression molded specimen was determined to see if the difference was due to the method of preparation. The investigation was also extended to a film cast specimen which had been immersed in methanol for several monthes to exhaustively extract any residual benzene (tha sample was kept at -15 °C during this time to minimize oxidation of the polybutadiene). In addition, tests were carried out in simple compression to see if the mode of testing (shear or uniaxial) made a difference. All the shift data gave very good agreement with the original shear data. These data are presented in the log a_T vs. temperature graph shown in Fig. 26 at a reference temperature of -60°C. A WLF plot of the data in Fig. 27 gives the constants $C_1 = 9.14$ and $C_2 = 52.4$°C at a reference temperature of -80°C. This WLF equation is shown as a solid line in Figures 26 and 27 (MELABS). The creep and stress relaxation results

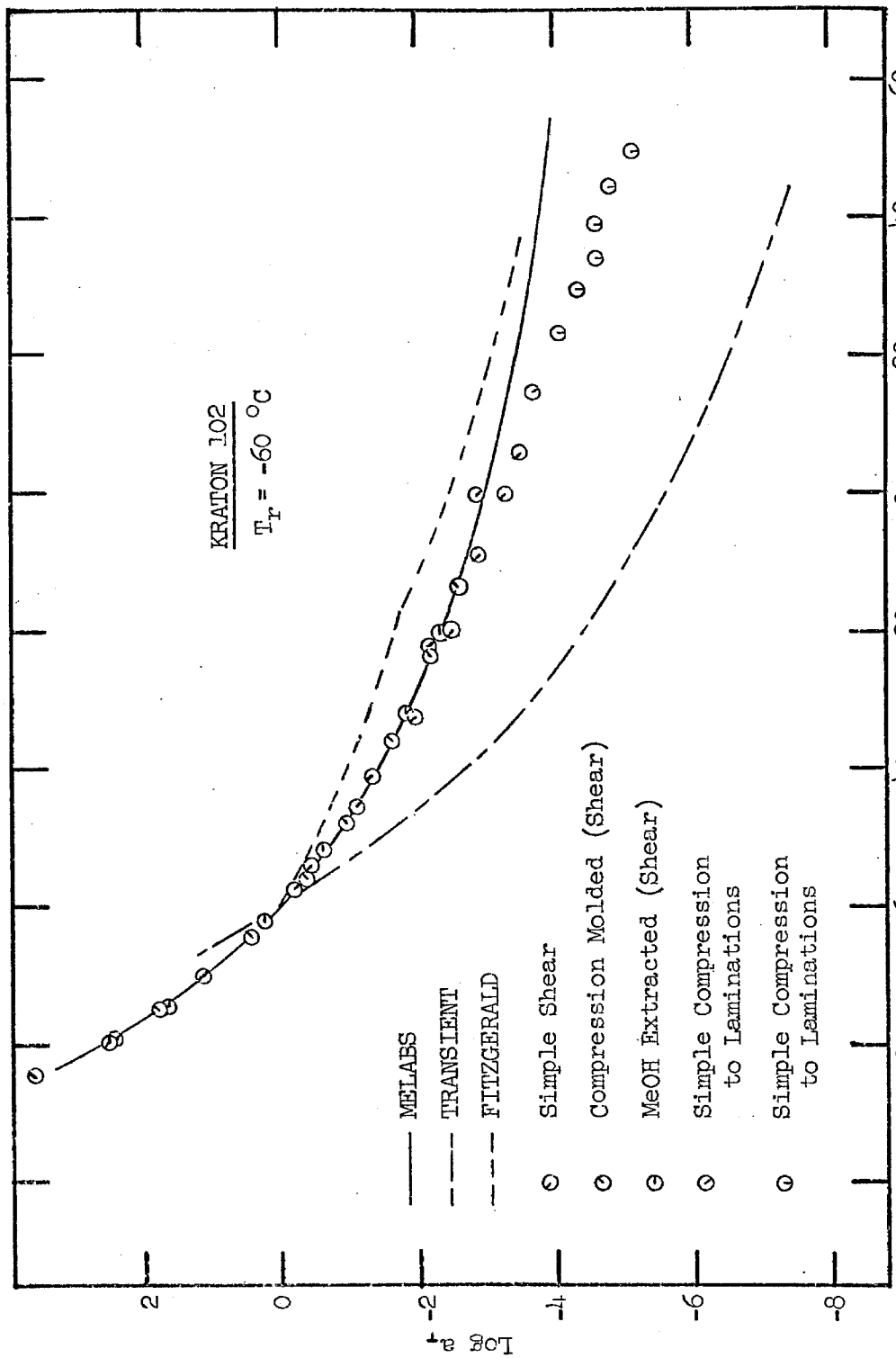

Figure 26. Time-Temperature Shifts for Kraton 102.

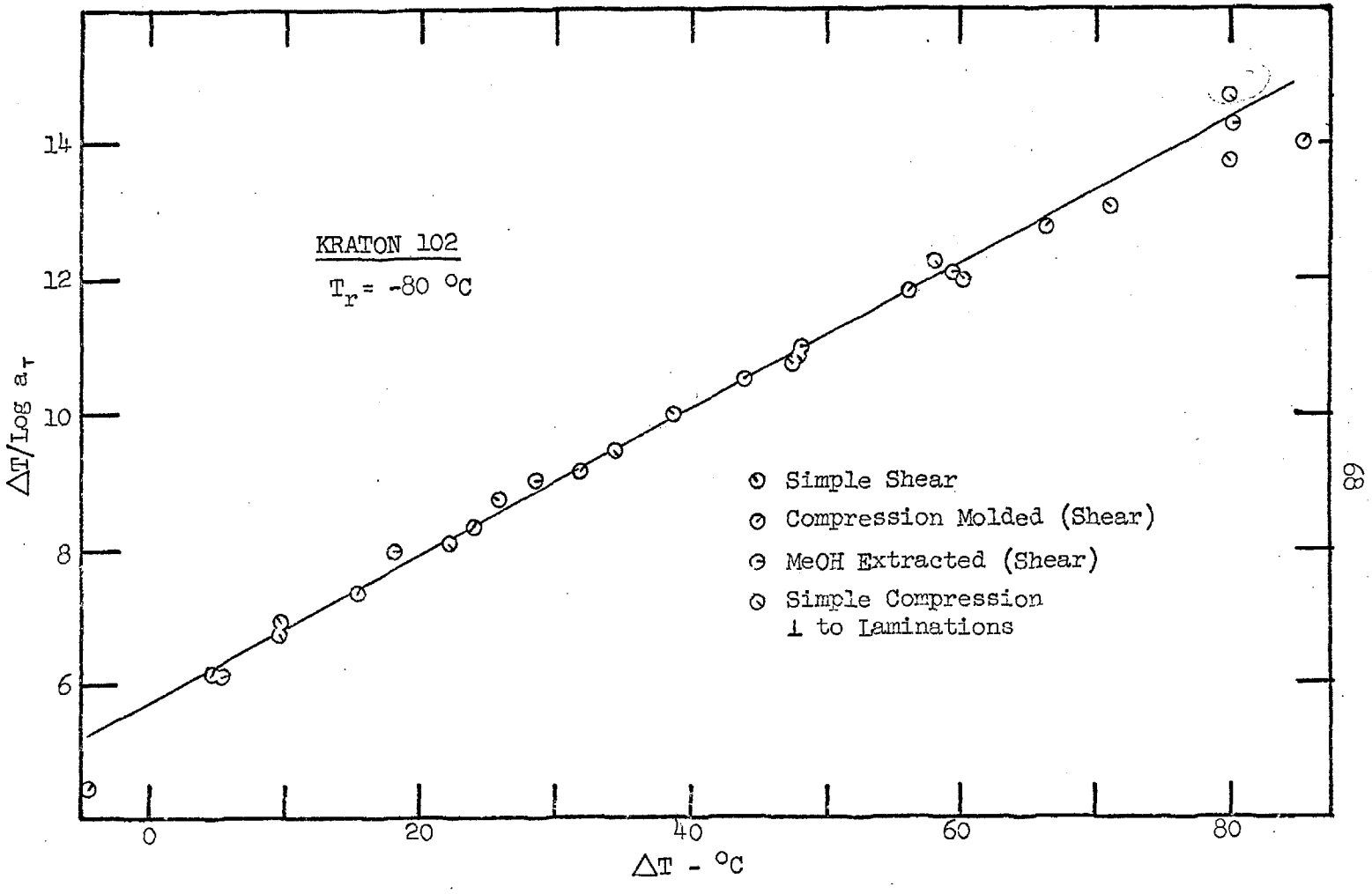

Figure 27. WLF Plot of the Data in Fig. 27.

(TRANSIENT) and the Fitzgerald dynamic results (FITZGERALD), both of which are represented by dashed lines, are also included in Fig. 26. The Fitzgerald data unfortunately cannot now be considered very accurate because later work revealed a malfunction of the apparatus at the time the data were obtained. The shift factors obtained, however, are probably fairly representative because they were based on the polybutadiene transition where the changes in the mechanical properties are large enough that the apparatus error should have had little adverse effect.

If the NBS 10/30/10 and Shell 16/78/16 log a_T data are shifted 5 and 3°C respectively to take into account the differences in T_g from that of Kraton 102 (as determined by DTA), they agree well with those data in Fig. 26. The three WLF curves are shown in Fig. 28.

The shift factors for the polybutadiene glass transition seen in these block copolymers shows remarkable consistency and reproducibility. The shifts are slightly steeper than the curve determined by Maekawa, Mancke, and Ferry (45) for polybutadiene. This is also included in Fig. 28, where it has been shifted 5°C assuming a T_g for that material of -93°C. Kraus et al. (26) have pointed out that a filler raises the apparent glass transition as seen in the mechanical properties by raising the rubbery modulus (of the plateau region here). This could account for the difference between Maekawa's data and the polybutadiene in block copolymers. The pronounced difference in the shifts seen here and those seen in

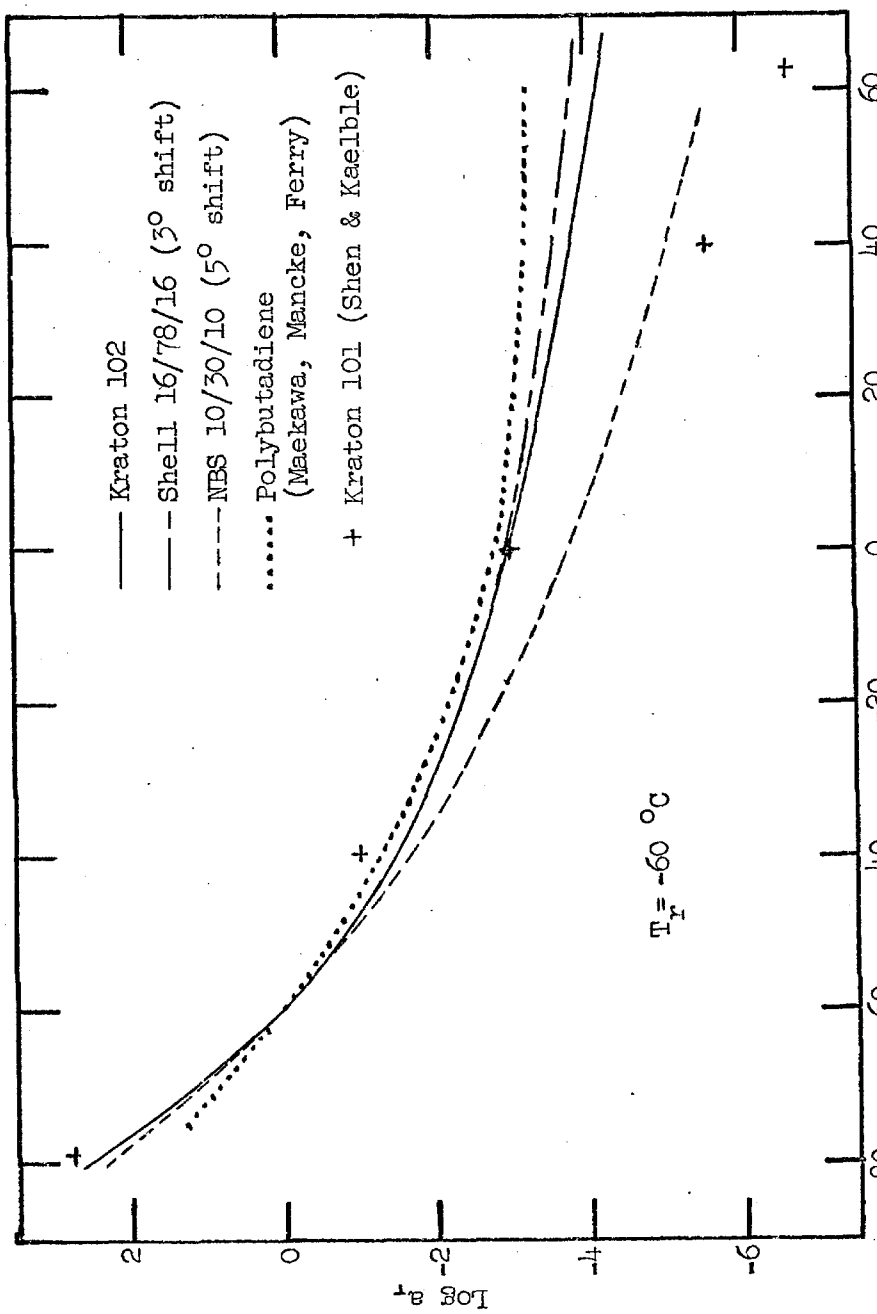

Figure 28. WLF Curves for the Polybutadiene Glass Transition in Block Copolymers.

the creep and stress relaxation experiments is very difficult to account for. Possible explanations are that 1) the finite strains used in the transient experiments affected the data or 2) since the specimens used there were unannealed and involved long strips of solvent cast films, perhaps the anisotropy affected the mechanical response. Very likely, these two factors could have interacted. The WLF equation determined by Shen and Kaelble also does not agree, although their data which fall within the temperature range explored here do seem to fit as is shown in Fig. 28. They used the universal form of the WLF equation, however, which may not be appropriate, and apparently weighted their lowest temperature data more heavily.

The shifts experienced at higher temperatures can be seen in Fig. 26 to follow much the same behavior as was seen for the Shell 16/78/16 material. The data at the intermediate temperatures in Fig. 27 are taken from the compliance data of a laminated specimen examined in simple compression with the strain parallel to the laminations. The lamination procedure was the same as that used for the Shell 16/78/16 specimens. In this case, though, the rheometer surfaces were not in contact with the original film surfaces, which were closely parallel, because of the specimen orientation. Therefore, two parallel cuts were milled into the laminated sample using soapy water as a lubricant, and then the trapezoidal specimen was cut out with a razor blade. The thickness was constant over the specimen within 0.003 cm. The specimen was installed in the rheometer and kept at 50°C under dry nitrogen for twenty-four hours

before measurements were begun. Six temperatures between 23 and 50°C were investigated. At the time of these experiments, the importance of annealing was not realized. Therefore, data taken over 50°C are suspect and are not considered here.

Probably the most meaningful way to shift these data is to follow the scheme used for the Shell 16/78/16 data with no provision for the interlayer. In that investigation, the polystyrene phase did not affect the shift below 80°C. Since there is evidence that the polystyrene phase glass transition does not occur below 80°C, it is unlikely that it would affect the data below 50°C presented here. Using the WLF equation determined from Fig. 27, then, and an Arrhenius expression of the same activation energy as was used for Shell 16/78/16, one obtains the compliance master curve shown in Fig. 29. The low temperature compliances here are from specimen U in which the strain was perpendicular to the laminations within the specimen. The shape factor of this specimen was too high to permit higher temperature measurements; and so data from specimen U4, for which the strain was parallel to the laminations, as already discussed, are included. The data agree very well except that the loss data for specimen U4 appear to be slightly higher than those of specimen U in the overlapping region. This may be due to experimental error in which case the data for specimen U4 should be more reliable since the measurements were more difficult for specimen U. This may also be a real difference resulting from anisotropy or differing amounts of static compression applied to the specimens.

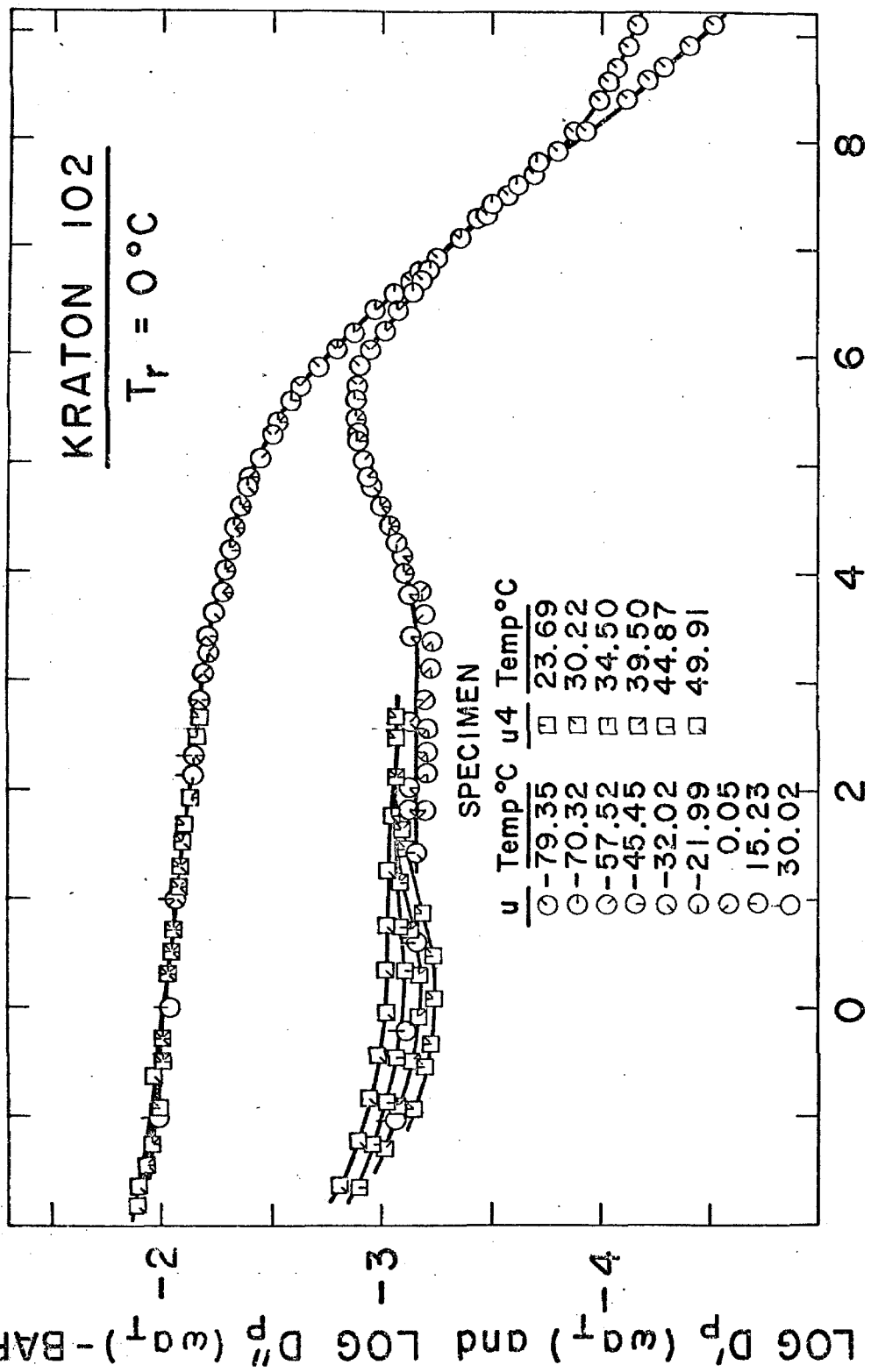

Fig. 29. Master Curves of Kraton 102.

Two other specimens, for which the strain was perpendicular to the laminations were examined at the higher temperatures, but specimen U4 was the only one that was annealed at 50°C for one day before testing and hence gave the only reliable data. Qualitatively, the storage and loss compliances in Fig. 30 are very similar to those determined for Shell 16/78/16. In fact, the polybutadiene transition at high frequencies superposes very well with the corresponding data of Shell 16/78/16 with only a small horizontal shift of about 0.5 decades, which is explained by the difference in T_g's (these data for Kraton 102 are probably best compared to the compliance of the Shell 16/78/16 unannealed specimen in Fig. 21). However, the loss compliance in the plateau region for Kraton 102 is slightly higher (with a correspondingly steeper slope of the storage compliance); and the lack of superposition, seen primarily in $D''(\omega)$ and attributed to the interlayer, is more pronounced here. The lack of high temperature data prohibits a more complete quantitative analysis, but one can already begin to explain the results obtained previously for Kraton 101 and 102. In shifting a single viscoelastic function, as is the case with the transient experiments, one would not necessarily see any significant lack of superposition as was evidenced by Fig. 16 for $D'(\omega)$ of Shell 16/78/16. The change in compliance due to the changing interlayer (with temperature) would therefore produce the relatively large shifts that have been interpreted as the glassy shift of polystyrene (22, 35). This also explains the very low temperatures at which this

behavior has been observed to be significant in the transient experiments as the time dependence of the interlayer was seen to be of the order of 10°C/decade in the case of the Shell 16/78/16 material. Thus, the interlayer effect observed here at 50°C would be expected to appear 30 to 40°C lower in a transient experiment where the times are generally about four decades longer (the value of 10°C/decade would tend to lower values as longer times are considered).

A very well defined maximum associated with the polybutadiene glass transition appears in the loss compliance of the block copolymers considered here ($10^{-2.83}$ bars^{-1} in simple compression for Shell 16/78/16 and Kraton 102 at -68.0°C and -51.5°C respectively and $10^{-3.32}$ bars^{-1} in simple shear at -71°C for NBS 10/30/10), and one is tempted to compare this maximum with the concentration of effective chains which can be calculated according to various theories. Although the equilibrium compliance, J_e, is more directly related to this, the use of the equilibrium compliance is prohibited because it is modified to an unknown extent by the filler, the polystyrene domains. It is also very difficult to establish J_e with the continued relaxation taking place in the plateau region. The maximum in the loss compliance can be related to the equilibrium compliance by various theories (cf. Ferry, reference 28, for a discussion of these) with values for J''_{max}/J_e ranging from 0.29 to 0.42. Kraus et al. (26) have shown that the loss modulus, G''_{max}, is insensitive to the presence of a filler. Unfortunately this fact precludes the use of J''_{max} for these calculations since it is related to both $G'(\omega)$, which depends strongly on

filler content, and $G''(\omega)$, which has increasing dependence as one moves away from the peak. Plugging the above maxima into the theoretically derived relationships results in abnormally high values for the density of effective strands (one obtains values of $4 \cdot 10^{-3}$ g moles/cc and higher). Although G''_{max} can be determined ($10^{3.70}$ bars in compression at -78.1°C for Shell 16/78/16, $10^{3.62}$ bars in compression at -79.4°C for Kraton 102, and $10^{2.20}$ bars in shear at -80.9°C for NBS 10/30/10), network theory is not adequate at present to relate this value to the equilibrium modulus in order to characterize the matrix network.

IV. APPARATUS

The dynamic moduli of the various samples studied were determined on a rheometer built and donated to this laboratory by Melabs, Inc. The operation of this rehometer is illustrated in Fig. 30.

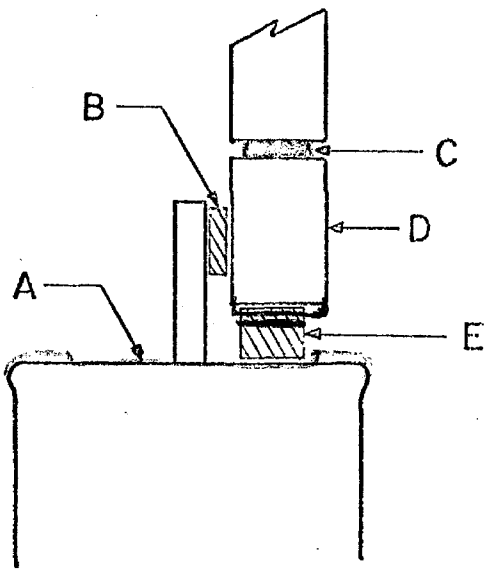

Fig. 30. Diagram Illustrating Compressive Mode in the Modified Melabs Apparatus. A: Driver; B: Specimen in Shear; C: Force Transducer; D: Force Monitor Plate; E: Specimen in Uniaxial Compression.

A sinusoidal displacement is applied to a specimen by a stack of piezoelectric disks driven by a function generator. The disks are contained in a stainless steel housing -- the housing acting as a linear retaining spring. The force generated is transmitted to a force monitor plate on the other side of the sample and converted with an extremely small displacement into an electrical charge. The amplitude ratio between the input voltage and the output charge is

measured, and the phase angle is determined using the differential Lissajous method of Tschoegl and Smith (47) -- a reprint of which is included in Appendix C.

The design is on the model of the Miles displacement driven shear generator (30). Several modifications had to be made to the apparatus and an extensive calibration scheme was developed in order to make the precision adequate for this investigation. The fully developed apparatus is capable of measuring the dynamic modulus of polymeric materials in shear or uniaxial compression over a temperature range of from -90° to 100°C and over a frequency range from 0.01 to 1000 Hz, although practical considerations has limited its use to frequencies above 0.1 Hz. Driver displacements have been estimated to be between 1000 and 5000 Å and the displacement of the force transducer is estimated to be less than 10 Å. Specimen elastances ranging from approximately 3×10^4 to 1.4×10^6 N/m can be measured and the phase difference between the drive and force signals can be determined to about 0.5 degrees of angle. Some description of the apparatus and ancillary equipment and details of the calibration, etc. are given in the Operation Manual, pertinent portions of which are included in Appendix B.

The apparatus was originally sold by Melabs as a shear rheometer capable of measurements from 60 to 1000 Hz. Since it was anticipated that a large frequency span would be necessary for block copolymers, a charge amplifier was added to the force measurement circuit so that low frequencies could be examined without significant charge drainage from the piezoelectric transducer. This proved very

fruitful allowing measurements, if one had the patience, as low as 0.01 Hz. Because of the high input impedence of the charge amplifier, however, pyroelectric effects became very significant, necessitating a complete redesigning of the temperature control scheme. Also shorting of the piezoelectric transducers became necessary during temperature changes to prohibit residual charges from building up which required long times to drain off.

Early in the evaluation of the rheometer, an inertial coupling between the driver and the force transducers was discovered. Resonances appearing at many frequencies between 100 and 1000 Hz prohibited an accurate determination of this coupling. By fastening a massive copper cylinder to the base, increasing the overall mass of the apparatus from about two kilograms to about ten kilograms, the inertial effect and the resonances were greatly reduced so that the coupling could be broken into a purely inertial term 180° out of phase with the driver, a frictional term 90° out of phase, and a single resonance occurring generally between 200 and 300 Hz. The inertial problem arises because the force transducer with the monitor plate acts as a very sensitive accelerometer detecting the small reaction of the rheometer base to the movements of the driver. This inertial contribution is seen alone by exciting the driver stack and monitoring the force transducer with no sample in between. Experience has indicated that this inertial coupling is not changed by the presence of a sample. Above the resonance the purely inertial portion is proportional to the square of the frequency with a finite intercept when extrapolated to zero Hz, and it becomes negligibly small below

the resonance. The frequency at which the resonance appears changes slightly with different monitor plates (apparently due to slight differences in the masses of different plates). The frictional portion is proportional to the frequency with a zero intercept and the resonance is superimposed on it.

One other serious problem is inherent in the Melabs shear rheometer design -- the extreme fragility of the force transducer. Clamping a sample in shear puts a torque on the force transducer which often breaks the piezoelectric transducer. This problem is compounded by the fact that the operator may not realize that the transducer is cracked and will continue taking erroneous data. This problem was overcome by straining the specimen in simple compression. Although the apparatus was not originally designed to do this and the range of specimen shape factor is subsequently very limited, the sensitivity range of the apparatus has allowed the present investigation to be made. In addition, one can put more trust in the calibration since that is also carried out in uniaxial compression (48).

With these changes the apparatus becomes a useful research tool for measuring the dynamic compliance of polymer samples. Calibration consists primarily of determining the constant relating of the force transducer charge/driver voltage ratio to the elastance of a specimen. This is done by testing three stainless steel calibration rings for which the elastance has been determined. The three values are averaged by plotting the amplitude ratios against the elastances on logarithmic graph paper and drawing a line of unit

slope through them. A detailed calibration goes much further, however, because this amplitude ratio is somewhat dependent on frequency and temperature. Also the phase angle depends on frequency and the measuring electronics. Of course, the inertial correction also has to be included. These calibrations and their application are detailed in Appendix B.

What knowledge has been gained from the evaluation of the Melabs Rheometer for this research is being applied to the construction of a new apparatus in this laboratory. This apparatus is being designed solely for uniaxial compression experiments, and improvements in design should improve the inertial and temperature characteristics, allow measurement of the clamped specimen's deformation, and admit a wide range of specimen shape factors. Also being considered is a capacitance displacement device (49) to permit direct measurement of the driver displacement.

Further evaluation of the now modified Melabs Rheometer was made by measuring the dynamic mechanical properties of Galcit I, which is highly cross-linked polyurethane rubber. Galcit I was developed as a laboratory standard at the California Institute of Technology and considerable characterization has been reported previously (50-54). This rubber is synthesized by reacting equal volumes of "prepolymer" (Thiokol's Solithane 113), with a "curing agent" (castor oil). Castor oil is the glyceryl ester of ricinoleic acid and is a triol. Solithane 113 is simply castor oil capped with tolylene diisocyanate. The glass transition temperature is about

-18°C. More extensive descriptions of Galcit I can be found in references 51 and 53. Other dynamic experiments on this material were made in shear on a Ferry-Fitzgerald apparatus, described elsewhere (55), simultaneous to this evaluation. The master curve dynamic compliance as determined with the Fitzgerald Apparatus is shown in Fig. 31 referred to 0°C. Two sets of twin specimens used for this were 0.95 cm and 2.54 cm diameter disks 0.254 cm thick. The data were actually referred to 31°C and this master curve was then shifted to 0°C using a WLF equation fit to the shift data. The shift factors are shown as open squares in Fig. 34.

Galcit I was examined on the Melabs Rheometer both in shear and in uniaxial compression. Shear data were obtained on a specimen with dimensions 0.89 x 0.49 x 0.11 cm thick and compression data were obtained on a specimen 0.30 x 0.52 x 0.48 cm long. Both samples were rinsed with methanol to remove any surface contamination and dried for at least 20 hours in vacuum. The assembled master curves of the dynamic compliance are shown in Figs. 32 and 33 for shear and simple compression, respectively. In both cases, superposition was excellent, and a frequency range of about 8 logarithmic decades was easily covered in this way. The shift factors are shown by open (shear) and full (compression) circles in Fig. 34. The shift factors at the two lowest temperatures were obtained in earlier measurements not shown in Fig. 32. The shift data represented by the open circles were fitted to a WLF-equation of the form

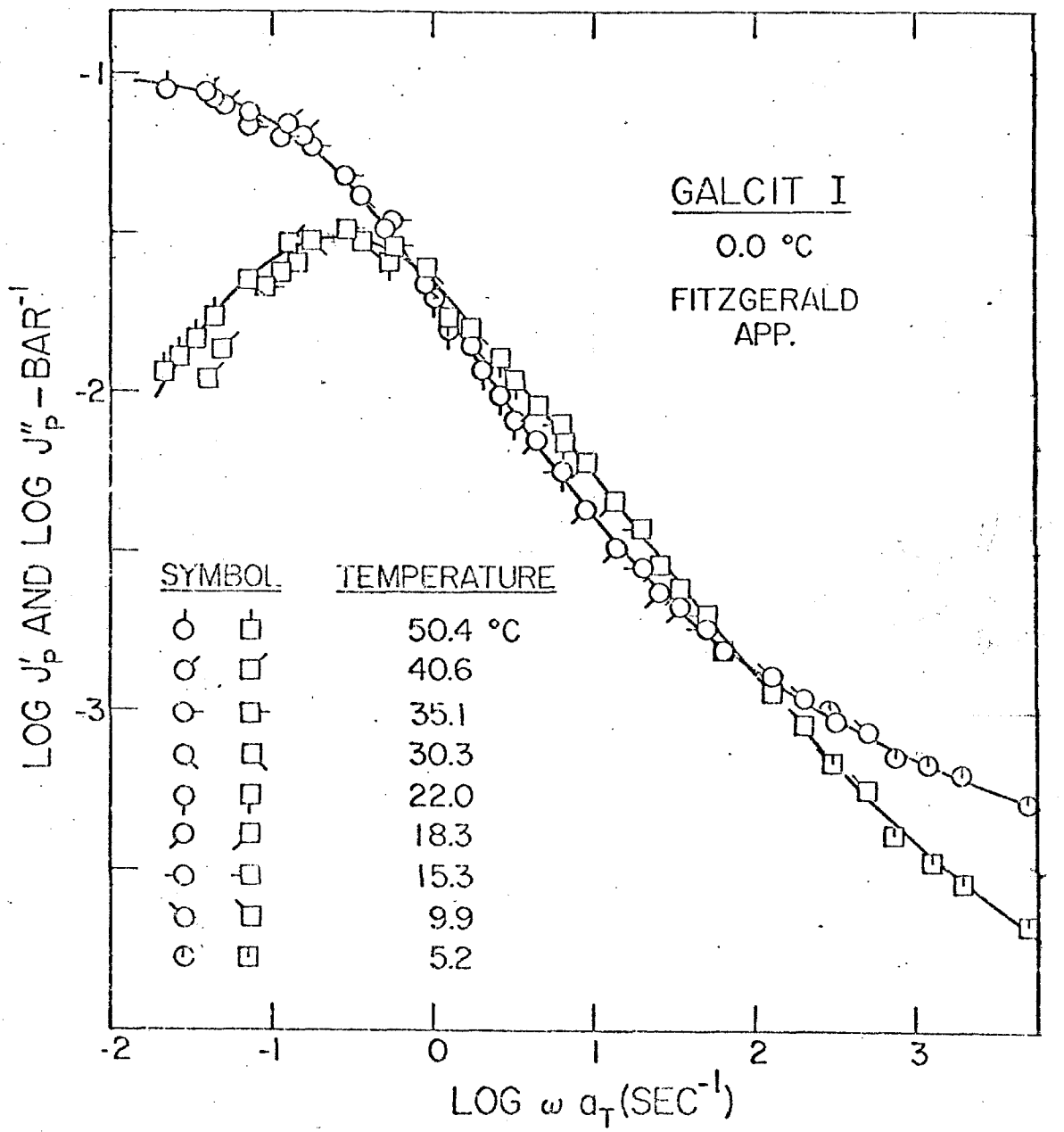

Figure 31. Master Curves of Log $J_p'(\omega)$ and Log $J_p''(\omega)$ vs. Log ωa_T Obtained in the Ferry-Fitzgerald Apparatus on Galcit I. Reference Temperature: 0°C.

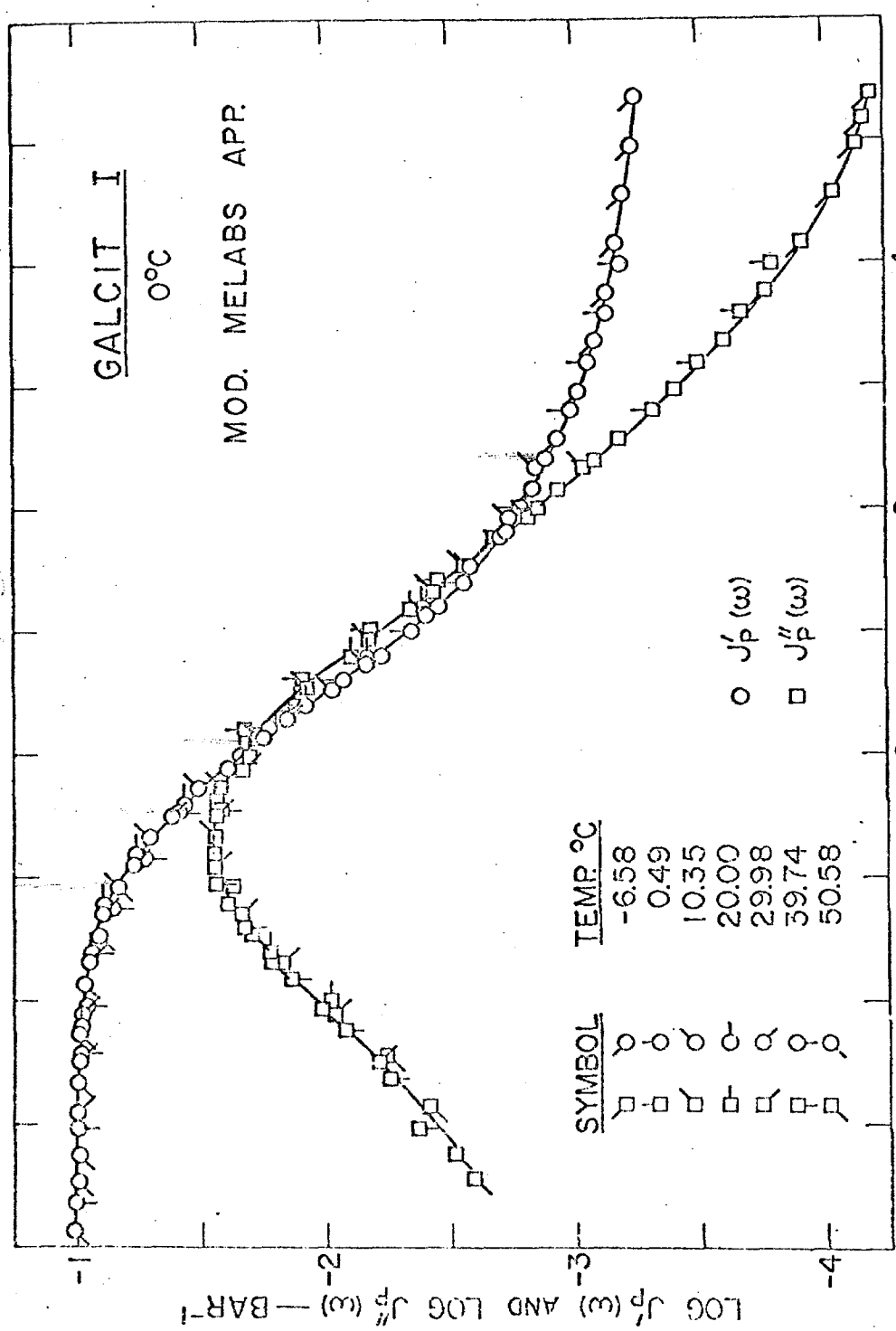

Figure 32. Master Curves of Log $J'_p(\omega)$ and Log $J''_p(\omega)$ vs. Log ωa_T Obtained in Shear in the Modified Melabs Apparatus on Galcit I. Reference Temperature: 0°C.

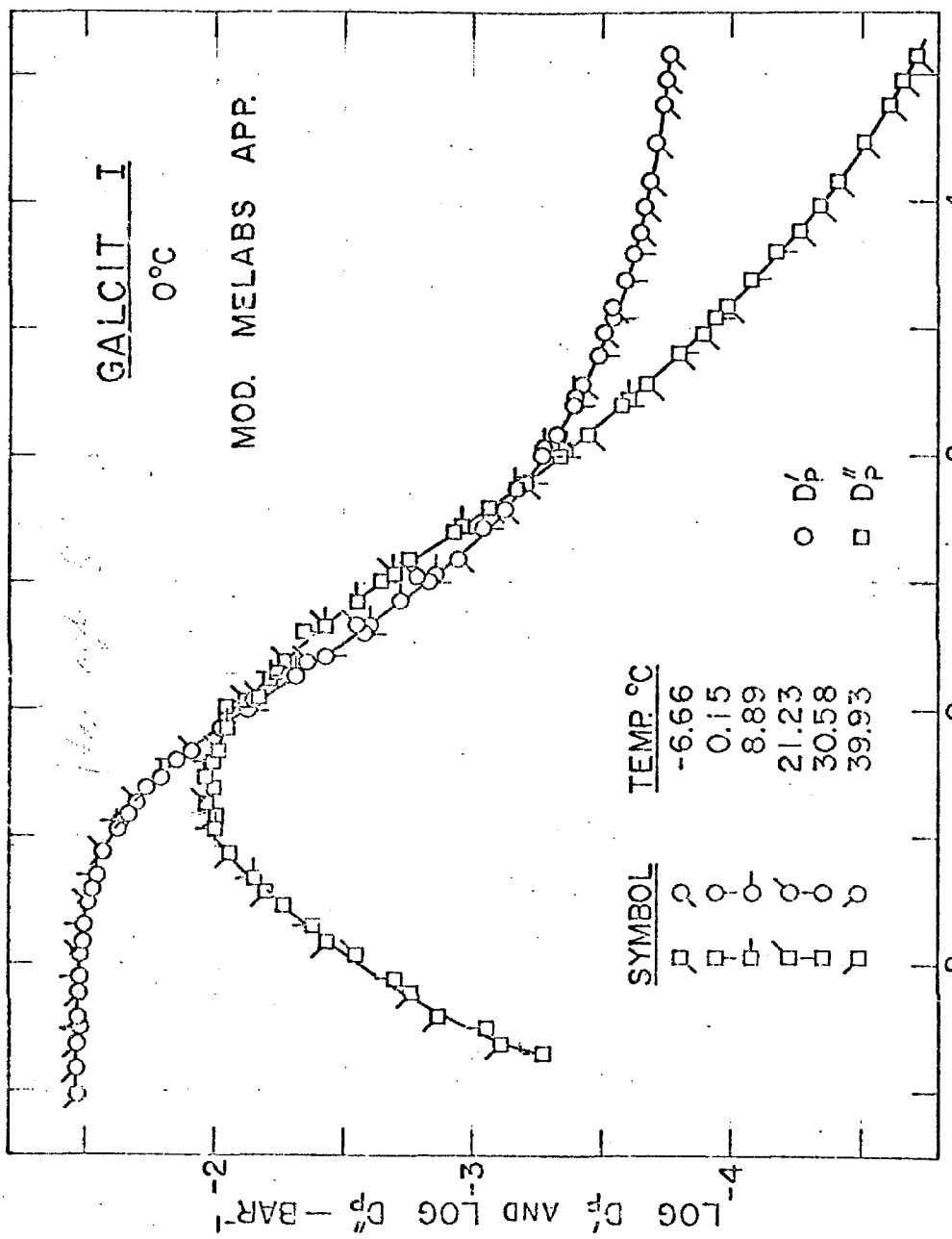

Figure 33. Master Curves of Log $D'_p(\omega)$ and Log $D''_p(\omega)$ vs. Log ωa_T Obtained in Simple Compression on Galcit I. Reference Temperature: 0 °C.

$$\log a_T = \frac{-9.84\ (T - 273.2)}{52.3 + (T - 273.2)} \qquad (21)$$

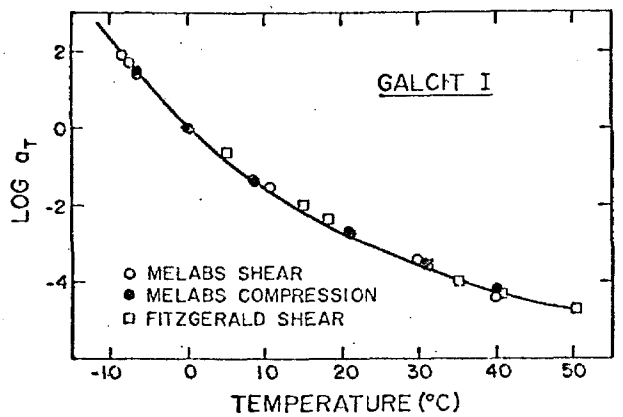

Fig. 34. Shift Factors, Log a_T, for Galcit I.

This is shown as the solid line in Fig. 34.

The data obtained in compression and shear show almost perfect superposition if the factor of 3 (0.48 log units) between the shear and uniaxial compliances is taken into account. The only discrepancy appears in the low frequency data (rubbery region) of $J_p''(\omega)$ and $D_p''(\omega)$ below the maximum. The measurement of very small phase angles in this region is difficult because they must be done at the highest sensitivity of the apparatus. A different force transducer was used in the two sets of experiments and hence different calibration factors were involved. The determination of $D''(\omega)$ was more recent and utilized somewhat more refined calibration corrections. Hence, the values for $D_p''(\omega)$ are felt to be more reliable.

One major difficulty was encountered in the Melabs experiments which threatened the extension of the use of the apparatus to examining block copolymers. Data taken at different

temperatures were slightly shifted vertically from one another. For the Galcit I experiments, this was more than compensated for by the large frequency range of the apparatus and an accurate vertical shift could be determined to achieve good superposition. Indeed, without any vertical shift other than the standard $\rho T/\rho_o T_o$ (28) (which is modified anyway in the transition to a glass) superposition could not be achieved and the data themselves were unreasonable. To examine block copolymers, where the mechanical properties change very little over large changes in time and temperature, this would be ambiguous. The effect is most pronounced in shear, and, fortunately, almost disappears in the compression experiments. Very likely, this effect is due to the torque placed on the force monitor plate as discussed previously. The effect appears to vary in a regular manner, though not reproducibly, with the changing stiffness or dimensions of the specimen with temperature. With special precautions, data were obtained on the block copolymers in compression which required no vertical shifting other than the temperature-density reduction factor. Occasionally a small shift would occur at some temperature which would produce a very obvious anomaly in the log a_T-temperature curve. This subject is discussed further in the experimental section for block copolymers (Part III).

Discussion of the Mechanical Properties of Galcit I

Comparison of the data obtained in the Ferry-Fitzgerald apparatus and in the modified Melabs instrument show very satisfactory agreement. The rubbery plateaus of the shear compliances determined in both apparatus agree very well. They also agree with the data of Knauss and Mueller (51) obtained in stress relaxation measurements. The only area of disagreement lies in the glassy region. The glassy compliance in shear, J_g, derived from the measurements in the modified Melabs instrument is higher than that from measurements in the Ferry-Fitzgerald apparatus. A check of the original measurements revealed that the elastances encountered in the Melabs instrument exceeded the calibration range. It is possible, therefore, that the higher compliances arise from the contribution of an added apparatus compliance in the modified Melabs shear rheometer. This would contribute negligibly to the loss compliance and would become noticeable only in the glassy region of the storage compliance. Time-temperature superposition would not be affected because a contribution of the apparatus to the compliance would be solely a function of the hardness of the specimen and not directly a function of temperature or frequency.

For the compliances in simple compression, $D'(\omega)$ and $D''(\omega)$, all measurements were within the calibration range. $3D''(\omega)$ agrees rather well with the $J''(\omega)$ values obtained in the Fitzgerald apparatus. $3D'(\omega)$, however, was slightly higher than $J'(\omega)$ as one would expect for a Poisson's ratio less than 0.5 in the glassy state.

For a viscoelastic material Poisson's ratio in dynamic measurements is a function of frequency. $D'(\omega)$ and $D''(\omega)$ are therefore related to $J'(\omega)$ and $J''(\omega)$ by

$$J'(\omega) = 2\,[1 + \nu'(\omega)]\,D'(\omega) - 2\,\nu''(\omega)\,D''(\omega) \tag{22}$$

and

$$J''(\omega) = 2\,[1 + \nu'(\omega)]\,D''(\omega) + 2\,\nu''(\omega)\,D'(\omega) \tag{23}$$

Since $D''(\omega)$ is necessarily small in the glassy region, the second term on the right of Eq. (22) is negligible in this region. Hence one may write

$$J'(\omega) \simeq 2\,[1 + \nu'(\omega)]\,D'(\omega) \qquad \text{(glassy region)} \tag{24}$$

The second term in Eq. (23) cannot be neglected. However, as $\nu'(\omega)\,D''(\omega)$ decreases, $\nu''(\omega)\,D'(\omega)$ tends to increase and thus the two terms may compensate each other sufficiently so that the overall shift between log $D''(\omega)$ and log $J''(\omega)$ remains constant at approximately 0.48. On these assumptions we can calculate both $\nu'(\omega)$ and $\nu''(\omega)$ from the four master curves for $D'(\omega)$, $D''(\omega)$, $J'(\omega)$ and $J''(\omega)$ using Eqs. (23) and (24). The result is shown in Fig. 35. It should be emphasized that this is a very indirect and inaccurate way of calculating Poisson's ratio, and quantitatively Fig. (35) is certainly not very accurate. Unfortunately very little is known of the dynamic Poisson's ratio, $\nu^*(\omega)$ (56), so Fig. 35 certainly does not appear to be unreasonable in light of present knowledge.

The time-temperature superposition shift factors

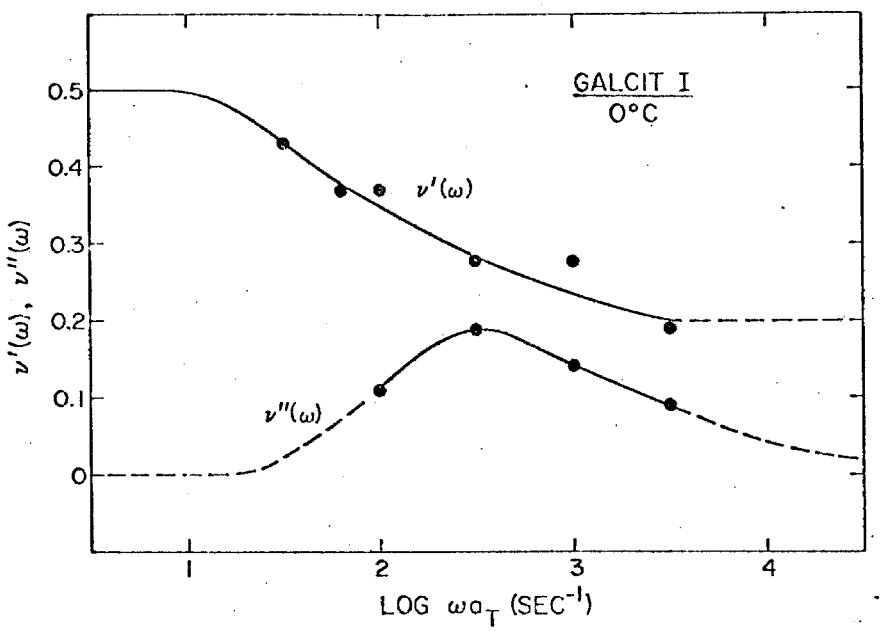

Fig. 35. Real and Imaginary Parts of Poisson's Ratio $\nu'(\omega)$, $\nu''(\omega)$ for Galcit I.

determined from the data obtained in the modified Melabs apparatus are extremely consistent and reproducible. Here, shifting is aided by the wide frequency range covered at a single temperature. The agreement with the shift factors determined from the data obtained in the Ferry-Fitzgerald apparatus is excellent as shown in Fig. 34. The shift factors obtained by Knauss and Mueller (51) from experiments on crack propagation, failure, and stress relaxation fall on the same curve (not shown). Knauss and Mueller expressed the temperature dependence by the "Universal" form of the WLF equation with a characteristic temperature, T_s, of 32°C(T_g = - 18°C). Equation (21) however, fits their shift factors better.

It is interesting to compare the ratio of the maximum in

$J_p''(\omega)$ to J_e, the equilibrium compliance, with theoretical predictions. From the data taken in the modified Melabs apparatus, $J''_{max}/J_e = 0.28$, $D''/D_e = 0.32$; and from the Fitzgerald data, $J''_{max}/J_e = 0.30$. This is considerably higher than the ratio of 0.21 determined for a lightly crosslinked Hevea rubber (28). The molecular weight between crosslinks for Galcit I would be expected to be more uniform. The calculated ratios thus support the contention that a distribution of the molecular weight between crosslinks, M_c, lowers the peak in $J_p''(\omega)$. Our values are still less than the value of about 0.4 predicted by the theory of Bueche (28). However, they are in substantial agreement with each other even though the samples used in the different sets of experiments were prepared at different times.

The equilibrium shear compliance for Galcit I is 0.10 bar^{-1} (cf. Figs. 31, 32 and 33). This may be used to calculate the number of moles of effective network chains per unit volume, ν_e, on the basis of the statistical theory of rubber elasticity. We have

$$\nu_e = \frac{1}{RTJ_e} \tag{25}$$

where T is the absolute temperature and R is the gas constant. Eq. (25) yields $\nu_e = 4.4 \times 10^{-4}$ g mole/cm^3, in excellent agreement with the average value of 4.4×10^{-4} g mole/cm^3 obtained by Landel (53) from compression tests on swollen specimens and the failure envelope for unswollen specimens. From the equilibrium stress relaxation modulus of Knauss and Mueller (51) one obtains

$\nu_e = 4.1 \times 10^{-4}$ g mole/cm^3. Their value of 5.8×10^{-4} g mole/cm^3 determined from stress-strain measurements on swollen Galcit I appears to be somewhat high.

REFERENCES

1. M. Szwarc, M. Levy, and R. Milkovich, J. Am. Chem. Soc., 78:2656 (1956).

2. L. J. Fetters, J. Poly. Sci., 26C:1(1967).

3. L. Fetters, J. Research NBS, 70A:5(1966).

4. M. Morton, R. Milkovich, D. McIntyre, L. Bradley, J. Poly. Sci., 1A:443 (1963).

5. D. J. Meier, J. Poly. Sci., 26A:81(1967).

6. T. Inoue, T. Soen, T. Hashimoto, H. Kawai, J. Poly. Sci., 7A2: 1283(1969).

7. T. Inoue, T. Soen, T. Hashimoto, H. Kawai, Macromolecules, 3:87 (1970).

8. S. Krause, J. Poly. Sci., 7A2:249 (1969).

9. O. Bianchi, Polymer Letters, 7:785(1969).

10. D. F. Leary, M. C. Williams, Polymer Letters, 8:335(1970).

11. S. Krause, Macromolecules, 3:84(1970).

12. D. J. Meier, private communication.

13. R. J. Ceresa, "Block and Graft Copolymers," (Washington: Butterworth, 1962).

14. H. A. J. Battaerd, G. W. Tregear, "Graft Copolymers," (New York: Interscience, 1967).

15. C. H. Basdekis, "ABS Plastics," (New York: Reinhold, 1964).

16. R. Ceresa, J. Poly. Sci., 53:9(1961).

17. V. Immergut, H. Mark, Makro. Chem., 18/19:322(1956).

18. J. Moacanin, G. Holden, N. W. Tschoegl (ed.), "Block Copolymers," J. Poly. Sci., Part C, 26(1969).

19. N. H. Canter, J. Poly. Sci.,6:155(1968).

20. M. Shen, E. H. Cirlin, D. H. Kaelble. To be published in "Colloidal and Morphological Behavior of Block and Graft Copolymers," G. E. Molau (ed.) (New York: Plenum Press).

21. M. Shen, D. H. Kaelble, Polymer Letters, 8:149(1970).

22. C. K. Lim, R. E. Cohen, N. W. Tschoegl, Adv. in Chem. Series (in press).

23. R. J. Angelo, R. M. Ikeda, M. L. Wallach, Polymer, 6:141(1965).

24. S. Miyata, T. Hata, private communication.

25. K. R. Arnold, D. J. Meier, J. Appl. Poly. Sci., 14:427 (1970).

26. G. Kraus, K. W. Rollmann, J. T. Gruver, Macromolecules, 3:87 (1970).

27. A. J. Staverman, F. Schwarzl. "Linear Deformation Behavior," in H. A. Stuart, Die Physik der Hochpolymeren, Vol. 4 (Berlin: Springer-Verlag, 1956).

28. J. D. Ferry. "Viscoelastic Properties of Polymers," 1st and 2nd ed. (New York: John Wiley and Sons, 1961, 1970).

29. D. J. Plazek, V. M. O'Rourke, J. Poly. Sci., 9A2:209 (1971).

30. D. O. Miles, J. Appl. Phys., 33:1422(1962).

31. G. Kraus, private communication.

32. N. W. Tschoegl, in: N. W. Tschoegl, et al., "A Research Program on Solid Propellant Physical Behavior," CHECIT PL 68-1, California Institute of Technology, AFRPL-TR-68-106,1968, pp. VI 1,30.

33. R. G. Mancke, private communication.

34. N. W. Tschoegl, D. Froelich, in: M. Morton, N. W. Tschoegl, D. Froelich, Air Force Materials Laboratory Technical Report, AFML-TR-408, Wright-Patterson Air Force Base, Ohio, 1969.

35. T. L. Smith, R. A. Dickie, J. Poly. Sci., 26C:163(1969).

36. K. Yagii, E. Maekawa, Nippon Gomukyokaishi, 40:46(1967).

37. K. C. Rusch, J. Macromol. Sci.-Phys., B2(2):179(1968).

38. J. J. Lohr, Trans. Soc. Rheology, 9:65(1965).

39. T. Hideshima, in: "Solid State Physics," 14 (New York: Academic Press, 1963), pp. 448,495-6.

40. N. R. Langley, J. D. Ferry, Macromolecules, 1:353(1968).

41. D. H. Kaelble, private communication.

42. J. F. Beecher, L. Marker, R. D. Bradford, S. L. Aggarwal, J. Poly. Sci.,26C:117(1969).

43. E. Fischer, J. F. Henderson, J. Poly. Sci., 30C:459(1970).

44. G. Kraus, F. E. Naylor, and K. W. Rollmann, Polymer Preprints, 12:362(1971).

45. E. Maekawa, R. G. Mancke, J. D. Ferry, J. Phys. Chem.,69:2811 (1965).

46. L. R. G. Treloar, in H. A. Stuart, Die Physik der Hochpolymeren, Vol. IV, Chapter V (Berlin: Springer-Verlag, 1956).

47. N. W. Tschoegl and J. R. Smith, in: "Viscoelastic Properties of Propellants and Propellant Binders," Final Report on SRI Projects PRM-3939,4660,5174, Stanford Research Institute, Menlo Park, California, 1966. Department of the Navy, Bureau of Naval Weapons Contract Nos. NOW 61-1057-d, NOW 64-0073-d, NOW 65-0061-d.

48. D. O. Miles, G. C. Knollman, A. S. Hamamoto, Rev. Sci. Instr., 36:158(1965).

49. D. Massa, Ph.D. Thesis, University of Wisconsin, Madison, Wisconsin(1971).

50. W. G. Knauss, J. F. Clauser, R. F. Landel, "Second Report on the Selection of a Crosslinked Polymer Standard," MATSCIT PS 66-1, California Institute of Technology, AFRPL-TR-66-21, Edwards, California, January, 1966.

51. W. G. Knauss, H. K. Mueller, "The Mechanical Characterization of Solithane 113 in the swollen and Unswollen State," AFRPL-TR-68-125, California Institute of Technology, Pasadena, California, December, 1967.

52. R. F. Landel, in: R. F. Landel, N. W. Tschoegl, "A Research Program on Solid Propellant Physical Behavior," MATSCIT PS 67-1, California Institute of Technology, AFRPL-TR-67-193, Edwards, California, June, 1967.

53. R. F. Landel, Part V in: N. W. Tschoegl, R. F. Landel, et al., "A Research Program on Solid Propellant Physical Behavior," CHECIT PL-68-1, California Institute of Technology, AFRPL-TR-68-106, Edwards, California, June 1968.

54. R. G. Mancke, R. F. Landel, in: N. W. Tschoegl, W. G. Knauss, R. F. Landel, et al., "A Research Program on Solid Propellant Physical Behavior," CHECIT PL-69-1, California Institute of Technology, AFRPL-TR-69-180, Edwards, California, August, 1969.

55. E. R. Fitzgerald, J. D. Ferry, J. Colloid Sci., 8:1(1953).

56. H. A. Waterman, Kolloid-Z., 192:1(1963).

Appendix A

A Derivation of a General Expression for

the Temperature Variation of Log a_T.

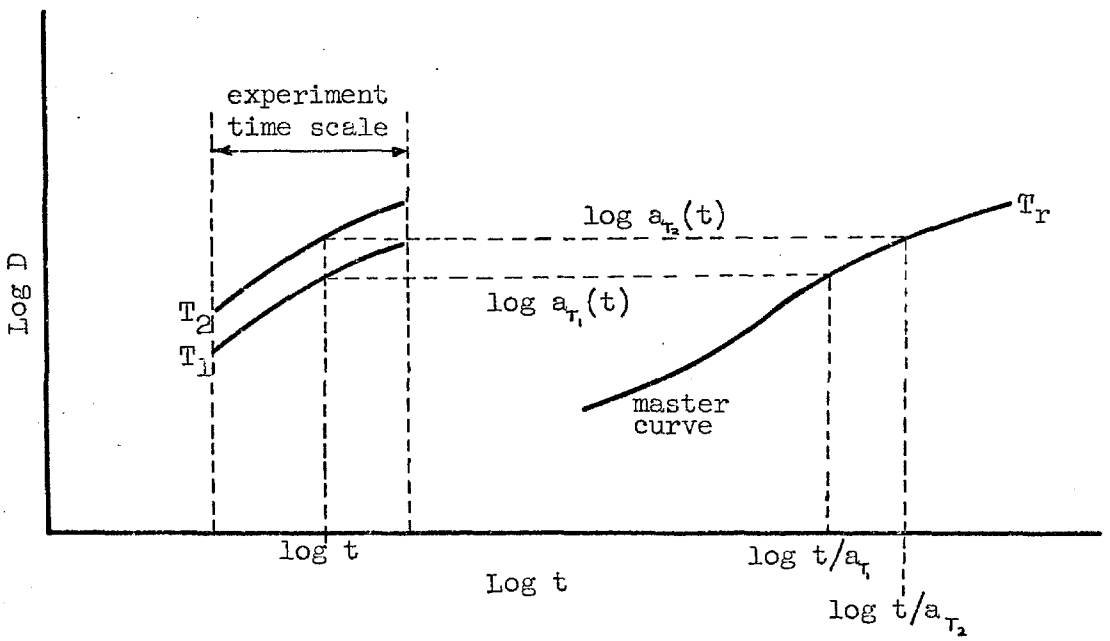

$\Delta T = T_2 - T_1$

$$\Delta_T \log D = \log D(t,T_2) - \log D(t,T_1) = \left(\frac{\partial \log D(t,T)}{\partial T}\right)_t\Big|_{T_1} (\Delta T) + \left(\frac{\partial^2 \log D(t,T)}{\partial T^2}\right)_t\Big|_{T_1} (\Delta T)^2 + \ldots \quad (1)$$

$$\Delta_T \log t/a_T = \log t/a_{T_2} - \log t/a_{T_1} = \left(\frac{\partial \log t/a_T}{\partial T}\right)_t\Big|_{T_1} (\Delta T) + \left(\frac{\partial^2 \log t/a_T}{\partial T^2}\right)_t\Big|_{T_1} (\Delta T)^2 + \ldots$$

or, since t is held constant,

$$\Delta_T \log t/a_T = -\left[\left(\frac{\partial \log a_T(t)}{\partial T}\right)_t\Big|_{T_1} (\Delta T) + \left(\frac{\partial^2 \log a_T(t)}{\partial T^2}\right)_t\Big|_{T_1} (\Delta T)^2 + \ldots\right] \quad (2)$$

$$\Delta_{t/a_T} \log D = \log D(t/a_{T_2},T_r) - \log D(t/a_{T_1},T_r) = \left(\frac{\partial \log D(t/a_T,T_r)}{\partial \log t/a_T}\right)_{T_r}\Big|_{t/a_{T_1}} (\Delta \log t/a_T) + \ldots \quad (3)$$

$$\Delta_{t/a_T} \log D = \Delta_T \log D \tag{4}$$

Substituting Eqs. (1) and (3) into Eq. (4), substituting Eq. (2), and dividing by ΔT, one obtains

$$\left(\frac{\partial \log D(t,T)}{\partial T}\right)\Big|_{t}\Big|_{T_1} + O(\Delta T) = -\left(\frac{\partial \log D(t/a_T, T_r)}{\partial \log t/a_T}\right)\Big|_{T_r}\Big|_{t/a_{T_1}} \cdot \left(\frac{\partial \log a_T(t)}{\partial T}\right)\Big|_{t}\Big|_{T_1} + O(\Delta T) \tag{5}$$

Taking the limit of Eq. (5) as $\Delta T \to 0$ yields

$$\left(\frac{\partial \log D(t,T)}{\partial T}\right)_t = -\left(\frac{\partial \log D(t/a_T(t), T_r)}{\partial \log t/a_T(t)}\right)_{T_r} \cdot \left(\frac{\partial \log a_T(t)}{\partial T}\right)$$

Appendix B

Part of the Operation Manual for the Modified Melabs Dynamic Rheometer with

I. Description of the Rheometer

II. Ancillary Equipment

III. Temperature Control

IV. Calibration Procedure

I. Description of the Rheometer

The Melabs Dynamic Rheometer utilizes a piezoelectrically driven displacement generator to strain a specimen in shear or uni-axial compression and a piezoelectric transducer to monitor the force. The arrangement is shown in Fig. 1.

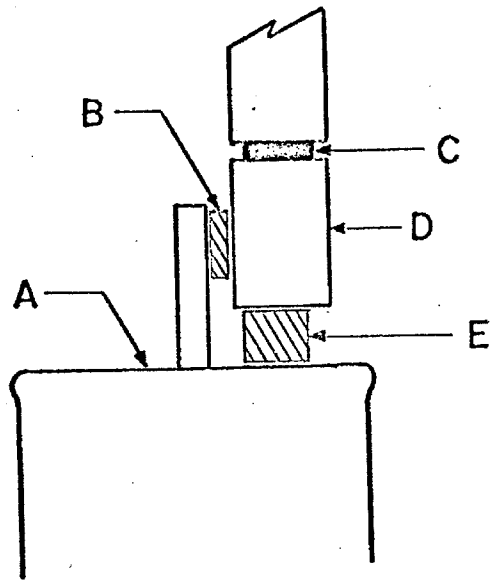

Figure 1. Diagram Illustrating the Operation of the Modified Melabs Apparatus. A: Driver; B: Specimen in Shear; C: Force Transducer; D: Force Monitor Plate; E: Specimen in Uni-axial Compression.

The original apparatus, a dynamic shear rheometer, was devised by D. O. Miles and described by him in reprints (1,2) included in the Appendix. Much of the description given here of the modified apparatus used in this laboratory also appears in annual reports to the Air Force. (3,4,5)

The displacement drive, the force monitor, and the supporting yoke together with the inertial block they rest on weigh about 5 kg. The generated displacement is estimated to be of the order of 3000 Å resulting in a strain less than 0.01%. The displacement of the force monitor is estimated to be less than one hundredth that of the driver. The driver excitation voltage and the force transducer charge are very nearly proportional to the driver displacement and the resultant force respectively. Their amplitude ratio and phase angle difference then allow calculation of the modulus of the material tested after taking into account the shape factor of the specimen. Calibration of the amplitude ratio of the voltage to charge for the actual ratio of the displacement to force is made by testing stainless steel rings of known elastance and zero phase angle.

The rheometer is encased in an environmental control chamber. Ancillary equipment is needed to excite the driver, measure and control the temperature, measure the force transducer charge, and compare the input and output signals. A block diagram of the equipment is shown in Fig. 2 and the arrangement of the apparatus is shown in Fig. 3.

II. Ancillary Equipment

The sinusoidal driving signal is provided by a Hewlett Packard 203A Function Generator. Since it generates only a 30 V peak-to-peak sine wave, a Zeltex 140B Transistorized Power Amplifier is used to boost the signal to a 200 V peak-to-peak amplitude, although

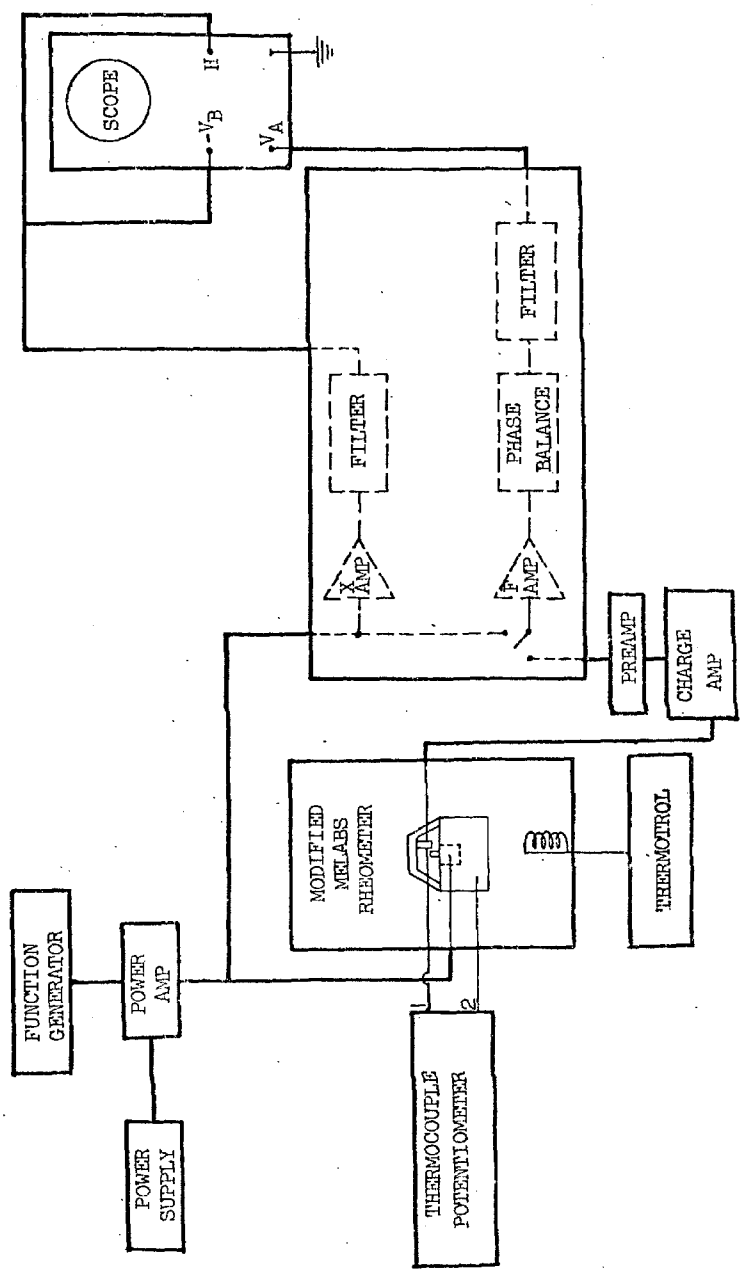

Figure 2. Block Diagram of the Modified Melabs Rheometer and Ancillary Equipment.

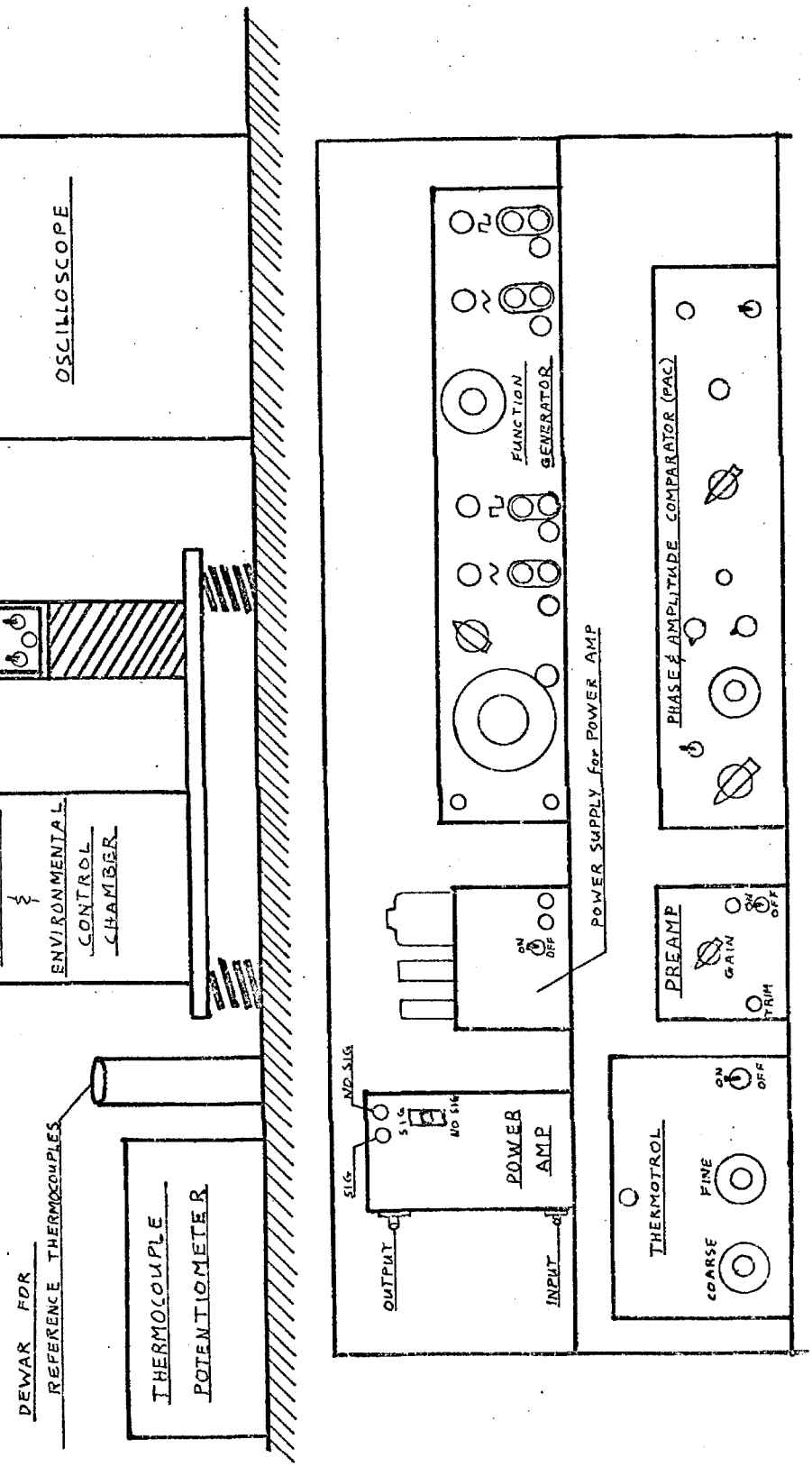

Figure 3. Modified Melabs Rheometer and Ancillary Equipment.

this voltage is usually kept below 50 V peak-to-peak. The output of the amplifier is limited to 20 milliamperes, and, because of the capacitive load placed on it by the piezoelectric driver, the signal is somewhat attenuated at frequencies above 200 Hz. However, this does not affect the performance of the apparatus.

The output signal generated by the piezoelectric force transducer is detected by a Kistler Model 566 Multi-range Electrostatic Charge Amplifier which converts the charge signal to a voltage signal. This amplifier is used at gains of 1 mV/pC or less, although it may be used cautiously at 2 mV/pC. Higher amplifications create large phase angles that are difficult to calibrate. The output of the charge amplifier is then amplified in seven steps up to 100 times by the Preamplifier (Preamp) which consists of two Zeltex Zel-1 operational amplifiers in series, both of which can be regarded as single pole amplifiers when calibrating them. A simplified schematic of this device together with the Phase and Amplitude Comparator discussed next is shown in Fig. 4. The signal from the Preamp is then amplified another 10 times and compared to the drive signal which is attenuated 20 times in the Phase and Amplitude Comparator (PAC). This device is used with the oscilloscope to measure the amplitude ratio of the two signals and their phase difference by the differential Lissajous method described by Tschoegl and Smith (6) which is included in the Appendix. The key components are two Zeltex Zel 1 operational amplifiers powered by a Solatron power supply which amplify the force signal and attenuate the drive signal. Switch S1, in the schematic allows angle calibration of the circuit and phase angle measurement in

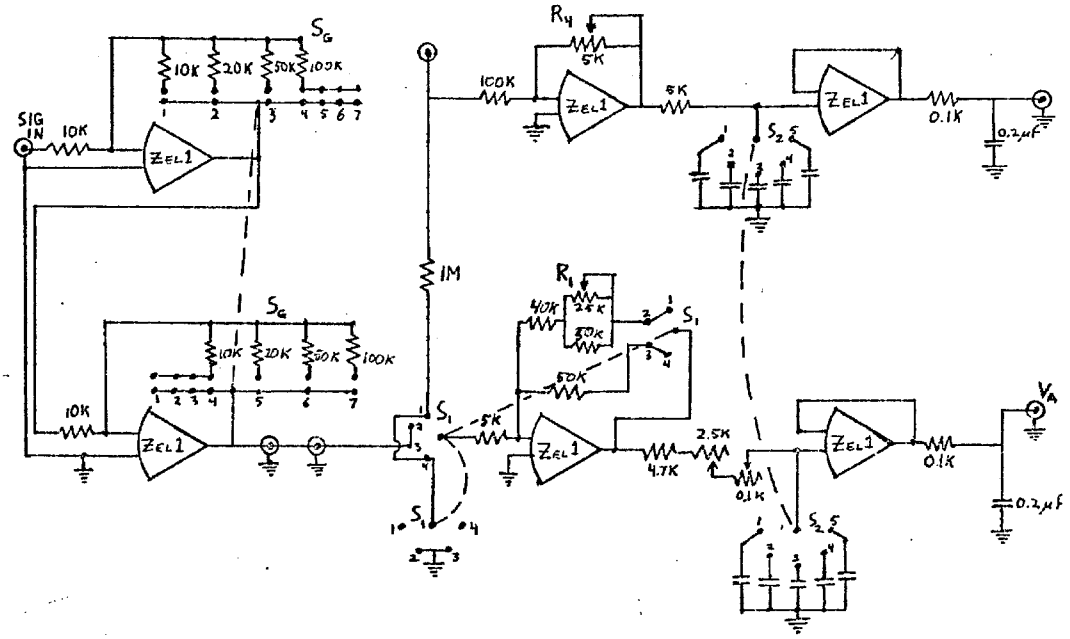

Figure 4. Schematic Diagram: Preamp and Phase and Amplitude Comparator.

positions 1 and 2, respectively, and measurement of the output signal amplitude and the drive signal amplitude on V_A in positions 3 and 4, respectively. Switch S_2 selects a proper capacitor for the frequency range to allow phase angle calibration. A physical description of the PAC is shown in Fig. 5. The output of the Phase and Amplitude Comparator, with an impedence of about 100 ohms, is displayed on a Tektronix Type 545B oscilloscope. A type W Plug-in Unit is generally used for the vertical axis amplification. A Type CA Double Beam Plug-in Unit can be used when large angles greater than 90° are encountered so that these phase angles can be measured directly from a simultaneous display of the two signals.

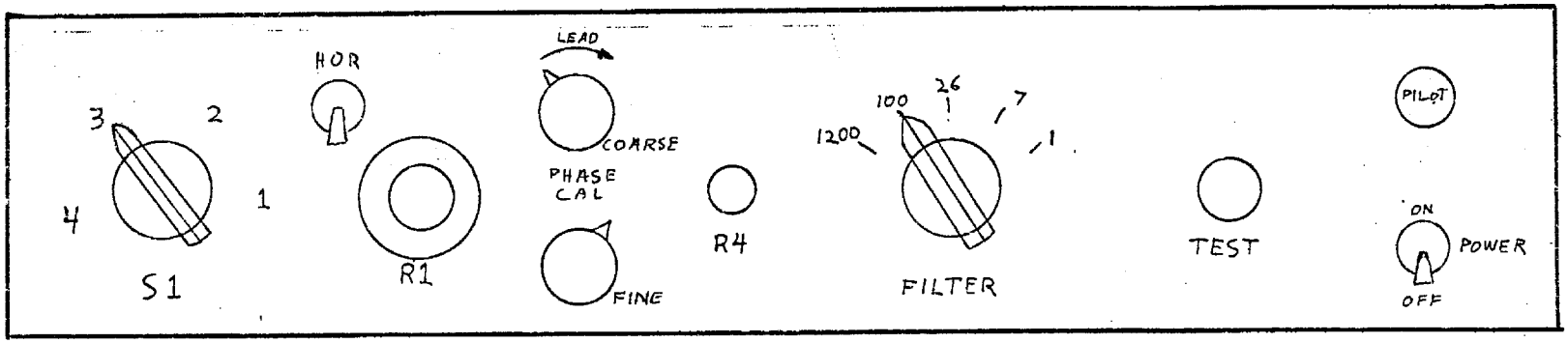

(a) Front

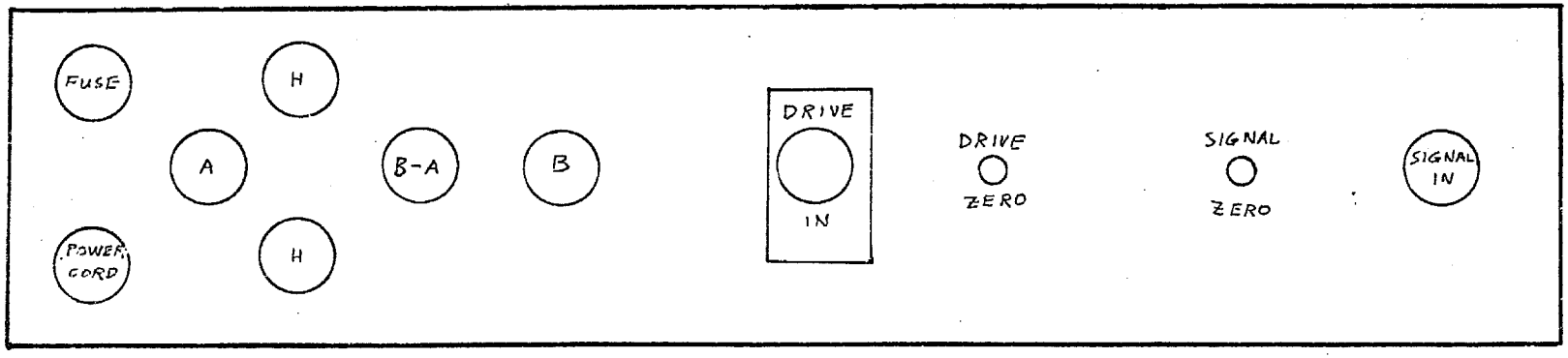

(b) Rear

Figure 5. Phase and Amplitude Comparator (PAC).

A Leeds and Northrup Potentiometer detects the EMF from two copper-constantan thermocouples located near the specimen and in the inertial block underneath. A Hallikainen Thermotrol Model 1053 is used to control the temperature. The temperature sensing element is a 200 ohm tungsten resistance thermometer mounted on the inside wall of the temperature control chamber. Temperature control is a critical part of the operation scheme and is discussed further in the next section.

III. Temperature Control

The problem of charge buildup on the piezoelectric force transducer as a result of changing temperature is very difficult to deal with. At high frequencies, the problem is not too severe because the oscilloscope can be AC coupled to eliminate the electrical drift from the amplified signal. At lower frequencies, when the oscilloscope must be DC coupled, temperature changes and the subsequent electrical drift must be reduced to negligible levels to allow phase angle measurements on the oscilloscope. With the fine temperature control required, one cannot set the temperature and wait for the apparatus to come to equilibrium, but one must adjust the temperature controller to come to the force transducer temperature. Since the Melabs controller was not designed to do this, the Hallikainen instrument was substituted for it. Monitoring the 200 ohm tungsten thermometer, this instrument is barely adequate by controlling the

thermometer to about 0.002°C.

A drawing of the environmental chamber is shown in Fig. 6. The housing is a section of 4.0 inch O.D. brass tubing of 1/8 inch wall thickness which is cut into two sections and machined so that the top section slides partially over the lower section. Circular brass plates are soldered onto the ends. A small hole in the lower section provides entrance for the various leads into the chamber. Another small hole in the top is needed for the resistance thermometer cemented to the inside wall of the top section. Also on top is an inert gas inlet for nitrogen blanketing, if required. Both sections are wrapped with asbestos paper. An 82 ohm Chromel A heater is wound around the top section in series with a similar 70 ohm heater around the bottom section. A third 97 ohm heater is wound independently around the bottom section for fast warm up. The heaters are wrapped with asbestos paper and the entire chamber is enclosed in polystyrene foam insulation.

In order to obtain optimal temperature control, a light-bulb is connected in series with the heaters to reduce the voltage applied to them. The light bulb can be changed to vary power input depending on the difference between the test temperature and ambient temperature. To operate below room temperature, a low temperature heat sink enclosing the insulated apparatus is required. This is achieved by sliding a 6 inch sealed end copper tube over the apparatus and allowing the bottom two inches of the tube to sit in a cooling bath of dry ice-acetone or liquid nitrogen. The copper tube is insulated where it is exposed to room temperature. All of this equipment is isolated from

mechanical vibration through substantial shock absorbing support.

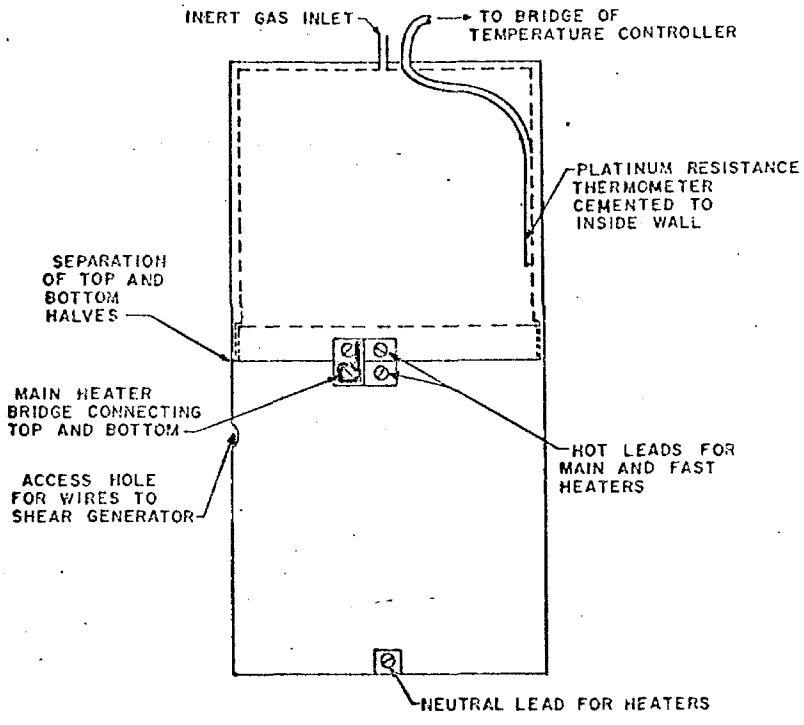

Figure 6. Environmental Chamber Containing the Rheometer.

REFERENCES

1. D. O. Miles, J. Appl. Phs., 33: 1422 (1962).

2. D. O. Miles, G. C. Knollman, A. S. Hamamoto, Rev. Sci. Instr., 36: 158 (1965).

3. N. W. Tschoegl, R. F. Landel, et al., "A Research Program on Solid Propellant Physical Behavior," CHECIT PL68-1, California Institute of Technology, Pasadena, California, AFRPL-TR-68-106, 1968, Part III.

4. N. W. Tschoegl, W. G. Knauss, R. F. Landel, et al., "A Research Program on Solid Propellant Physical Behavior," CHECIT PL69-1, California Institute of Technology, Pasadena, California, AFRPL-TR-69-180, 1969, Part XIII.

5. N. W. Tschoegl, W. G. Knauss, R. F. Landel, et al., "A Research Program on Solid Propellant Physical Behavior," CHECIT PL70-1, California Institute of Technology, Pasadena, California, AFRPL-TR-70-143, 1970, Part VII.

6. N. W. Tschoegl, J. R. Smith in T. L. Smith, J. R. Smith, N. W. Tschoegl, Final Report on "Viscoelastic Properties of Solid Propellants and Propellant Binders," SRI Projects PRU-3939,4660, 5174, Stanford Research Institute, Menlo Park, California, 1966, Appendix A. Department of the Navy, Bureau of Naval Weapons Contracts No. NOW 61-1057-d, NOW 64-0073-d, NOW 65-0061-d.

IV. Calibration

Five different calibration factors affecting the phase angle and amplitude ratio measurements have to be determined and included in the computer program for proper analysis of the data. These factors have to be redetermined whenever modification is made to the rheometer or the measuring equipment.

Factors important in the apparatus calibration include:

1. The Amplitude Ratio
2. The Frequency Dependence of the Amplitude Ratio
3. The Phase Angle Contribution at Various Frequencies
4. The Inertial Contribution
5. The Temperature Dependence of the Amplitude Ratio

The calculations are summarized in Part 6.

1. The Amplitude Ratio

A calibration is determined by examining three stainless steel rings of known elastance. Data are taken for the rings at 30 °C in the same way as for a polymer sample as described in the procedure section. The amplitude ratio (AR) is proportional at a specified frequency (usually 1 Hz) to the ring's elastance. The rest of the data obtained over the frequency range will be used in computing other calibration factors. The three points are plotted as shown in Fig. 7a, and a straight line with unit slope is fit to the points. The elastances of the rings are determined from the dimensions of the rings, and therefore the larger rings are probably the most accurate and should be weighted most heavily. Another point can be calculated from the equilibrium modulus of a specimen of

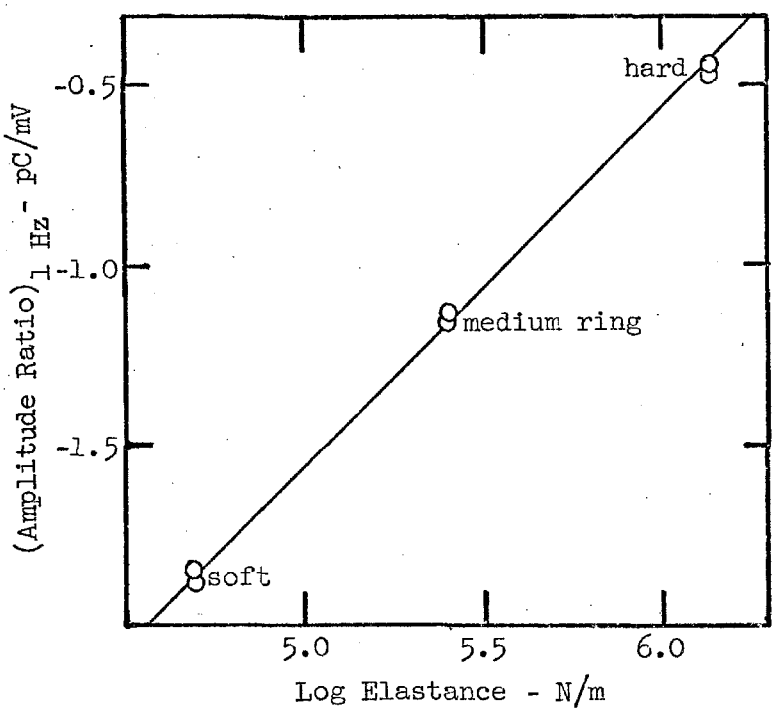

Figure 7a. Amplitude Calibration.

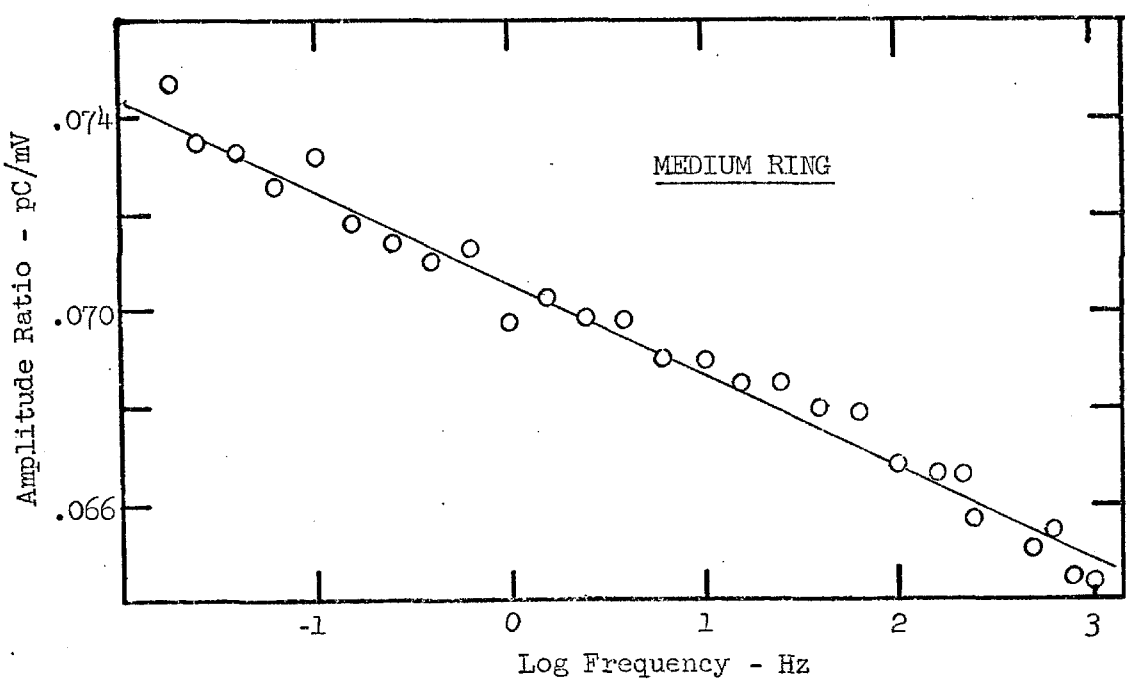

Figure 7b. Frequency Calibration of Amplitude Ratio.

a known crosslinked rubber such Galcit I (this point will usually lie near the point determined for the softest ring). The calibration constant is determined by taking any point on the line and dividing the attenuation by the elastance, obtaining for this transducer a value of 3.7×10^6 (N/m)/(pC/mV) or 3,700. (bar·cm)/(pC/mV), the latter being the proper units for the computer subroutine CALIB.

2. Amplitude Ratio vs. Frequency

Taking measurements of a calibration ring at various frequencies, one sees that the amplitude ratio increases with decreasing frequency. The variation is very nearly linear when the AR is plotted against the logarithm of the frequency as shown in Fig. 7b for the medium ring. The slope of the line normalized by the amplitude ratio at 1 Hz is constant for the three rings, having a value of about -0.031 as determined from this graph. The value used in the subroutine CALIB is an average value for the three rings. Together with the factor in Part 1, then, the elastance of a specimen is calculated from the measured AR as

$$\text{Elastance}^* = 3700 \times [1 + 0.031 \times \log_{10}(\text{HZ})] \times (\text{AR}) \quad \text{bar·cm} \quad (1)$$

for this transducer where HZ is the frequency. With some transducers, the amplitude ratio deviates from the straight line relationship at very low frequencies, increasing more that the straight line indicates. If this is the case, tabulated data better describe the nonlinear behavior and an interpolation scheme should be included in the CALIB subroutine along with Eq. (1).

*The elastance multiplied by the shape factor gives the absolute value of the complex modulus G^*.

3. The Phase Angle

The phase angle of the apparatus changes radically with frequency. This variation is shown in Fig. 7c which is a plot of the tangent of the phase angle between the drive signal and the lagging force signal for the medium stainless steel calibration ring. Since the ring contributes essentially no phase angle, the lag is attributed to the apparatus. At very low frequencies, the increase in phase lag is approximately proportional to the reciprocal of the square root of the frequency. No explanation is offered for this behavior. At intermediate frequencies, the phase angle shows small variation approximately proportional to the logarithm of the frequency. At high frequency, the change is proportional to the frequency and is clearly electronic since it is also proportional to the amplifier gains employed. The phase angle changes only negligibly with temperature except for frequencies below 0.1 Hz at temperatures above 40°C.

To correct for this, the lag phase angle of the apparatus, as determined by testing calibration rings, must be added to the lead phase angle measured for a polymer sample. Once a constant term plus a high frequency term proportional to the frequency and the amplifier gain have been subtracted from the apparatus phase angle, interpolation between frequencies of the resultant data yields the best results.

The high frequency phase angles, after applying an intertial correction (Section 4), for one of the rings, usually the medium one, are plotted against the frequency as shown in Fig. 7d. A straight

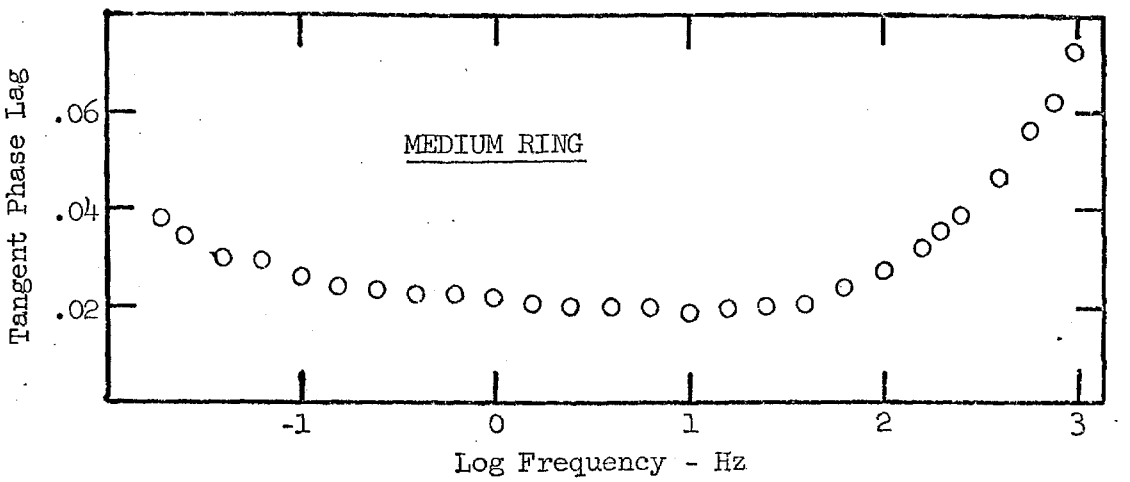

Figure 7c. Frequency Calibration of Phase Angle.

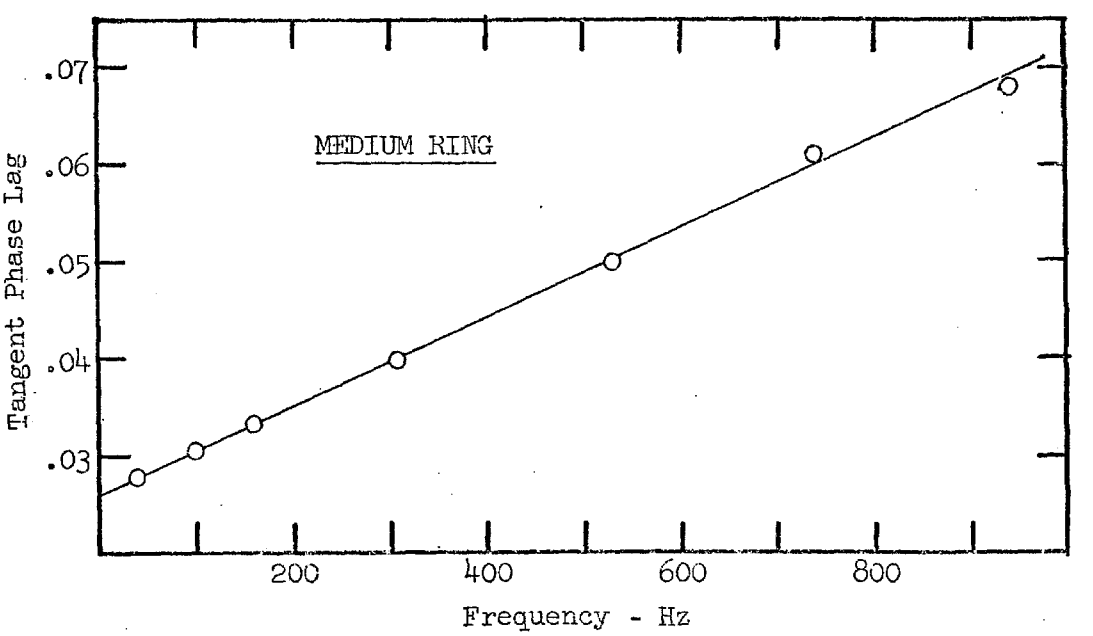

Figure 7d. High Frequency Calibration of Phase Angle.

line is drawn through the data yielding

$$\phi_1 = 0.030 + 4.75 \cdot 10^{-10} \times (HZ) \tag{2}$$

The dependence of the phase angle on the gain of the preamp has been determined to be

$$\phi_g = \begin{cases} 1.24 \cdot 10^{-6} \times GAIN \times HZ & GAIN \leq 10 \\ 1.24 \cdot 10^{-6} \times (10 + GAIN/10) \times HZ & 10 < GAIN \leq 100 \end{cases} \tag{3}$$

from attenuation measurements at very high frequency. The amplification used in obtaining the data fit by Eq. (2) was 10 x. Eq. (2) and Eq. (3) can be combined to yield

$$\phi_a = 0.024 + \begin{cases} 3.5 + 1.2 \cdot 10^{-6} \times GAIN \times HZ & GAIN \leq 10 \\ 3.5 + 1.2 \cdot 10^{-6} \times (10 + GAIN/10) \times HZ & 10 < GAIN \leq 100 \end{cases} \tag{4}$$

Eq. (2), or Eq. (4) with the gain set equal to 10 is then subtracted from the experimentally determined phase angles over the entire frequency span. The remainder is then used in an interpolation scheme to determine ϕ_i which is added to ϕ_a to get the whole phase angle correction ϕ.

$$\phi = \phi_a + \phi_i \tag{5}$$

If one intends to investigate frequencies below 0.1 Hz, a term proportional to $1/\sqrt{Hz}$ should be added to Eq. (4) before subtraction.

The phase angle measured for a calibration ring has some systematic error in it. The data are generally reproducible, but will change as the same ring is reinstalled in the apparatus. The ring should be installed and tested several times at 30°C until a minimum phase angle is measured. This minimum phase angle appears

to be most characteristic of the apparatus. The phase angle also changes slightly, often erratically, with temperature. Once a minimum phase angle is seen at 30°, the measurement should be made at several other temperatures subtracting Eq. (4) from the computed phase angles. A table of these data for various frequencies and temperatures show trends that develop. The variation, however, is small enough that a single set of smoothed values for various frequencies will suffice. If one is interested in very low frequencies (below 0.4 Hz) and above about 40°C, one should take the temperature variation into account. A double interpolation scheme between frequencies and temperatures can then be used.

The phase angle can also change with time, usually decreasing slightly over several days if the temperature is controlled steadily. This is very small, fortunately, and can be neglected.

The phase angle correction is carried out in the computer subroutine ANGCOR.

4. Inertial Contribution

When no sample or calibration ring is installed in the rheometer, so that there is no direct connection between the driver plate and the force transducer, one can still observe a small output to an imposed sinusoidal drive. This output is measurable at frequencies above 100 Hz. The amplitude ratio is obtained by comparing the input and output signals at high amplifier sensitivity. The output lags the input by an angle of from $\pi/2$ to π radians which

is out of the range for the differential Lissajous method on the PAC. The angle can be determined by direct measurement by first centering the input signal on the oscilloscope so that one cycle occupies the full horizontal scale, triggering it by an independent signal at the same frequency. Switching to the output signal shows it as it is displaced by a part of a cycle. The shift is measured as a fraction of a cycle. The PAC S1 is set on pos'n 4 for measurement of the drive signal and on 3 for measurement of the output signal. The comparison of the two signals can be made easier by using the CD Dual Channel Plug-in on the scope, but its maximum amplification is not as great as that available on the W-Plug-in unit so that the amplitude ratio is harder to measure. The real and imaginary parts of the amplitude ratio are plotted against the frequency squared and the frequency, respectively, as shown in Fig. 7e. One immediately notes a prominent resonance peak at 250 Hz which precludes measurements in that region (the exact location depends on the monitor plate used). Below the resonance, the real part is very small and can be neglected. The measured amplitude here is very nearly equal to the imaginary part. Above the resonance, the real part is significant and the imaginary part is very sensitive to the phase angle and therefore also sensitive to the phase angle correction discussed in the last section. Thus that correction has to be applied to the data. Similarly, the phase angle correction (particularly at high gains) is even more sensitive to the inertial correction, so these have to be applied iteratively to each other to obtain proper factorization of the two effects. The imaginary portion below the

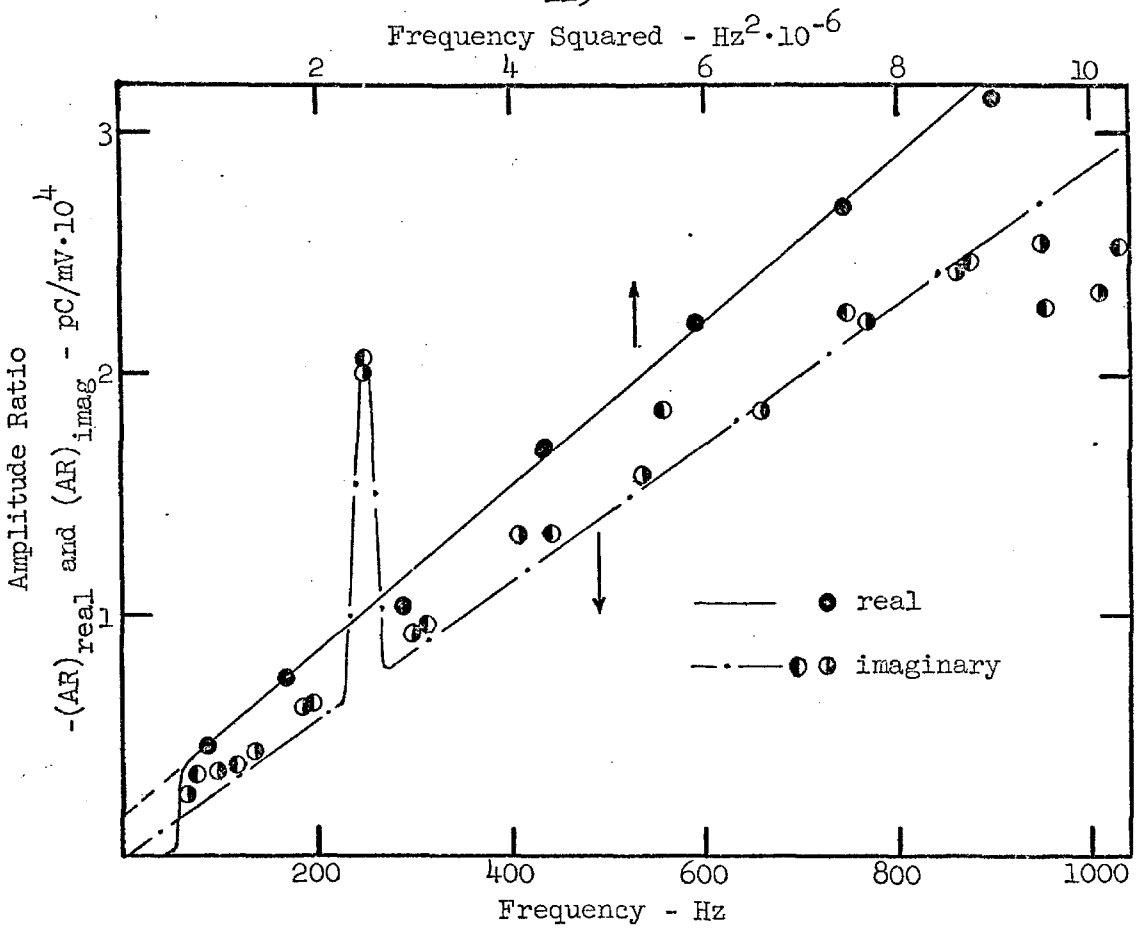

Figure 7e. Inertial Calibration.

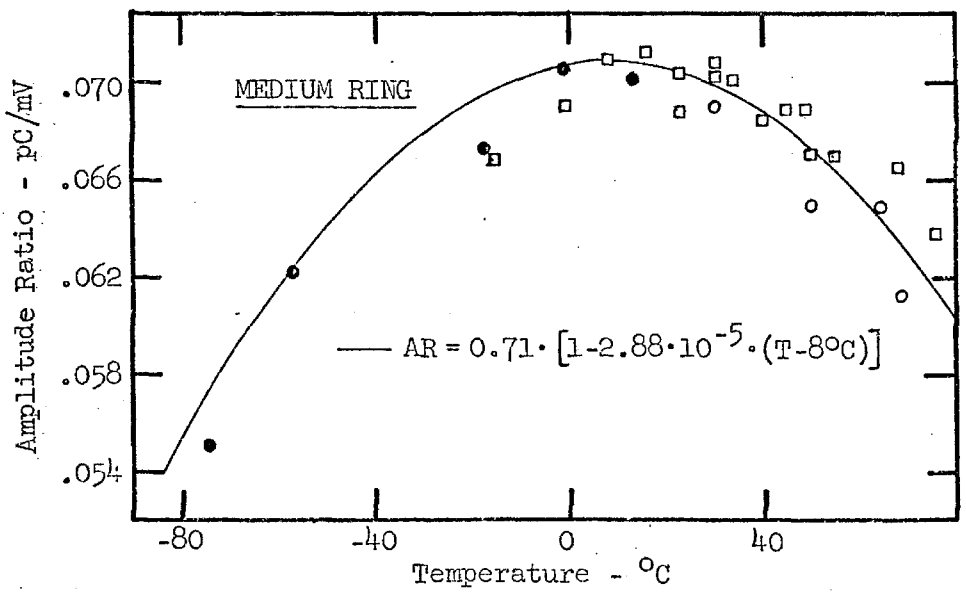

Figure 7f. Temperature Calibration of Amplitude Ratio.

resonance is much less sensitive to the phase angle, and by extrapolating these data above the resonance, one can quickly obtain the desired data approximately. The real and imaginary parts in Fig. 7e can be represented by

$$\mathrm{Re[AR]} = \begin{cases} -(1.7\cdot10^{-5} + 3.42\cdot10^{-10} \times \mathrm{HZ}^2) & \mathrm{HZ} > 250 \\ 0.0 & \mathrm{HZ} < 250 \end{cases} \tag{6}$$

$$\mathrm{Im[AR]} = 2.86\cdot10^{-7} \times \mathrm{HZ} \tag{7}$$

These quantities are subtracted from the real and imaginary parts respectively of the amplitude ratio measured in an experiment. This subtraction is carried out in the computer subroutines ARRC and ARIC.

It was mentioned that the phase angle at high frequencies was influenced by the inertial contribution. The real part has very little affect other than increasing the measured amplitude ratio of a ring by a few percent (especially for the softest ring). The phase angle is most influenced by the imaginary part. For the small phase angles considered, it generally suffices to divide Eq. (7) by the amplitude ratio for the ring, and subtract this from the uncorrected tangent of the phase angle (this action assumes that the phase angle and its tangent and sine are all nearly equivalent).

5. Temperature Calibration of the Amplitude Ratio

If the amplitude ratio for a calibration ring is determined at different temperatures at a single frequency, a dependence like that in Fig. 7f is seen. This curve is established primarily with the medium ring as the hard ring must be reinstalled after large changes in temperature, apparently because its small deformation

cannot allow for changes due to thermal expansion. Some hard ring data can be acquired, however, and included by normalizing the value at 30°C to that value observed for the medium ring and then normalizing values at other temperatures by the same factor. Also data can be included from other specimens, such as Galcit I data in the rubbery region, in the same manner. At each temperature, data are taken from 60 to 1000 Hz and the points appearing in Fig. 7f are the 100 Hz values on the line drawn through these data. The temperature dependence seems to be represented quite well by a parabola which in this instance has the form

$$[AR]_{100Hz} = 0.0710 \times \left[1 - 2.88 \cdot 10^{-5} \times (T-8°)^2\right] \qquad (8)$$

where the temperature T is expressed in degrees centigrade and 0.0710 is the amplitude ratio for the medium ring at 100 Hz and 8°C. Therefore, to correct amplitude ratios determined at different temperatures, the measured value is multiplied by the normalization factor f_n where

$$f_n = \left[1 - 2.88 \cdot 10^{-5} \times (t-8°)^2\right]^{-1} \qquad (9)$$

in the computer subroutine ARTEMP. This correction is slightly smaller than the magnitude of the T/T_o correction applied for time-temperature superposition over the temperature range of interest.

6. Calculation and Calibration Summary

In Fortran computer program MELAB, the storage and loss moduli, G' and G'', of a material at a given temperature and frequency are calculated according to the relationships

$$G' = H \cdot C(f) \cdot \{AR \cdot f_n(T) \cdot \cos[\theta - \phi(f)] - I(f)\} \quad (10)$$

$$G'' = H \cdot C(f) \cdot \{AR \cdot f_n(T) \cdot \sin[\theta - \phi(f)] + F(f)\} \quad (11)$$

where

f ... frequency in Hz

H ... shape factor; see Appendix C

T ... temperature (°C)

AR ... measured amplitude ratio for a sample; function of f, T

θ ... measured phase angle for a sample; function of f, T

and the various correction factors are given in Table I.

Table I

Correction Function	computer subroutine	Eq in text
$C(f) = 3700 \cdot [1.0 + 0.03 \cdot \log_{10}(f)]$ (bar)/(pC/mV)	CALIB	(1)
$\phi(f) = \phi_a(f) + \phi_i(f)$ radians	ANGCOR	(5)
$\phi_a = 0.024 + \begin{cases} 3.5+1.2 \cdot 10^{-6} \cdot GAIN \cdot f & GAIN \leq 10 \\ 3.5+1.2 \cdot 10^{-6} \cdot (10+GAIN/10) \cdot f & 10 < GAIN \leq 100 \end{cases}$		(4)
ϕ_i is determined by interpolation		
$I(f) = \begin{cases} -1.7 \cdot 10^{-5} - 3.42 \cdot 10^{-10} \cdot f^2 \text{ (pC/mV)} & f > 250 \text{ Hz} \\ 0 & f < 250 \text{ Hz} \end{cases}$	ARRC	(6)
$F(f) = 2.86 \cdot 10^{-7} \cdot f$ (pC/mV)	ARIC	(7)
$f_n(T) = [1.0 - 2.88 \cdot 10^{-5} \cdot (T-8)^2]^{-1}$	ARTEMP	(9)

Appendix C

The Measurement of Small Phase Angles in the Subaudio Frequency Range

N.W. Tschoegl* and J.R. Smith
Stanford Research Institute, Menlo Park, California

ABSTRACT

A method is described which allows the measurement of small phase angles with excellent accuracy and is suitable for work at subaudio frequencies. The weaker signal, F, is connected to the positive terminals of an oscilloscope which has a double differential amplifier input. The stronger signal, X, is connected to the negative terminals of the vertical amplifier. The ellipse which appears on the screen is leveled (zero angle of tilt) by changing the gain of a solid state operational amplifier in the path of the F-signal. The phase angle φ is then obtained from $\sin \varphi = d_D s_v / d_X s'_v$, where d_D and d_X are the peak-to-peak distances of the difference signal and the X-signal, respectively, and s_v and s'_v are the sensitivities of the vertical scope amplifier, at which the distances were recorded.

A simultaneous determination of the gain through the operational amplifier permits the amplitude ratio to be calculated. The signals may be filtered. The attenuation through the two filters is equalized and any phase shift through them is eliminated by a simple balancing

*Present address: California Institute of Technology, Pasadena, California.

procedure.

Known phase angles of the order of 0.0001 radians have been measured at frequencies of 0.25 and 0.05 cps in an experiment designed to evaluate the method.

INTRODUCTION

Various types of forced vibration experiments are widely used in the measurement of dynamic mechanical properties. These measurements require the determination of the amplitude ratio and the phase angle between a sinusoidal excitation and response. Because of the ease and precision with which such measurements can be made electronically, conversion of force and displacement (or torque and angular displacement) into electric signals is the preferred method. Most of the measurements are made in the audio and/or subaudio frequency range. Instrumentation and techniques in the audio range are highly developed because of the interest of the electronics industry in this range. In the subaudio range, from essentially zero to about 20 cps, only a few, generally costly, precise methods are available. In this paper, a relatively simple technique is described for the measurement of small phase angles which is suitable in the subaudio range, although it may be used with advantage at higher frequencies with the same excellent accuracy. The method allows filtering of the signals by compensating automatically for any phase shift introduced by the filters--an advantage in eliminating the effect of hum, spurious vibrations, and induced voltages.

PRINCIPLE OF METHOD

The method is based on the principle of vector composition, as illustrated in Fig. 1, in which F refers to the force signal, X to the displacement signal, D to the difference signal, and the subscript zero denotes peak values.

For the general case, illustrated in Fig. 1a, the law of cosines yields

$$\cos \varphi = (F_0^2 + X_0^2 - D_0^2)/2F_0X_0. \qquad (1)$$

However, for small phase angles this method requires very precise measurements of the peak amplitudes of the three signals. When $F_0 = X_0$ the law of sines gives

$$\sin (\varphi/2) = D_0/2X_0 = D_0/2F_0 \qquad (2)$$

as shown in Fig. 1b. This method has limited applicability, since the equality of the two signals is usually difficult to ensure.

A third possibility, demonstrated in Fig. 1c, consists in making the angle enclosed by F_0 and D_0 equal to $\pi/2$. We then have

$$\cos \varphi = F_0/X_0 \qquad (3)$$

$$\tan \varphi = D_0/F_0 \qquad (4)$$

$$\sin \varphi = D_0/X_0 \qquad (5)$$

For the purpose of this paper we shall assume that $F_0 \leq X_0 \cos \varphi$, since this condition can always be obtained by exchanging terminals.

Methods based on Eq. (5) have been described by Marvin, Fitzgerald, and Ferry,[1] and by Markovitz, Yavorsky, Harper, Zapas, and deWitt,[2] for the audio frequency range. Vacuum tube voltmeters were used to measure the voltages. The stronger signal was attenuated until the difference

signal became a minimum. The chief disadvantage of this method is that the time required to find the minimum with the same accuracy increases as the frequency decreases. In addition, voltmeters cannot be employed in the subaudio frequency range.

In the method to be described, an oscilloscope (or, alternatively, a pen recorder) is used to measure the peak voltages. Solid state operational amplifiers serve to increase the signal level to achieve the conditions embodied in Eqs. (3) through (5). This is done by rotating in the manner detailed below, an ellipse on the oscilloscope screen until it is level. The method is shown to be quite sensitive even at low frequencies.

THEORY OF PHASE ANGLE DETERMINATION

A block diagram of the phase meter network is shown in Fig. 2. To understand the principle of the technique, let it be assumed that the filters are by-passed and that the switch S1 is in position 2. The gain through the F-amplifier is g, that through the X-amplifier is g_X. With the force signal appearing at the terminals of the horizontal scope amplifier and the difference signal appearing at the terminals of the vertical amplifier, the oscilloscope screen displays an ellipse whose major axis, in general, will be tilted by an angle θ (the angle of tilt) with respect to the horizontal screen axis. This situation is shown in Fig. 3. The difference signal arriving at the vertical amplifier is

$$D = gF_o \sin(\omega t + \varphi) - g_X X_o \sin \omega t \qquad (6)$$

and the signal at the horizontal amplifier becomes

$$gF = gF_0 \sin(\omega t + \varphi). \qquad (7)$$

In the preceding equations, ω is the radian frequency, t is time, and φ is the phase angle between the signals. Equations (6) and (7) refer to a displacement driven system, but this involves no loss of generality. The angle of tilt of the ellipse is

$$\tan\theta = D_{(F = F_0)}/gF_0 \qquad (8)$$

where $D_{(F = F_0)}$ is the value of D when gF is at its peak value. For F to achieve its peak value F_0, $\omega t + \varphi$ must equal $\pi/2$, and therefore

$$D_{(F = F_0)} = gF_0 - g_X X_0 \sin\left(\frac{\pi}{2} - \varphi\right) = gF_0 - g_X X_0 \cos\varphi. \qquad (9)$$

Substituting into Eq. (8)

$$\tan\theta = 1 - g_X X_0 \cos\varphi/gF_0. \qquad (10)$$

If g is varied so that $gF_0 = g_X X_0 \cos\varphi$, then the angle of tilt becomes zero. But when the ellipse is levelled, $\tan\varphi = D_0/gF_0$, or $\sin\varphi = D_0/g_X X_0$ (cf. Eqs. (4) and (5)).

The minor axis of the levelled ellipse is D_0, and its major axis is gF_0. If d_D and d_F stand for the distance in cm of the ellipse axes on the oscilloscope (or an X-Y recorder), and s_v and s_h are the sensitivities of the vertical and horizontal scope (or recorder) amplifiers in mV/cm, then

$$\tan\varphi = d_D s_v/d_F s_h. \qquad (11)$$

This method (which may be called the differential Lissajous method because it makes use of the difference of the two signals) bears some resemblance to the well-known Lissajous method for determining phase

angles. In the normal Lissajous method, however, as shown in Fig. 4, the measurements are derived from the ellipse itself, and the ellipse must be correctly positioned with respect to the center of the screen to obtain A. Furthermore, with small phase angles, A becomes very small. It can be enlarged by increasing the sensitivity, but then only the center section of the ellipse remains on the screen, and the correct positioning of the ellipse becomes doubtful. Consequently, the normal Lissajous method is not capable of high precision at small phase angles. In the differential Lissajous method, however, the ellipse is used only to ensure the necessary conditions, and then peak-to-peak amplitude measurements can be used to derive the phase angle.

Levelling of the ellipse in the differential Lissajous method is facilitated if, during this process, s_v is kept fairly low, and s_h is adjusted, using the vernier, to extend the major axis over the entire screen grid width. Instead of Eq. (11) one may use

$$\sin \varphi = d_D s_v / d_X s_v' \qquad (12)$$

where d_X is the peak-to-peak distance of the $g_X X$ signal and s_v' is the corresponding sensitivity. It is not necessary to know either g or g_X to obtain φ. Figure 5 shows a photograph of an ellipse and $g_X X$ signal taken in this way.

With the filters in the circuit, it is necessary, of course, to ensure that no additional phase shift be introduced; this is achieved by balancing the two filters against each other. When the switch S1 is in position 1, the same (X) signal will pass through both paths. If the phase shift through the two paths is not zero, an ellipse will

appear on the scope screen. By collapsing the ellipse through adjusting the X-filter, and, if necessary, levelling it by changing the gain through the X-amplifier, the phase shift between the two paths is readily eliminated.

THEORY OF AMPLITUDE RATIO MEASUREMENTS

Let f be the force in dynes, x the displacement in cm, K_F the force transducer constant in dynes/mV, K_X the displacement transducer constant in cm/mV, F the force signal in mV, and X the displacement signal in mV. The desired amplitude ratio is then

$$A_r = f_o/x_o = F_o K_F / X_o K_X. \tag{13}$$

Now let the gain through the X amplifier be g_X, the gain through the F-amplifier g_B (>1), and the gain (<1) through the X- and F-filters g_{XF} and g_{FF}. When the phase shift between the two paths is eliminated in the manner described in the previous section, the attenuation through the filters becomes identical, since the attenuation is a function only of the phase shift at the same frequency. Consequently,

$$g_X \, g_{FX} = g_B \, g_{FF}, \tag{14}$$

and the signals arriving at the oscilloscope will be

$$X' = g_X \, g_{XF} X = g_B g_{FF} X \tag{15}$$

and

$$F' = g_B g_{FF} F. \tag{16}$$

When the ellipse has been levelled with switch S1 in position 2,

$$F' = g \, g_{FF} F. \tag{17}$$

The amplitude ratio between force and displacement then becomes

$$A_r = \frac{K_F\, g_B\, F_0'}{K_X\, g\, X_0'} = \frac{K_F\, g_B\, s_{vX}\, d_F}{K_X\, g\, s_{vF}\, d_F} \qquad (18)$$

since g_{FF} cancels. The vertical scope amplifier sensitivities s_{vX} and S_{vF} refer to the sensitivities used in recording the X- and F-signal, respectively. The amplifier gains g_B and g must, of course, be known and are determined as described below.

Evidently Eq. (18) can be correct only if the phase shift through the F-amplifier does not change when the gain is changed from g_B to g. This gain dependent phase shift is examined in the Appendix. It is usually negligible, but a correction can be made if necessary.

The reason for initially setting the gain through the F-amplifier at $g_B > 1$ is to ensure proper levelling of the ellipse. This can only be achieved if the ellipse can be rotated through zero angle of tilt so that the level position can be approached from both sides. We can distinguish three cases:

1. If $F_0 < X_0 \cos\varphi$, the angle of tilt will be negative for $1 < g < X_0 \cos\varphi/F_0$, zero for $g = X_0 \cos\varphi/F_0$, and positive for $g > X_0 \cos\varphi/F_0$. The ellipse can therefore be rotated through zero tilt.

2. If $F_0 = X_0 \cos\varphi$, the angle of tilt is zero for $g = 1$, and positive for $g > \cos\varphi$. It cannot be negative since $g > 1$. The ellipse can be levelled, but it cannot be rotated through zero tilt.

3. If $X_0 \cos\varphi < F_0 < X_0$, the angle of tilt is always positive, and the ellipse cannot be levelled at all.

To insure the proper rotation of the ellipse in cases (2) and (3) an arbitrary "base gain" g_B can be introduced into the X-path by the proper adjustment of the feedback loop of the operational amplifier in this path (cf. Eq. (15). The equation for the angle of tilt then becomes

$$\tan \theta = 1 - g_B X_0 \cos \varphi / g F_0 \qquad (19)$$

and, provided $g_B > 1/\cos \varphi$, it will always be possible to rotate the ellipse through zero tilt. The extent of the negative tilt depends on the magnitude of g_B. In normal operation one would expect an angle of 45° to be the largest to be measured by this method. One finds

$$\cos \varphi = \cos \pi/4 = 1/\sqrt{2}, \qquad (20)$$

i.e., g_B should not be less than $\sqrt{2}$. Making $g_B = 2$ is the logical choice and should be adequate for most practical cases.

DESCRIPTION AND OPERATION OF PHASEMETER

A schematic of the phasemeter network is shown in Fig. 6. The two amplifiers are Burr-Brown Model 1507 operational amplifiers connected in the noninverting mode. The amplifiers provide isolation of the signal sources, as well as amplification. The feedback loops (gain control) around the amplifiers is provided by resistors R_1 and R_2, and R_4 and R_5, respectively. R_1 and R_4 are 1 kilo ohm fixed resistors. R_2 is a variable 10 kilo ohm, and R_5 a variable 100 kilo ohm resistor. These variable resistors (as well as R_3 and R_7) have smaller variable resistors (not shown) in series for fine control.

The two filters consist of two 1 μF fixed capacitors, C_1 and C_2, and the resistors R_3 and R_6. R_3 is a 75 kilo ohm fixed resistor in

series with a variable 50 kilo ohm resistor which is used in equilizing the phase shift through the two paths. R_6 is a fixed 100 kilo ohm resistor which determines the 3-db-down point of the two filters. R_7 is a voltage divider through which a d.c. calibration signal taken from a 1.35 volt mercury cell may be injected into the F-path. S1 is a multiple 4-position switch used to select the mode of operation. S2 is used in the gain calibration. It should be noted that with S1 in positions 3 or 4 for gain calibration, the filters are out of the circuits.

When operating the phasemeter, the first step consists in calibrating the base gain g_B. With S1 in position 3 and S2 in position 1, R_7 is regulated until a convenient mV output is obtained on the Rubicon potentiometer. S2 is then put into position 2, and R_5 is varied until the reading on the Rubicon potentiometer is exactly twice the previous reading. The base gain g_B then is exactly 2.

S2 is now put into position 3, and S1 into position 1. R_2 and R_3 are varied until the ellipse is a level straight line, which completes the preliminaries. The actual measurements are taken by putting S1 into position 2 and varying R_5 to level the ellipse. A photographic record is made of d_D, d_F, and d_X.

The gain g is read similarly to g_B with S1 in position 3 and S2 first in position 1, then in position 2. The ratio of the two readings will be g. If g is too high to be read conveniently in this way, two horizontal lines are displayed (and photographed) with S1 first in position 3, then in position 4. The distance between the two lines, d_G, then yields the gain from

$$g = d_F S_{vF}/V_p \qquad (21)$$

where V_p is the potentiometer reading obtained with S2 in position 1.

EXPERIMENTAL RESULTS

The method was checked by measuring small known phase angles at several low frequencies. The manner in which the known phase angles were produced is shown diagrammatically in Fig. 7. A Hewlett Packard Model 202A Function Generator was used as the signal source. R_1 is a 5000-ohm shunt resistance equal to the output impedance of the generator, which thus operates at design load. R_1 is also used for fine regulation of the signal amplitude. The signal is split, one portion being fed to the F (force) terminal of the phasemeter network shown in Fig. 6, while the other portion goes to a phase shifting network consisting of a general Radio Corporation Model 1432-P Decade Resistance Box (1,111,100 ohms total, in steps of 10 ohms) and a 1.0006 μF fixed capacitor C whose capacitance was determined precisely in a capacitance bridge. The phase-shifted signal is then passed through a Burr-Brown Model 1507 operational amplifier to the X (displacement) terminal of the phasemeter network. The amplifier effectively isolates the signal.

The phase shift between the two signals is thus obtained as the ratio between the imaginary and real parts of the transfer function of the phase shifting network. The transfer function G_p is given by

$$G_p = 1/(1 + j\omega CR) \qquad (22)$$

and consequently the generated phase shift is

$$\tan \varphi = \text{Im } G_p/\text{Re } G_p = \omega CR. \qquad (23)$$

The measured phase angle is obtained from Eq. (12).

Figure 8 shows plots of measured vs. calculated phase angles at various frequencies. The measured angles are plotted on the ordinates as sin φ; the calculated angles are plotted on the abscissa as tan φ. The straight lines represent the theoretical relationship between sin φ and tan φ, which are identical for these low angles. Evidently, at frequencies as low as 0.25 cps, phase angles of the order of only a few thousandths of a radian can be measured with very good accuracy. The lowest frequency at which measurements were attempted was 0.05 cps, and even at this frequency the accuracy was excellent.

APPENDIX

Calculation of Frequency and Gain Dependence of Phase Shift Through a Single-Pole Amplifier

Since the Burr-Brown operational amplifier is closely approximated by a single-pole (single time constant) amplifier,[3] the open loop phase shift φ_0 is given by the equation[4a]

$$\tan \varphi_0 = f/f_H, \qquad (A\text{-}1)$$

where f is the operating frequency and f_H (the break frequency) is the frequency at which the open loop gain g_0 is down 3 decibels from the D.C. open loop gain, $\bar{g}_0$; the frequency dependence of the open loop gain is[4a]

$$g_0 = \frac{\bar{g}_0}{\sqrt{1 + (f/f_H)^2}} \quad . \qquad (A\text{-}2)$$

The phase shift in feedback operation can be shown[5] to be

$$\tan \varphi = \frac{\tan \varphi_0}{1 - \beta . g_0 \sqrt{1 + \tan^2 \varphi_0}} \qquad (A\text{-}3)$$

where β is the feedback factor[4b] given by

$$g = \frac{g_0}{1-\beta\, g_0} , \tag{A-4}$$

g being the gain with feedback.

Subsbituting Eq. (A-1) into Eq. (A-2) yields

$$g_0 = \frac{\bar{g}_0}{\sqrt{1 + \tan^2 \varphi_0}} = \bar{g}_0 \cos \varphi_0 \tag{A-5}$$

and Eq. (A-3) transforms into

$$\tan \varphi = \frac{f/f_H}{1-\beta\, \bar{g}_0} . \tag{A-6}$$

Using Eq. (A-4) leads to

$$\tan \varphi = \frac{g\, f}{\bar{g}_0\, f_H + g\, f_H(1-\bar{g}_0/g_0)} . \tag{A-7}$$

But from Eq. (A-5)

$$\bar{g}_0/g_0 = 1/\cos \varphi_0 \tag{A-8}$$

and

$$\bar{g}_0\, f_H = f_c \tag{A-9}$$

where f_c is the open loop unity gain crossover frequency.

This finally leads to

$$\tan \varphi = \frac{g\, f}{f_c + g\, f_H(1-1/\cos \varphi_0)} \tag{A-10}$$

as the equation for the frequency and gain dependence of the phase shift through a single-pole amplifier. The design parameters apearing in Eq. (A-10) are the open loop unity gain crossover frequency f_c and the break frequency f_H.

If

$$f_c \gg g\, f_H(1-1/\cos \varphi_0) , \tag{A-11}$$

the phase shift may be found with good approximation from the simple equation

$$\tan \varphi = g\, f/f_c \qquad \text{(A-12)}$$

ACKNOWLEDGMENTS

The authors with to extend their thanks to Mr. J. Van Geen for his advice and to Mr. I. Illing for building the phasemeter and for his painstaking measurements.

This work was supported by the Bureau of Naval Weapons under Contract No. NOw 65-0061-d, ARPA Order No. 22.

REFERENCES

1. R.S. Marvin, E.R. Fitzgerald, and J.D. Ferry, Journal of Applied Physics 21, 197 (1950).
2. H. Markovitz, P.M. Yavorsky, R.C. Harper, L.J. Zapas, and T.W. DeWitt, Review of Scientific Instruments 23, 430 (1952).
3. Burr-Brown Research Corporation, Handbook of Operational Amplifier Applications, Tucson, Arizona, 1963.
4. J.D. Ryder, Engineering Electronics, McGraw-Hill, New York, 1957: (a) pp. 87 ff; (b) p. 185.
5. F. Langford-Smith, Ed., Radiotron Designer's Handbook, Radio Corporation of America, Harrison, New Jersey, 1952, p. 389.

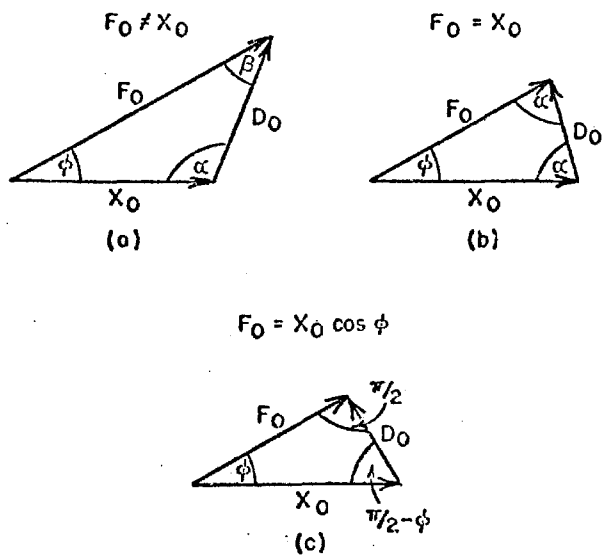
$F_0 \neq X_0$
F_0
D_0
β
ϕ
α
X_0
(a)
$F_0 = X_0$
F_0
D_0
α
ϕ
α
X_0
(b)
$F_0 = X_0 \cos\phi$
F_0
$\pi/2$
D_0
ϕ
X_0
$\pi/2-\phi$
(c)
RA-4660-9R

Fig. 1

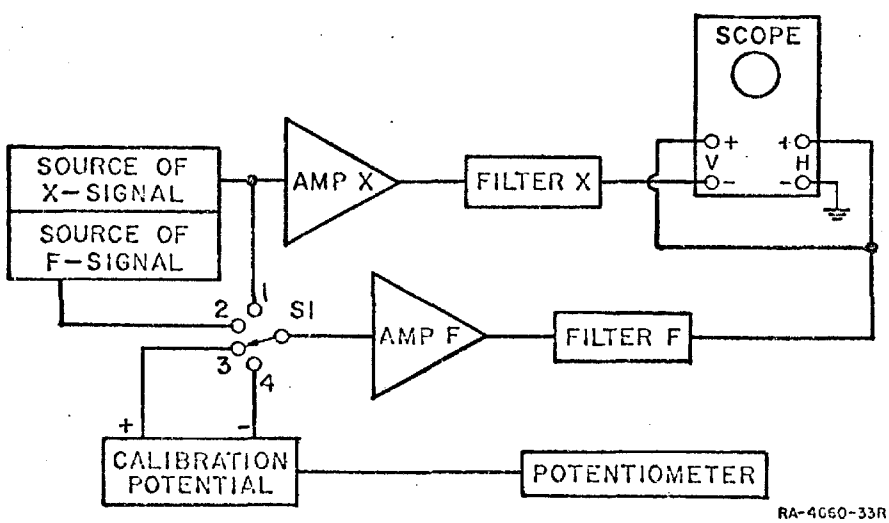
SCOPE
SOURCE OF X-SIGNAL
SOURCE OF F-SIGNAL
AMP X
FILTER X
V
H
2
1
S1
AMP F
FILTER F
3
4
+
-
CALIBRATION POTENTIAL
POTENTIOMETER
RA-4660-33R

Fig. 2

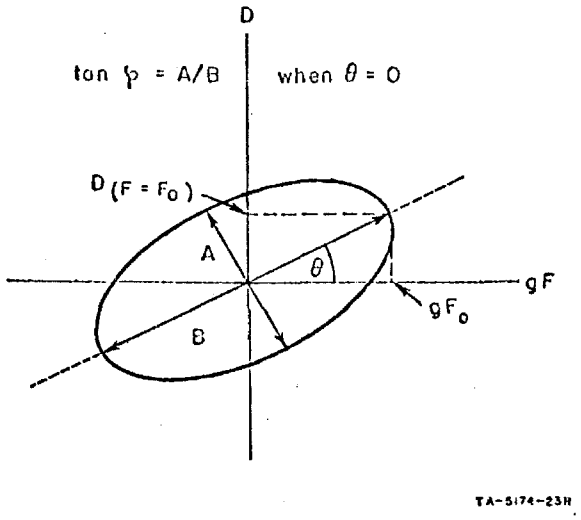

Fig. 3

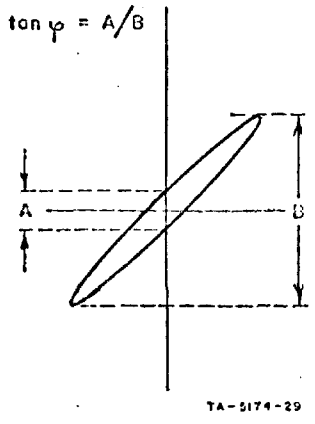

Fig. 4

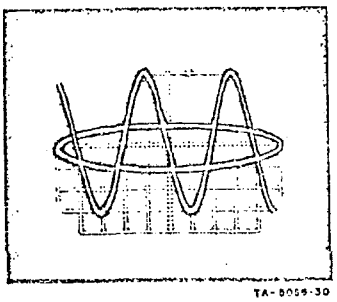

Fig. 5

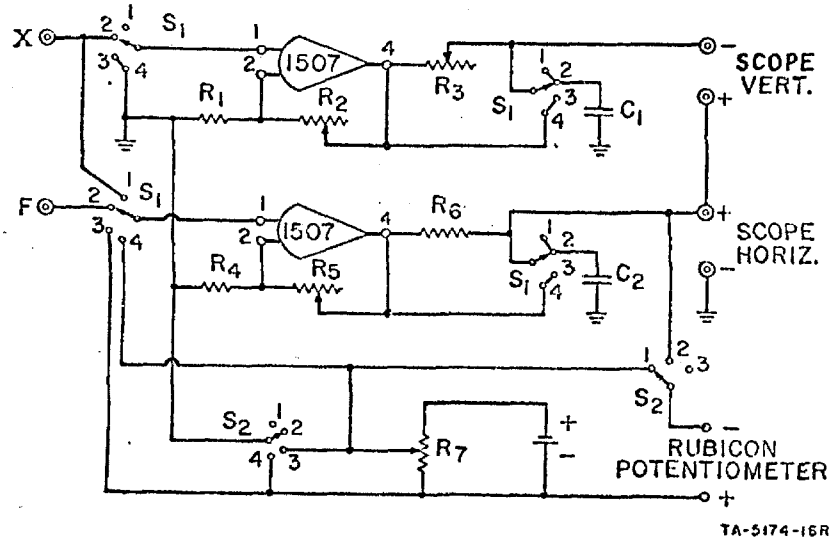
X
F
S1
S2
1507
R1
R2
R3
R4
R5
R6
R7
C1
C2
SCOPE VERT.
SCOPE HORIZ.
RUBICON POTENTIOMETER
TA-5174-16R

Fig. 6

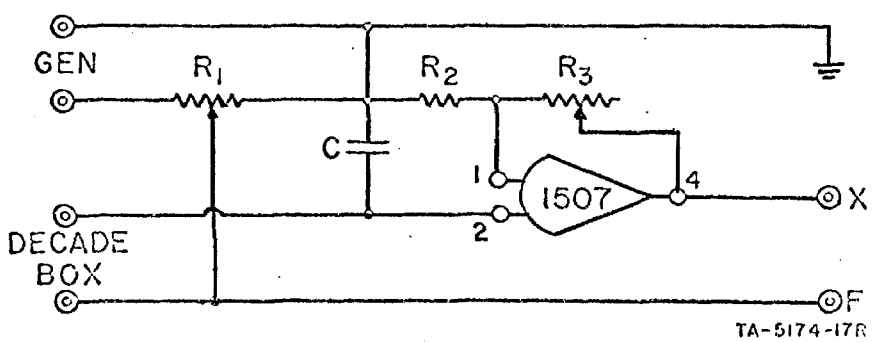
GEN
DECADE BOX
R1
R2
R3
C
1507
X
F
TA-5174-17R

Fig. 7

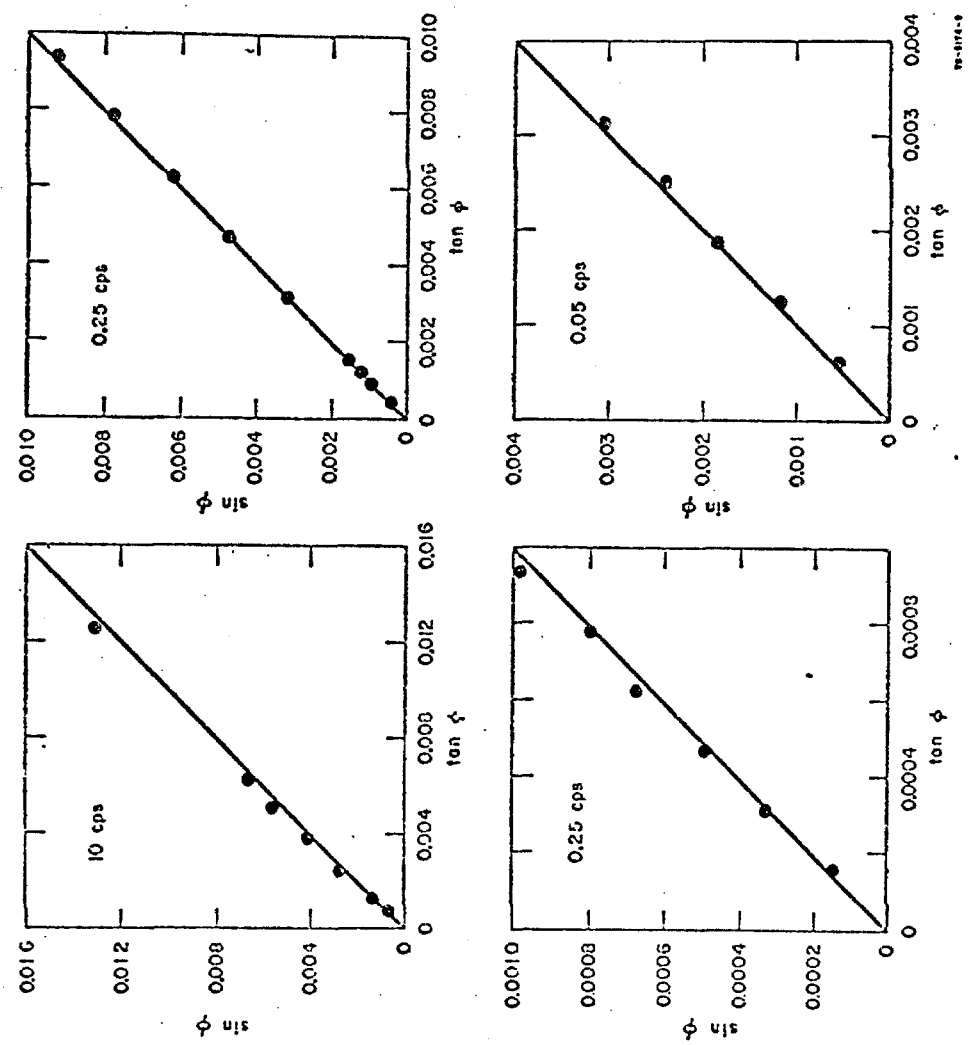
0.25 cps
sin φ
tan φ
0.010
0.008
0.006
0.004
0.002
0
0.002
0.004
0.006
0.008
0.010
0.05 cps
0.004
0.003
0.002
0.001
0.001
0.002
0.003
0.004
10 cps
0.016
0.012
0.008
0.004
0.004
0.008
0.012
0.016
0.25 cps
0.0010
0.0008
0.0006
0.0004
0.0002
0.0004
0.0008

Fig. 8

Appendix D

Characterization of Shell Research-Grade Block Copolymers

EXPERIMENTAL BLOCK COPOLYMERS

In recent years, there has been a great deal of interest in block copolymers which have the unique property of being both rubbers and thermoplastics. As a commercial manufacturer of these products, the Shell Chemical Company has received many requests for samples to be used for research. Three polymers have now been specially made and carefully characterized for this purpose.

All three polymers have the general configuration poly (styrene-b-butadiene-b-styrene)* and were synthesized by sequential anionic polymerization in a hydrocarbon solvent. Details of quite similar systems have been discussed in recent articles[2,3]. In these particular polymerizations, to keep the molecular weight distribution of the final polystyrene segments as narrow as possible, a small amount (about 0.3% volume of the total solution) of diethyl ether was added to the reaction mixture at the end of the butadiene polymerization[4]. This increases the ratio between the initiation rate and the propagation rate of the polymerization of the subsequent polystyrene segment. Polymerization of each segment was continued for greater than 10 half lives of the reaction before the next monomer increment was added, thus avoiding tapering of one segment into another.

The polymers were characterized by measuring the intrinsic viscosities of the first segments in toluene at 30°C and the styrene content of the subsequent materials by infrared spectroscopy. These values, together with the segmental molecular weights calculated from them, are given in Table I.

The molecular weight of the first (S1) segment was obtained from the intrinsic viscosity measurement using the relationship given in Table I. The molecular weight of the second (B) segment was obtained from the S1 molecular weight and the measured styrene content of the S1-B polymer by the relationship,

$$\bar{M}_B = \frac{\bar{M}_{S1}}{\phi_{S1-B}} - \bar{M}_{S1}$$

where ϕ_{S1-B} is the styrene content of the S1-B polymer and $\bar{M}_B$ and $\bar{M}_{S1}$ are the molecular weights of the B and S1 segments, respectively.

The molecular weight of the final (S2) segment was obtained from the molecular weight of the previous S1 segment and the measured styrene content of the S1-B and S1-B-S2 polymer by the relationship,

---

* The nomenclature is that of Ceresa[1].

1) R. J. Ceresa. "Block and Graft Copolymers", Butterworth, Inc., Washington, D. C. 1962.
2) R. Zelinski and C. W. Childers. Rubber Chem. and Tech. 41 161 (1968).
3) L. J. Felters. J. Poly. Sci. C26 1 (1969).
4) "Carbanions, Living Polymers and Electron Transfer Processes", M. Szwarc. Interscience Publishers, New York 1968, Chapter 7.

$$\bar{M}_{S2} = \bar{M}_{S1} \cdot \frac{\phi_{S1\text{-}B\text{-}S2} - \phi_{S1\text{-}B}}{(1-\phi_{S1\text{-}B\text{-}S2}) \cdot \phi_{S1\text{-}B}}$$

where $\phi_{S1\text{-}B\text{-}S2}$ is the styrene content of the final S-B-S polymer and $\bar{M}_{S2}$ is the molecular weight of the final polystyrene segment.

The intrinsic viscosities of the S1-B-S2 polymer was also measured and are given in Table I for reference purposes.

The relative amounts of cis 1,4, trans 1,4 and 1,2 addition in the butadiene portion of two polymers were measured by infrared spectroscopy and are also given in Table I. The other one is expected to be similar.

Stabilization and Purification

The polymers are essentially pure materials, containing only ~ 0.2% of Antioxidant 330**. If further purification is required for light scattering measurements, etc., they may be dissolved, filtered as required, and reprecipitated***.

If the polymers are to be exposed to relatively high temperature (> 100°C), it is suggested that up to 0.5% each of Plastanox LTDP**** and Antioxidant 330** be added. This can be done by dissolving and reprecipitating as previously described. Like other polymers containing unsaturation in the backbone chain, these materials can be degraded by excessive exposure to light. If prolonged exposure is necessary, they can be established by the addition of Tinuvin P*****.

Credit

The polymerization and characterization of these materials should be credited to Mr. A. R. Bean and Mrs. M. J. Papavasiliou, Elastomers Technical Center, Shell Chemical Company, Torrance, California.

These polymers were produced for research purposes and are not intended to be representative of commercial products.

** 1,3,5-Trimethyl-2,4-tris (3,5-di-tert-butyl-4-hydroxybenzyl) benzene, ex Ethyl Corporation.

*** Our usual procedure is to make a 10% solution of the polymer in cyclohexane and to add 1 volume of this solution to 5 volumes of well stirred methanol. The mixture is stirred for about one hour, the excess liquid decanted off and the precipitate filtered and vacuum dried. If it is desired to have n% of some additive (i.e., an antioxidant) in the dried polymer, then about 5 n gm/liter of this material should be dissolved in the methanol.

**** Dilaurylthiodipropionate, ex American Cyanamid Co.

***** 2(2' Hydroxy-5' methylphenol) benzotriazole, ex Geigy Chemical Company.

TABLE I

Characterization of Experimental Block Polymers

	Polymer Number		
	TR-41-1649	TR-41-1648	TR-41-1647
Intrinsic Viscosity, $[\eta]$, $Dl/gm^{a)}$			
$[\eta]_{S1}$	0.130	0.141	0.089
$[\eta]_{S1-B-S2}$	0.648	1.004	0.662
Styrene Content, ϕ, (Weight Fraction)			
ϕ_{S1-B}	0.319	0.170	0.164
$\phi_{S1-B-S2}$	0.482	0.293	0.268
Calculated Molecular Weights, $\bar{M}$ (in thousands)			
$\bar{M}_{S1}$ b)	14	16	7
$\bar{M}_{B}$	30	78	36
$\bar{M}_{S2}$	14	16	6
Polybutadiene Microstructure, (%)			
cis 1,4	-	41	44
trans 1,4	-	49	46
1,2	-	10	10

a) In toluene at 30°C.
b) Using the relationship $\log [\eta] = 0.648 \log \bar{M}_{S1} - 3.564$.

APPENDIX E

Data*

1. Storage and Loss Compliance Data of Low Molecular Weight (16,400) Polystyrene Used to Calculate the Polystyrene Contribution to the Time-Temperature Shifts of Block Copolymers.
2. Storage Compliance Data of Shell 16/78/16 (unannealed) used to Calculate the Polybutadiene Contribution to the Time-Temperature Shifts of Block Copolymers.
3. Raw Dynamic Compliance in Simple Compression Data for Shell 16/78/16 (annealed) as Determined with the Modified Melabs Rheometer.
4. Raw Dynamic Shear Compliance Data for NBS 10/30/10 as Determined with the Modified Melabs Rheometer.

*The data included here are presented in support of statements made in this thesis and in the hope that others can apply them.

1. Storage and loss compliance data of low molecular weight (16,400) polystyrene used to calculate the polystyrene contribution to the time-temperature shifts of block copolymers. These data were obtained by converting the shear creep compliance data of D. J. Plazek and J. M. O'Rourke (J. Poly. Sci., 9A2:209 (1971)) via the Maegawa-Yagii Technique. The reference temperature is 100.6°C. Compliances are in bars^{-1}.

Log ω	Log D'	Log D"
-3.4	-0.72	0.12
-3.2	-0.74	-0.08
-3.0	-0.83	-0.26
-2.8	-0.94	-0.43
-2.6	-1.11	-0.61
-2.4	-1.33	-0.78
-2.2	-1.61	-0.95
-2.0	-1.82	-1.13
-1.8	-2.02	-1.30
-1.6	-2.20	-1.48
-1.4	-2.35	-1.65
-1.2	-2.49	-1.83
-1.0	-2.62	-2.00
-0.8	-2.73	-2.18
-0.6	-2.83	-2.35
-0.4	-2.92	-2.63
-0.2	-2.99	-2.70
0	-3.05	-2.89
0.2	-3.10	-3.04
0.4	-3.15	-3.18
0.6	-3.20	-3.33
0.8	-3.25	-3.48
1.0	-3.29	-3.60
1.2	-3.32	-3.72
1.4	-3.35	-3.84
1.6	-3.38	-3.97
1.8	-3.40	-4.11
2.0	-3.42	-4.22
2.2	-3.43	-4.33
2.4	-3.435	-4.43
2.6	-3.44	-4.52
2.8	-3.444	-4.61
3.0	-3.448	-4.70
3.2	-3.451	-4.78
3.4	-3.454	-4.84
3.6	-3.457	-4.90
3.8	-3.46	-4.95

For frequencies higher than log $\omega = 3.8$,

$$\log D'(\omega) = -3.46 - 0.014 \cdot (\omega - 3.8)$$

and

$$\log D''(\omega) = -4.95 - 0.014 \cdot (\omega - 318)$$

2. Storage compliance data of Shell 16/78/16 (unannealed) used to calculate the polybutadiene contribution to the time-temperature shifts of block copolymers. These data are taken from Fig. 22 appearing in the text. The reference temperature is 0°C. Compliances are in bars^{-1}.

Below frequencies of

$\log \omega = 4.0$,

$\log D' = -2.3 - 0.039 \cdot (\log \omega - 4.0)$

Log ω	Log D'
4.0	-2.30
4.2	-2.31
4.4	-2.325
4.6	-2.335
4.8	-2.35
5.0	-2.375
5.2	-2.40
5.4	-2.425
5.6	-2.47
5.8	-2.505
6.0	-2.565
6.2	-2.64
6.4	-2.71
6.6	-2.81
6.8	-2.91
7.0	-3.01
7.2	-3.10
7.4	-3.215
7.6	-3.35
7.8	-3.47
8.0	-3.57
8.2	-3.68
8.4	-3.765
8.6	-3.845
8.8	-3.93
9.0	-4.01
9.2	-4.06
9.4	-4.13
9.6	-4.165
9.8	-4.19
10.0	-4.215
10.2	-4.24
10.4	-4.26
10.6	-4.28

3. Raw dynamic compliance in simple compression data for Shell 16/78/16 (annealed) as determined with the Modified Melabs Rheometer. Compliances are in $bars^{-1}$.

undeformed dimensions of specimen:

in direction of strain: 0.404 cm

cross-sectional area: 0.176 cm^2

RUN NUMBER 254 TEMPERATURE 86.44 C

LOG OMEGA	LOG D'	LOG D''
3.767	-2.141	-3.028
3.598	-2.132	-3.006
3.400	-2.112	-2.987
3.099	-2.083	-2.946
3.099	-2.077	-2.945
2.798	-2.063	-2.935
2.598	-2.042	-2.903
2.400	-2.033	-2.901
2.099	-1.999	-2.887
1.798	-1.974	-2.889
1.598	-1.957	-2.864
1.400	-1.923	-2.818
1.099	-1.916	-2.797
0.798	-1.899	-2.727
0.598	-1.877	-2.695
0.400	-1.867	-2.654
0.099	-1.514	-2.512

RUN NUMBER 253 TEMPERATURE 82.15 C

LOG OMEGA	LOG D'	LOG D''
3.780	-2.150	-3.042
3.598	-2.139	-3.028
3.400	-2.123	-2.994
3.099	-2.097	-2.975
2.798	-2.066	-2.946
2.598	-2.053	-2.921
2.400	-2.035	-2.925
2.200	-2.022	-2.926
2.002	-2.005	-2.924
1.798	-1.984	-2.913
1.598	-1.971	-2.930
1.400	-1.963	-2.925
1.200	-1.955	-2.911
1.002	-1.933	-2.883
0.798	-1.919	-2.858
0.598	-1.904	-2.821
0.400	-1.890	-2.741
0.200	-1.879	-2.725
0.002	-1.872	-2.724

RUN NUMBER 252 TEMPERATURE 77.02 C

LOG OMEGA	LOG D'	LOG D''
3.786	-2.167	-3.098
3.598	-2.154	-3.074
3.400	-2.137	-3.060
3.099	-2.114	-3.030
3.099	-2.109	-3.016
2.798	-2.090	-3.005
2.598	-2.049	-2.958
2.400	-2.058	-2.967
2.200	-2.032	-2.950
2.002	-2.028	-2.966
1.798	-2.010	-2.971
1.598	-1.998	-2.983
1.400	-1.990	-2.987
1.099	-1.958	-2.943
0.798	-1.955	-2.918
0.598	-1.916	-2.866
0.400	-1.912	-2.844
0.200	-1.891	-2.798
0.002	-1.905	-2.800

RUN NUMBER 251 TEMPERATURE 68.00 C

LOG OMEGA	LOG D'	LOG D''
3.786	-2.172	-3.152
3.598	-2.164	-3.096
3.400	-2.145	-3.085
3.099	-2.131	-3.059
2.798	-2.104	-3.030
2.598	-2.093	-3.018
2.400	-2.077	-3.002
2.200	-2.060	-2.986
2.002	-2.047	-2.993
1.798	-2.028	-2.996
1.598	-2.006	-2.983
1.400	-1.996	-3.012
1.200	-1.986	-3.020
1.002	-1.972	-3.023
0.798	-1.937	-3.000
0.598	-1.942	-3.001
0.400	-1.936	-2.956
0.200	-1.914	-2.917

RUN NUMBER 250 TEMPERATURE 60.98 C

LOG OMEGA	LOG D'	LOG D''
3.778	-2.188	-3.175
3.598	-2.175	-3.139
3.400	-2.158	-3.139
3.099	-2.142	-3.120
2.798	-2.116	-3.086
2.598	-2.108	-3.074
2.400	-2.096	-3.058
2.200	-2.078	-3.037
2.002	-2.069	-3.031
1.798	-2.046	-3.033
1.598	-2.031	-3.051
1.400	-2.018	-3.074
1.099	-2.003	-3.068
0.798	-1.988	-3.083
0.598	-1.973	-3.059
0.400	-1.969	-3.035
0.099	-1.949	-2.987

RUN NUMBER 249 TEMPERATURE 56.94 C

LOG OMEGA	LOG D'	LOG D''
3.785	-2.188	-3.170
3.598	-2.174	-3.140
3.400	-2.161	-3.131
3.099	-2.139	-3.117
2.798	-2.120	-3.105
2.598	-2.109	-3.083
2.400	-2.100	-3.071
2.099	-2.074	-3.040
1.798	-2.048	-3.037
1.598	-2.036	-3.057
1.400	-2.025	-3.061
1.099	-2.008	-3.083
0.798	-1.990	-3.118
0.598	-1.973	-3.070
0.400	-1.972	-3.038
0.200	-1.951	-3.019
0.002	-1.949	-2.988

RUN NUMBER 229 TEMPERATURE 49.74 C

LOG OMEGA	LOG D'	LOG D''
3.774	-2.178	-3.166
3.598	-2.169	-3.162
3.400	-2.165	-3.169
3.099	-2.141	-3.154
2.798	-2.125	-3.140
2.598	-2.121	-3.138
2.400	-2.197	-3.119
2.200	-2.092	-3.111
2.002	-2.074	-3.069
1.798	-2.068	-3.118
1.598	-2.055	-3.092
1.400	-2.030	-3.083
1.200	-2.026	-3.086
1.002	-1.989	-3.047
0.798	-2.008	-3.111
0.400	-1.983	-3.054
0.200	-1.975	-3.037
3.099	-2.142	-3.157

RUN NUMBER 230 TEMPERATURE 44.38 C

LOG OMEGA	LOG D'	LOG D''
3.776	-2.190	-3.178
3.598	-2.178	-3.189
3.400	-2.171	-3.182
3.099	-2.146	-3.176
2.798	-2.132	-3.168
2.598	-2.118	-3.143
2.400	-2.105	-3.132
2.200	-2.097	-3.117
2.002	-2.082	-3.092
1.798	-2.076	-3.090
1.598	-2.055	-3.083
1.400	-2.045	-3.099
1.200	-2.032	-3.101
1.002	-2.027	-3.116
0.798	-2.009	-3.124
0.598	-2.003	-3.140
0.400	-1.996	-3.105
0.200	-1.983	-3.078
0.002	-1.962	-3.039
-0.202	-1.965	-3.055

RUN NUMBER 231 TEMPERATURE 40.00 C

LOG OMEGA	LOG D'	LOG D''
3.776	-2.181	-3.169
3.606	-2.173	-3.164
3.400	-2.159	-3.168
3.099	-2.143	-3.163
2.798	-2.127	-3.143
2.598	-2.119	-3.138
2.400	-2.108	-3.117
2.200	-2.095	-3.101
2.002	-2.078	-3.086
1.798	-2.066	-3.063
1.598	-2.054	-3.059
1.400	-2.036	-3.061
1.200	-2.026	-3.075
1.002	-2.019	-3.087
0.798	-2.005	-3.098
0.598	-1.994	-3.094
0.400	-1.986	-3.088
0.200	-1.974	-3.114
0.002	-1.967	-3.120
-0.202	-1.951	-3.115

RUN NUMBER 234 TEMPERATURE 24.64 C

LOG OMEGA	LOG D'	LOG D''
3.798	-2.199	-3.174
3.598	-2.182	-3.177
3.400	-2.172	-3.213
3.099	-2.155	-3.202
2.798	-2.134	-3.186
2.798	-2.136	-3.185
2.400	-2.118	-3.161
2.196	-2.097	-3.128
2.002	-2.091	-3.127
1.798	-2.080	-3.116
1.598	-2.067	-3.093
1.400	-2.056	-3.080
1.200	-2.035	-3.075
1.002	-2.020	-3.053
0.798	-2.001	-3.052
0.598	-1.994	-3.061
0.400	-2.015	-3.064
0.200	-1.990	-3.038
0.002	-1.976	-2.992
-0.202	-1.964	-3.025
2.598	-2.129	-3.168

RUN NUMBER 236 TEMPERATURE 17.41 C

LOG OMEGA	LOG D'	LOG D''
3.798	-2.205	-3.181
3.598	-2.191	-3.180
3.400	-2.173	-3.220
3.099	-2.166	-3.218
2.798	-2.144	-3.218
2.598	-2.146	-3.226
2.400	-2.131	-3.185
2.400	-2.120	-3.185
1.798	-2.099	-3.184
1.598	-2.068	-3.106
1.200	-2.047	-3.084
1.002	-2.030	-3.070

RUN NUMBER 235 TEMPERATURE 12.04 C

LOG OMEGA	LOG D'	LOG D''
3.798	-2.208	-3.184
3.598	-2.194	-3.193
3.400	-2.182	-3.215
3.099	-2.168	-3.227
2.798	-2.149	-3.208
2.400	-2.134	-3.205
2.196	-2.114	-3.179
2.002	-2.108	-3.172
1.798	-2.100	-3.145
1.598	-2.077	-3.130
1.400	-2.077	-3.100
1.200	-2.074	-3.112
1.002	-2.040	-3.050
0.798	-2.044	-3.063
0.598	-2.011	-3.014
0.400	-2.006	-3.048
0.200	-1.990	-3.037
0.002	-2.002	-3.044
-0.202	-2.016	-3.051

RUN NUMBER 237 TEMPERATURE 5.32 C

LOG OMEGA	LOG D'	LOG D''
3.798	-2.226	-3.188
3.598	-2.206	-3.194
3.400	-2.196	-3.222
3.099	-2.178	-3.240
2.798	-2.166	-3.244
2.798	-2.159	-3.250
2.196	-2.130	-3.209
2.002	-2.125	-3.208
1.798	-2.113	-3.181
1.598	-2.097	-3.176
1.400	-2.087	-3.140
1.200	-2.080	-3.111
1.002	-2.056	-3.090
0.798	-2.051	-3.058
0.598	-2.041	-2.992
0.400	-2.016	-3.037
0.200	-2.008	-3.040
0.200	-2.024	-3.074
0.200	-2.019	-3.069
2.400	-2.145	-3.246
2.598	-2.154	-3.234

RUN NUMBER 239 TEMPERATURE -14.12 C

LOG OMEGA	LOG D'	LOG D''
3.798	-2.262	-3.159
3.598	-2.240	-3.135
3.400	-2.230	-3.195
3.099	-2.212	-3.246
2.798	-2.196	-3.290
2.598	-2.187	-3.295
2.400	-2.180	-3.305
2.196	-2.168	-3.296
2.002	-2.157	-3.296
1.798	-2.154	-3.292
1.598	-2.136	-3.280
1.400	-2.126	-3.262
1.200	-2.118	-3.230
1.002	-2.103	-3.201
0.798	-2.095	-3.170
0.598	-2.090	-3.148
0.400	-2.074	-3.109
0.200	-2.064	-3.141
0.002	-2.043	-3.145
3.798	-2.252	-3.139

RUN NUMBER 238 TEMPERATURE 1.18 C

LOG OMEGA	LOG D'	LOG D''
3.798	-2.230	-3.201
3.598	-2.216	-3.200
3.400	-2.199	-3.203
3.099	-2.183	-3.232
2.798	-2.165	-3.241
2.598	-2.161	-3.251
2.400	-2.151	-3.254
2.196	-2.137	-3.227
2.002	-2.127	-3.217
1.798	-2.119	-3.189
1.598	-2.102	-3.175
1.400	-2.094	-3.160
1.200	-2.079	-3.132
1.002	-2.071	-3.094
0.798	-2.053	-3.071

RUN NUMBER 240 TEMPERATURE -23.88 C

LOG OMEGA	LOG D'	LOG D''
3.794	-2.305	-3.028
3.598	-2.274	-3.076
3.400	-2.258	-3.126
3.099	-2.230	-3.199
2.798	-2.214	-3.262
2.598	-2.208	-3.300
2.400	-2.189	-3.305
2.200	-2.188	-3.315
2.002	-2.176	-3.323
1.798	-2.168	-3.318
1.598	-2.146	-3.307
1.400	-2.155	-3.300
1.200	-2.146	-3.279
1.200	-2.146	-3.279
1.002	-2.134	-3.256
0.798	-2.121	-3.237
0.598	-2.113	-3.210
0.400	-2.103	-3.163
0.200	-2.088	-3.149
0.002	-2.084	-3.117
-0.202	-2.052	-3.089
3.400	-2.256	-3.121

RUN NUMBER 241 TEMPERATURE -32.39 C

LOG OMEGA	LOG D'	LOG D''
3.790	-2.346	-2.925
3.598	-2.311	-2.981
3.400	-2.288	-3.040
3.099	-2.263	-3.130
2.798	-2.242	-3.213
2.598	-2.231	-3.253
2.400	-2.216	-3.274
2.200	-2.210	-3.311
2.002	-2.201	-3.325
1.798	-2.190	-3.339
1.598	-2.183	-3.349
1.400	-2.174	-3.338
1.200	-2.160	-3.320
1.002	-2.153	-3.306
1.002	-2.159	-3.315
0.798	-2.144	-3.281
0.598	-2.136	-3.251
0.400	-2.113	-3.202
0.200	-2.113	-3.160
0.002	-2.105	-3.169

RUN NUMBER 242 TEMPERATURE -44.90 C

LOG OMEGA	LOG D'	LOG D''
3.798	-2.519	-2.823
3.602	-2.448	-2.832
3.400	-2.395	-2.865
3.077	-2.326	-2.941
2.798	-2.286	-3.028
2.598	-2.272	-3.089
2.400	-2.251	-3.211
2.196	-2.241	-3.194
2.002	-2.230	-3.241
1.798	-2.216	-3.202
1.598	-2.210	-3.313
1.400	-2.194	-3.331
1.200	-2.190	-3.330
1.002	-2.179	-3.332
0.798	-2.153	-3.329
0.598	-2.150	-3.302

RUN NUMBER 243 TEMPERATURE -53.11 C

LOG OMEGA	LOG D'	LOG D''
3.798	-2.741	-2.907
3.598	-2.648	-2.856
3.400	-2.568	-2.832
3.077	-2.452	-2.837
2.798	-2.373	-2.868
2.598	-2.334	-2.932
2.400	-2.309	-2.980
2.200	-2.286	-3.052
2.002	-2.266	-3.113
1.798	-2.253	-3.180
1.598	-2.212	-3.228
1.400	-2.224	-3.264
1.200	-2.219	-3.296
1.002	-2.215	-3.314
0.798	-2.195	-3.314
0.598	-2.187	-3.316
0.400	-2.176	-3.279
0.200	-2.167	-3.285
0.002	-2.165	-3.292

RUN NUMBER 244 TEMPERATURE -59.58 C

LOG OMEGA	LOG D'	LOG D''
3.785	-3.011	-3.060
3.598	-2.905	-2.985
3.400	-2.778	-2.902
3.077	-2.649	-2.859
2.798	-2.528	-2.828
2.598	-2.446	-2.818
2.400	-2.406	-2.854
2.200	-2.364	-2.900
2.002	-2.322	-2.940
1.798	-2.297	-3.020
1.598	-2.279	-3.076
1.400	-2.267	-3.158
1.200	-2.261	-3.219
1.002	-2.230	-3.245
0.798	-2.223	-3.287
0.598	-2.216	-3.297
0.400	-2.213	-3.316
0.200	-2.210	-3.310
0.002	-2.165	-3.294

RUN NUMBER 245 TEMPERATURE -68.00 C

LOG OMEGA	LOG D'	LOG D''
3.799	-3.485	-3.446
3.598	-3.376	-3.338
3.400	-3.257	-3.240
3.081	-3.065	-3.093
2.798	-2.916	-2.993
2.598	-2.802	-2.921
2.400	-2.712	-2.882
2.200	-2.617	-2.849
2.002	-2.535	-2.832
1.798	-2.474	-2.840
1.598	-2.416	-2.866
1.400	-2.404	-2.944
1.200	-2.334	-2.976
1.002	-2.283	-3.011
0.798	-2.267	-3.057
0.400	-2.239	-3.103
0.200	-2.233	-3.176

RUN NUMBER 246 TEMPERATURE -78.06 C

LOG OMEGA	LOG D'	LOG D''
3.798	-4.027	-4.241
3.598	-3.972	-4.126
3.400	-3.969	-3.995
3.099	-3.757	-3.869
2.598	-3.554	-3.512
2.400	-3.431	-3.390
2.099	-3.251	-3.239
1.798	-3.069	-3.086
1.598	-2.954	-3.010
1.400	-2.828	-2.933
1.099	-2.684	-2.854
0.598	-2.471	-2.800
0.400	-2.410	-2.830
0.200	-2.359	-2.844
0.002	-2.303	-2.870

RUN NUMBER 247 TEMPERATURE -82.89 C

LOG OMEGA	LOG D'	LOG D''
3.977	-4.222	-4.777
3.798	-4.189	-4.715
3.598	-4.166	-4.604
3.400	-4.130	-4.503
3.099	-4.071	-4.344
2.798	-3.995	-4.166
2.598	-3.946	-4.029
2.400	-3.867	-3.911
2.099	-3.735	-3.724
1.798	-3.581	-3.534
1.598	-3.467	-3.402
1.400	-3.345	-3.290
1.099	-3.168	-3.137
0.798	-2.977	-3.013
0.598	-2.853	-2.931
0.400	-2.744	-2.878
0.200	-2.650	-2.816

4. Raw dynamic shear compliance data for NBS 10/30/10 as determined with the Modified Melabs Rheometer. Compliances are in bars^{-1}.

undeformed dimensions of specimen:

length: 0.866 cm

width: 0.554 cm

thickness: 0.188 cm

Run 149 T = 86.99 °C

Log ω	Log J'	Log J"
3.798	-2.219	-2.742
3.598	-2.178	-2.639
3.400	-2.134	-2.553
3.200	-2.090	-2.469
3.002	-2.039	-2.371
2.798	-1.991	-2.288
2.598	-1.940	-2.189
2.400	-1.886	-2.104
2.200	-1.821	-2.002
2.002	-1.743	-1.905
1.798	-1.675	-1.815
1.598	-1.598	-1.731
1.400	-1.517	-1.642
1.200	-1.420	-1.575
1.002	-1.338	-1.511
0.798	-1.250	-1.459
0.598	-1.173	-1.413
0.400	-1.111	-1.403
0.200	-1.056	-1.375
0.002	-0.995	-1.328

Run 148 T = 76.59 °C

Log ω	Log J'	Log J"
3.598	-2.376	-3.137
3.400	-2.352	-3.083
3.200	-2.328	-3.033
3.002	-2.305	-2.976
2.798	-2.285	-2.919
2.598	-2.258	-2.858
2.400	-2.232	-2.792
2.200	-2.201	-2.723
2.002	-2.151	-2.631
1.798	-2.125	-2.565
1.598	-2.085	-2.484
1.400	-2.040	-2.397
1.200	-1.996	-2.315
1.002	-1.945	-2.220
0.798	-1.893	-2.127
0.598	-1.831	-2.033
0.400	-1.766	-1.936
0.200	-1.690	-1.846
0.002	-1.618	-1.755

Run 147 T = 66.37 °C

Log ω	Log J'	Log J"
3.767	-2.438	-3.444
3.598	-2.424	-3.403
3.400	-2.406	-3.367
3.200	-2.394	-3.335
3.002	-2.380	-3.302
2.798	-2.364	-3.261
2.598	-2.344	-3.217
2.400	-2.325	-3.176
2.200	-2.313	-3.141
2.002	-2.294	-3.095
1.798	-2.280	-3.054
1.598	-2.260	-3.005
1.400	-2.238	-2.953
1.200	-2.219	-2.903
1.002	-2.193	-2.845
0.798	-2.168	-2.785
0.598	-2.141	-2.725
0.400	-2.114	-2.669
0.200	-2.080	-2.585
0.002	-2.052	-2.524
-0.202	-2.010	-2.448

Run 146 T = 57.25 °C

Log ω	Log J'	Log J"
3.598	-2.420	-3.525
3.400	-2.406	-3.495
3.200	-2.398	-3.474
3.002	-2.386	-3.444
2.798	-2.377	-3.424
2.598	-2.365	-3.396
2.400	-2.349	-3.368
2.200	-2.344	-3.351
2.002	-2.324	-3.318
1.598	-2.300	-3.259
1.400	-2.286	-3.229
1.200	-2.275	-3.197
1.002	-2.262	-3.149
0.798	-2.244	-3.106
0.598	-2.224	-3.067
0.400	-2.215	-3.037
0.200	-2.194	-2.993
0.002	-2.179	-2.949

Run 145 T = 44.52

Log ω	Log J'	Log J"
3.598	-2.426	-3.640
3.400	-2.419	-3.621
3.200	-2.406	-3.603
3.002	-2.406	-3.596
2.798	-2.396	-3.579
2.598	-2.384	-3.560
2.400	-2.377	-3.539
2.200	-2.367	-3.518
2.002	-2.361	-3.505
1.798	-2.350	-3.486
1.598	-2.344	-3.469
1.400	-2.333	-3.440
1.200	-2.325	-3.425
1.002	-2.309	-3.391
0.798	-2.299	-3.363
0.598	-2.292	-3.341
0.400	-2.278	-3.306
0.200	-2.272	-3.285
0.002	-2.256	-3.251
-0.202	-2.246	-3.226

Run 144 T = 29.53 °C

Log ω	Log J'	Log J"
3.598	-2.430	-3.730
3.400	-2.423	-3.730
3.200	-2.414	-3.726
3.002	-2.411	-3.723
2.798	-2.406	-3.717
2.598	-2.400	-3.704
2.400	-2.395	-3.695
2.200	-2.389	-3.680
2.002	-2.383	-3.667
1.798	-2.376	-3.654
1.598	-2.367	-3.634
1.400	-2.361	-3.623
1.200	-2.357	-3.606
1.002	-2.348	-3.584
0.798	-2.343	-3.566
0.598	-2.336	-3.540
0.400	-2.330	-3.515
0.200	-2.320	-3.478
0.002	-2.313	-3.441
-0.202	-2.302	-3.407

Run 131 T = 29.74 °C

Log ω	Log J'	Log J"
3.786	-2.491	-3.783
3.598	-2.469	-3.780
3.400	-2.464	-3.779
3.200	-2.454	-3.775
3.002	-2.451	-3.774
2.798	-2.446	-3.764
2.598	-2.440	-3.748
2.400	-2.435	-3.736
2.200	-2.429	-3.719
2.002	-2.423	-3.697
1.798	-2.415	-3.678
1.598	-2.406	-3.656
1.400	-2.404	-3.641
1.200	-2.386	-3.618
1.002	-2.377	-3.595
0.798	-2.369	-3.574
0.598	-2.363	-3.559
0.400	-2.352	-3.529
0.200	-2.346	-3.502
0.002	-2.338	-3.478

Run 132 T = 19.60 °C

Log ω	Log J'	Log J"
3.794	-2.543	-3.893
3.598	-2.528	-3.886
3.400	-2.521	-3.893
3.200	-2.516	-3.906
3.002	-2.511	-3.908
2.798	-2.507	-3.907
2.598	-2.506	-3.906
2.400	-2.496	-3.892
2.200	-2.492	-3.878
2.002	-2.485	-3.859
1.798	-2.481	-3.843
1.598	-2.476	-3.834
1.400	-2.476	-3.823
1.200	-2.467	-3.804
1.002	-2.464	-3.790
0.798	-2.455	-3.767
0.598	-2.450	-3.744
0.400	-2.442	-3.718
0.200	-2.437	-3.696
0.002	-2.429	-3.665
-0.202	-2.424	-3.635

Run 133 T = 9.56 °C

Log ω	Log J'	Log J"
3.794	-2.596	-3.940
3.598	-2.580	-3.940
3.400	-2.573	-3.945
3.200	-2.569	-3.954
3.002	-2.563	-3.968
2.798	-2.561	-3.972
2.598	-2.554	-3.970
2.400	-2.552	-3.969
2.200	-2.548	-3.965
2.002	-2.545	-3.955
1.798	-2.542	-3.947
1.598	-2.534	-3.937
1.400	-2.528	-3.925
1.200	-2.527	-3.918
1.002	-2.522	-3.898
0.798	-2.517	-3.883
0.598	-2.513	-3.864
0.400	-2.509	-3.843
0.200	-2.504	-3.821
0.002	-2.497	-3.790
-0.202	-2.493	-3.762

Run 134 T = 0.03 °C

Log ω	Log J'	Log J"
3.796	-2.642	-3.955
3.598	-2.627	-3.957
3.400	-2.630	-3.975
3.200	-2.624	-3.992
3.002	-2.619	-4.008
2.798	-2.613	-4.019
2.598	-2.612	-4.032
2.400	-2.609	-4.039
2.200	-2.602	-4.033
2.002	-2.598	-4.033
1.798	-2.589	-4.023
1.598	-2.583	-4.010
1.400	-2.581	-4.012
1.200	-2.578	-3.999
1.002	-2.571	-3.988
0.798	-2.566	-3.971
0.598	-2.562	-3.957
0.400	-2.560	-3.943
0.200	-2.557	-3.923
0.002	-2.553	-3.900
-0.202	-2.546	-3.863

Run 135 T = -10.22 °C

Log ω	Log J'	Log J"
3.785	-2.683	-3.940
3.598	-2.671	-3.952
3.400	-2.669	-3.975
3.200	-2.660	-3.988
3.002	-2.659	-4.011
2.798	-2.653	-4.027
2.598	-2.651	-4.047
2.400	-2.650	-4.061
2.200	-2.643	-4.070
2.002	-2.640	-4.075
1.798	-2.634	-4.077
1.598	-2.630	-4.074
1.400	-2.625	-4.066
1.200	-2.622	-4.066
1.002	-2.619	-4.053
0.798	-2.616	-4.046
0.598	-2.613	-4.034
0.400	-2.609	-4.018
0.200	-2.606	-3.996
0.002	-2.599	-3.967

Run 138 T = -34.83 °C

Log ω	Log J'	Log J"
3.798	-2.581	-3.561
3.598	-2.561	-3.571
3.400	-2.545	-3.594
3.200	-2.538	-3.633
3.002	-2.531	-3.669
2.798	-2.523	-3.709
2.598	-2.517	-3.739
2.400	-2.514	-3.770
2.200	-2.510	-3.796
2.002	-2.506	-3.823
1.798	-2.498	-3.839
1.598	-2.494	-3.853
1.400	-2.491	-3.869
1.200	-2.488	-3.873
1.002	-2.485	-3.879
0.798	-2.484	-3.878
0.598	-2.476	-3.864
0.400	-2.474	-3.857
0.002	-2.472	-3.830
0.200	-2.474	-3.845

Run 141 T = -58.01 °C

Log ω	Log J'	Log J"
3.798	-2.688	-3.368
3.598	-2.655	-3.359
3.400	-2.632	-3.366
3.200	-2.611	-3.381
3.002	-2.590	-3.397
2.798	-2.576	-3.432
2.598	-2.559	-3.458
2.400	-2.549	-3.488
2.200	-2.537	-3.517
2.002	-2.527	-3.551
1.798	-2.518	-3.581
1.598	-2.514	-3.616
1.400	-2.502	-3.636
1.200	-2.497	-3.659
1.002	-2.488	-3.672
0.798	-2.484	-3.684
0.598	-2.478	-3.693
0.400	-2.474	-3.695
0.200	-2.467	-3.704
0.002	-2.463	-3.691

Run 142 T = -80.91 °C

Log ω	Log J'	Log J"
3.598	-2.950	-3.784
3.400	-2.939	-3.627
3.400	-2.934	-3.722
3.200	-2.917	-3.663
3.002	-2.896	-3.601
2.798	-2.879	-3.543
2.598	-2.855	-3.488
2.400	-2.825	-3.435
2.200	-2.792	-3.392
2.002	-2.764	-3.366
1.798	-2.737	-3.366
1.400	-2.668	-3.356
1.200	-2.645	-3.366
1.002	-2.636	-3.387
0.798	-2.604	-3.386
0.598	-2.592	-3.402
0.400	-2.578	-3.409
0.200	-2.564	-3.404
0.002	-2.551	-3.478
-0.202	-2.541	-3.492

Run 143 T = -71.13 °C

Log ω	Log J'	Log J"
3.798	-2.862	-3.411
4.002	-2.907	-3.484
3.598	-2.826	-3.371
3.400	-2.793	-3.350
3.200	-2.741	-3.322
3.002	-2.714	-3.328
2.598	-2.661	-3.349
2.400	-2.639	-3.365
2.200	-2.617	-3.379
2.002	-2.603	-3.404
1.798	-2.586	-3.427
1.598	-2.570	-3.452
1.400	-2.557	-3.476
1.200	-2.546	-3.504
1.002	-2.535	-3.531
0.798	-2.524	-3.556
0.598	-2.514	-3.588
0.400	-2.509	-3.612
0.200	-2.502	-3.630
0.002	-2.495	-3.643
-0.202	-2.489	-3.640

PROPOSITION I

INSTABILITY OF THE Z-FORM NUMERICAL METHOD OF INVERSE LAPLACE TRANSFORMATION FOR LARGE TIME INCREMENTS

Abstract

The strength of the Z-form numerical method of determining the inverse Laplace transform lies in being able to treat Laplace fractions of high order since the method does not require the evaluation of the roots of the characteristic equation. The technique becomes very accurate as smaller time increments are taken. Interest in the real time response, however, may very well lie in the long time response, and one may want to use large time increments to reduce computational errors or simply to make the scheme more economical.

The proposition is made that large time increments generally cannot be used for the Z-form method because of instability deriving from the presence of short time contributions to the response. An analysis of this instability is presented.

Laplace Inversion by the Z-Form Numerical Technique

A technique for numerically making the inverse Laplace transformation has been presented by Boxer and Thaler (1) and further discussed by Gibson (2). The inverse Laplace integral is first approximated by a finite integral

$$f(t) = \frac{1}{2\pi i} \int_{-i\infty}^{i\infty} F(s)\, e^{st}\, ds \cong \frac{1}{2\pi i} \int_{-i\pi/T}^{i\pi/T} f(s)\, e^{st}\, ds \qquad (1)$$

Letting $t = nT$ and substituting $z = e^{Ts}$

$$f(nT) = \frac{1}{2\pi i} \oint \frac{1}{T}\, F(\ell n\, z/T)\, z^{n-1}\, dz \qquad (2)$$

The contour on the s-plane goes over to a unit circle on the z-plane. The contour is closed so that the integral can be found by the residue theorem. First, however, an approximation is made for $\ell n\, z$ which gives rise to the z-forms tabulated by Boxer and Thaler and Gibson. For reasons of convergence, the z-forms are substituted for negative powers of s; and the resulting expression, $\overline{f(z)}$, is arranged as a fraction with polynomials of z^{-1} forming the numerator and denominator. Instead of computing the residues directly, the fraction is expanded in ascending powers of z^{-1}. The coefficients of these terms automatically become f(nT), the constant term giving f(0); the coefficient of z^{-1}, f(T); the coefficient of z^{-2}, f(2T); and so on. Barring computational round-off error, this method becomes more accurate with smaller time increments (T). The technique is well suited to computer computations, and in the course of this study, the author has developed a Fortran subroutine to do this.

The Z-Form Method at Long Times

As described above, the Z-form method numerically generates the inverse Laplace transform at discrete intervals starting at zero time. Occasionally it is desirable to examine the inverse transform at long times, particularly in the case of high order Laplace functions. Since the use of a small time interval in the numerical procedure may result in too much accumulated error due to repeated round-off or truncation, or perhaps simply too much computation time, the question arises of what consequences are brought about by the use of a large time interval. Ideally, those factors which determine the short time response could be made negligible. Consider, then, the effect of using time increments (T) that are large compared to the small time constants of terms making up F(s).

First, one can examine the approximation of truncating the Laplace integral in Eq. (1) as T becomes large. Two cases should be considered-- a negative real pole and a pole at zero. For a negative pole, one can start with the expression

$$f(t) = \mathcal{L}^{-1}\left\{f(s)\right\} \cong \frac{1}{2\pi i}\int_{-i\pi/T}^{i\pi/T} \frac{e^{st}}{s+a}\,ds \qquad (3)$$

Making the substitution $y = s + a$

$$f(t) = \frac{e^{-at}}{2\pi i}\int_{-a-i\pi/T}^{-a+i\pi/T} \frac{e^{yt}}{y}\,dy \qquad (4)$$

This integral can be represented by an infinite series

$$f(t) = \frac{e^{-at}}{2\pi}\left[\log y + yt + \frac{(yt)^2}{2\cdot 2!} + \frac{(yt)^3}{3\cdot 3!} + \cdots\right]_{y=-a-\frac{i\pi}{T}}^{y=-a+\frac{i\pi}{T}} \qquad (5)$$

The series converges faster than an exponential, so one would expect $f(t)$ to vanish as T gets large, remembering that $t = nT$, so that it should make little contribution at long times. Treating the pole at zero is a little more difficult. It can be considered by deforming the usual contour, shown as A in Fig. 1 into the semicircle shown as contour B.

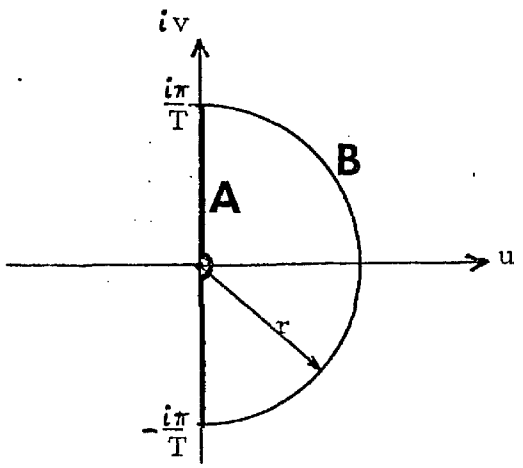

Fig. 1. Pole at $s = 0$.

The integrals are equal. Letting $s = re^{i\theta}$, where $r = \pi/T$,

$$f(t) = f(nT) \cong \frac{1}{2\pi i}\int_{-\pi/2}^{\pi/2} \frac{e^{nTre^{i\theta}}}{re^{i\theta}}\, ire^{i\theta}\, d\theta$$

$$\cong \frac{1}{2\pi}\int_{-\pi/2}^{\pi/2} e^{n\pi e^{i\theta}}\, d\theta$$

Taking absolute values,

$$\left| \frac{1}{2\pi} \int_{-\pi/2}^{\pi/2} e^{n\pi(\cos\theta + i\sin\theta)}\, d\theta \right| \leq \frac{1}{\pi} \int_{0}^{\pi/2} e^{n\pi\cos\theta}\, d\theta$$

$$< \frac{1}{\pi} \int_{0}^{1} e^{n\pi(1-x^2)}\, dx$$

$$< \operatorname{erf}(1)\, \frac{e^{n}}{\pi\sqrt{n\pi}}$$

Thus, we might expect the effect of a pole at zero on the calculated response to die out slightly faster than an exponential of n. This looks promising, but there are other facets of the z-form method that are worth considering.

Let us treat three individual cases.

Case 1. $F(s) = s^{-1}$; single pole at zero

From Gibson, $\bar{f}(z^{-1}) = \frac{T}{2}\,(1+z^{-1})/(1-z^{-1})$

Then $f(nT) = \frac{1}{2\pi i} \oint \frac{1}{2}\left[(1+z^{-1})\, z^{n-1}/(1-z^{-1})\right] dz$

$$= \frac{1}{2}\, R\left\{(z+1)\, z^{n-1}/(z-1)\right\}_{z=1} = 1 \text{ independent of } T\,.$$

where $R\{\bar{f}(z)\}$ indicates the evaluation of residues.

Case 2. $F(s) = (as + 1)^{-1}$; single negative pole

$$\overline{f(z)} = \frac{T}{2}\,(1+z^{-1})/[(1-z^{-1})a + \frac{T}{2}\,(1+z^{-1})] \approx 1 \text{ as } T \to \infty$$

Then $f(nT) \cong \frac{1}{2\pi i} \oint z^{n-1}/T\ dz \to 0$ as $T \to \infty$.

Case 3. $F(s) = (as^2 + s)^{-1}$

$$\overline{f(z)} = \frac{T^2}{12}\,(1+10z^{-1}+z^{-2})/[a(1-z^{-1})^2 + \frac{T}{2}\,(1+z^{-1})(1-z^{-1})]$$

$$\approx \frac{T}{6}\,(z^2+10z+1)/(z^2-1) \text{ as } T \to \infty$$

Evaluating residues, $f(nT) \cong 1 + \frac{2}{3}\,(-1)^{n-1}$ as $T \to \infty$.

These three cases treat simple z-form approximations to the Laplace inversion when the time increment is taken to be large. Instead of expanding $\overline{f(z)}$, however, its poles are found so that a closed form of the solution can be evaluated from the residues. Case 1 treats a single pole in the s-plane at $s = 0$. This is a unit step function in time and is seen to transform well. Case 2 treats a single negative pole and the contribution of this term is seen to vanish like $1/T$ as T becomes large. This is not as fast as the exponential decay that should appear, but it would probably be sufficient for many applications. In Case 3, which represents the combination of Cases 1 and 2, one sees that the solution is oscillatory and will not decay.

In general, z-forms are substituted for powers of (s^{-1}). For a term s^{-n}, the z-form appears as

$$\frac{T^n}{k_n}\,\frac{N_n(z^{-1})}{(1-z^{-1})^n} \qquad (6).$$

where k_n is a constant and $N_n(z^{-1})$ is a polynomial of z^{-1} in which the highest order term is z^{-n}. Thus, if $F(s)$ is a single fraction with polynomials of s^{-1} (or of s) in the numerator and denominator, and we let T be large, only the highest order terms (in s^{-1}) will be important after substitution of the z-forms. We can therefore discuss two

general cases, keeping only the highest order terms in s^{-1}.

Case 4.

$$F(s) = \frac{1 + \cdots\cdots + s^{m-1}}{1 + \cdots\cdots + s^{m}} \cong \frac{s^{-m}}{s^{-m}}$$

Then $\overline{f(z)} \cong 1$

and $f(nT) \to 0$ like $\frac{1}{T}$ as $T \to \infty$.

Case 5.

$$F(s) = \frac{1 + \cdots\cdots + s^{m-1}}{s + \cdots\cdots + s^{m}} \cong \frac{s^{-m}}{s^{-m+1}}$$

Then $\overline{f(z)} \cong \frac{k_m T}{k_{m-1}} \frac{N_m(z^{-1})}{(1-z^{-1})\, N_{m-1}(z^{-1})}$

and $f(nT) \cong \oint \frac{N_m(z^{-1})\ z^{n-1}}{(1-z^{-1})\, N_{m-1}(z^{-1})}\, dz$, neglecting the k_i's.

In the two cases shown above, F(s) has a numerator which is a polynomial of s of smaller order than the denominator. This is true of almost any physical problem. Case 4 includes Case 2 as a special case. Both numerator and denominator have a constant term, 1, so that clearing the fraction of positive powers of s results in a fraction with the highest power of s^{-1} in both the numerator and the denominator. In substituting the z-forms, the numerator and denominator approach one another as T gets large. We are then left with the same situation as Case 2 in which the integral approaches zero like 1/T. If the numerator is missing the constant term, one can see that the resulting z-form approximation will go to zero even faster.

Case 5 includes Case 3 as a special case. F(s) has a pole at s = 0; or in other words, the denominator of F(s) is missing the constant term while the numerator still has it. As a result, z-form substitution yields a numerator withe T raised to one power higher than the denominator. This T cancels with the 1/T in the integral in Eq. (2) leaving no T dependence. It is now necessary to consider the poles of $\overline{f(z)}$. If any of the poles have real parts that are greater in absolute value than unity, the z^{n-1} term in the integral will cause exponential growth. By examining the numerators of the first few z-forms given in Gibson, one can say that usually there will be poles of this type. In fact, the z-forms for s^{-1} and s^{-3} are probably the only ones that do not cause exponential growth under these circumstances; s^{-1} is of trivial importance and s^{-3} imparts an oscillatory nature to the result as shown in Case 3. This applies well to the practical example presented by Boxer and Thaler. For illustration, they provide a very well behaved function

$$F(s) = \frac{1}{s + s^2 + s^3}$$

When the preceeding analysis is applied to this problem, the response becomes for large T

$$f(nT) = \frac{1}{6}\left[1 - \frac{1}{2}(-5 + 2\sqrt{6})^n - \frac{1}{2}(-5-2\sqrt{6})^n\right]$$

One can see that the third term in the expression grows exponentially in n and that f(nT) will change sign with each successive n.

Theoretically, the z-form method should still work, since the contour for the integral in Eq. (2) is taken on the unit circle. The poles outside the contour should not be counted. In the numerical treatment however, everything is included, causing the approximation to "blow up." One can see that exponential growth will normally result from these unwanted poles and the 1/T decay seen in Case 4 will certainly not be able to overcome this.

The preceeding discussion takes T large relative to the total real time response. In a practical application one would be interested in a choice for T that is small relative to the large time constants involved, but larger (though perhaps not much larger) than the smallest time constants. The result would be the same. Poles in the s-plane that lie outside the contour which should not be counted are indiscriminitely included in the numerical calculations, leading to instability.

A practical example which illustrates this unstable behavior lies in attempting to recover a real time viscoelastic function for a polymer from a Laplace expression that can arise in the process of interconversion from another viscoelastic function (3,4). The variation of the viscoelastic function typically covers many decades of time. By using various values for the time increment, T, in the z-form method, one can easily show varying degrees of instability that result.

References

1. R. Boxer, S. Thaler, "A Simplified Method of Solving Linear and Nonlinear Systems," Proc. IRE, 44:89(1956).

2. J. E. Gibson, Nonlinear Automatic Control, pp. 147-159, New York: McGraw-Hill(1963).

3. J. D. Ferry, Viscoelastic Properties of Polymers, New York: John Wiley(1961).

4. R. A. Schapery, "A Simple Collocation Method for Fitting Viscoelastic Models to Experimental Data," Contract No. AF33(616)-8399: GALCIT, SM 61-23 A, February, 1962.

PROPOSITION II

CHOOSING AN APPROXIMATION FOR CALCULATING THE RELAXATION SPECTRUM FROM STORAGE MODULUS DATA

Abstract

Tschoegl[1] has examined some approximation methods for deriving the relaxation spectrum from the storage modulus. He is able to derive various approximations by truncating an infinite series of logarithmic derivatives of the storage modulus. Truncation of the series after the r^{th} order logarithmic derivative results in r different approximations. He shows that for an odd order truncation one of the approximations is centered and symmetric while the other approximations are skewed and shifted in time. Even order truncations result in skewed and shifted approximations only.

It is proposed that the accuracy of these approximations is dependent upon the slope of the relaxation spectrum and that the choice of approximation, whether symmetric or skewed, should be made with regard to the slope of the spectrum.

Introduction*

In studying the mechanical behavior of viscoelastic materials, several loading patterns are needed. If stress is measured as the response to an imposed strain, the experiment is said to be of the relaxation type. The function obtained is a time or frequency dependent modulus. The time regime - independent function is known as the relaxation spectrum, $H(\tau)$, in which τ is the relaxation time; and it is related to the modulus by an integral equation. We are concerned here with the storage modulus, $G'(\omega)$, which is a measure of the stress in phase with the strain imposed as a sinusoidal deformation (ω is the frequency).

$G'(\omega)$ and $H(\tau)$ are related by the equation

$$G'(\omega) = \int_0^\infty H(\tau) \frac{\omega^2 \tau^2}{1 + \omega^2 \tau^2} \, d \ln \tau \qquad (1)$$

We assume that the relaxation spectrum can be represented by a series expansion in terms of logarithmic derivatives of the source function and that approximations to the spectrum can be made by truncating the series.

$$H_k'(\tau) = \sum_{i=1}^{k} a_i \frac{d^i G'(\omega)}{d \ln^i \omega} \Bigg|_{\omega = 1/\tau} \qquad (2)$$

---

* Tschoegl's derivations are beyond the scope of this paper; rather, they are merely summarized here. Details may be found in reference (1). The nomenclature adopted is the same as his in order to avoid confusion.

$H_k'(\tau)$ is the k^{th} approximation to the relaxation spectrum determined from $G'(\omega)$ by truncating the series after the k^{th} term. For practical reasons we are limited to two or three terms.

Changing the integration variable in Eq. (1) to θ, using $\omega = 1/\tau$, and substituting into Eq. (2) gives

$$H_k'(\tau) = \int_o^\infty H(\theta)\, I_k'(\theta/\tau)\, d\, \ell n\, \theta \qquad (3)$$

where,

$$I_k'(\theta/\tau) = \sum_{i=1}^{k} a_i \frac{d^i}{d\, \ell n^i\, \omega} \left[\frac{\theta^2 \omega^2}{1 + \theta^2 \omega^2} \right] \qquad (4)$$

$I_k'(\theta/\tau)$ is called the intensity function for the approximation. With the transformations $\theta = \exp z$ and $\tau = \exp n$, Eq. (3) becomes

$$\overline{H}_k'(n) = \int_{-\infty}^{\infty} \overline{H}(z)\, \overline{I}_k'(z-n)\, dz \qquad (5)$$

One easily sees that $\overline{H}_k'(n) = \overline{H}(n)$ if $\overline{I}_k'(z-n)$ is the delta function.

Tschoegl evaluates Eq. (4) to obtain intensity functions corresponding to the first three approximations and utilizes the normalization of the intensity function along with the condition that the intensity function can have only one maximum to evaluate the a_i's. The approximations are then obtained by substituting these coefficients into Eq. (2)

$$I_1'(\theta/\tau) = \frac{2\,\theta^2/\tau^2}{(1+\theta^2/\tau^2)^2} \tag{6a}$$

$$I_{2L}'(\theta/\tau) = \frac{4\,\theta^2/\tau^2}{(1+\theta^2/\tau^2)^3} \tag{6b}$$

$$I_{2R}'(\theta/\tau) = \frac{4\,\theta^4/\tau^4}{(1+\theta^2/\tau^2)^3} \tag{6c}$$

$$I_3'(\theta/\tau) = \frac{12\,\theta^4/\tau^4}{(1+\theta^2/\tau^2)^4} \tag{6d}$$

$$I_{3L}'(\theta/\tau) = \frac{6\,\theta^2/\tau^2}{(1+\theta^2/\tau^2)^4} \tag{6e}$$

$$I_{3R}'(\theta/\tau) = \frac{6\,\theta^6/\tau^6}{(1+\theta^2/\tau^2)^4} \tag{6f}$$

These intensity functions are plotted in Fig. 1. Functions (6a) and (6d) are symmetric and centered on log $(\theta/\tau) = 0$. I_{2R}' and I_{3R}' are shifted to the right and are slightly skewed although the skewness is not apparent in Fig. 1. I_{2L}' and I_{3L}' are mirror images of I_{2R}' and I_{3R}' respectively with the axis of reflection at log $(\theta/\tau) = 0$. The peak of I_{2R}' is at log $(\theta/\tau) = \log \sqrt{2}$ and that for I_{3R}' is at log $(\theta/\tau) = \log \sqrt{3}$. The median of I_{2R}' occurs at log $(\theta/\tau) = \log (1.553)$ and that of I_{3R}' is at log $(\theta/\tau) = \log (1.961)$.

In general, there are as many approximations for a truncation of the series as the order of the approximation. The approximations corresponding to the intensity functions in Eqs. (6) are:

$$H_1'(\tau) = \frac{d\,G'(\omega)}{d\,\ell n\,\omega}\Big|_{\omega = 1/\tau} \tag{7a}$$

$$H_{2L}'(\tau/\sqrt{2}) = \frac{d\,G'(\omega)}{d\,\ell n\,\omega} + \frac{1}{2}\frac{d^2 G'(\omega)}{d\,\ell n^2\,\omega}\Big|_{\omega = 1/\tau} \tag{7b}$$

$$H_{2R}'(\sqrt{2}\,\tau) = \frac{d\,G'(\omega)}{d\,\ell n\,\omega} - \frac{1}{2}\frac{d^2 G'(\omega)}{d\,\ell n^2\,\omega}\Big|_{\omega = 1/\tau} \tag{7c}$$

$$H_3'(\tau) = \frac{d\,G'(\omega)}{d\,\ell n\,\omega} - \frac{1}{4}\frac{d^3 G'(\omega)}{d\,\ell n^3\,\omega}\Big|_{\omega = 1/\tau} \tag{7d}$$

$$H_{3L}'(\tau/\sqrt{3}) = \frac{d.G'(\omega)}{d\,\ell n\,\omega} + \frac{3}{4}\frac{d^2 G'(\omega)}{d\,\ell n^2\omega} + \frac{1}{8}\frac{d^3 G'(\omega)}{d\,\ell n^3\,\omega}\Big|_{\omega = 1/\tau} \tag{7e}$$

$$H_{3R}'(\sqrt{3}\tau) = \frac{d\,G'(\omega)}{d\,\ell n\,\omega} - \frac{3}{4}\frac{d^2 G'(\omega)}{d\,\ell n^2\,\omega} + \frac{1}{8}\frac{d^3 G'(\omega)}{d\,\ell n^3\,\omega}\Big|_{\omega = 1/\tau} \tag{7f}$$

where shifts have been made to account for the location of some of the intensity functions. The shifts were made so that the peak of the intensity function would lie at the point of interest.

To test the accuracy of the various approximations, Tschoegl uses an analytic function which closely approximates the $G'(\omega)$ data for polyisobutylene.

$$\frac{G'(\omega) - G_e}{G_d - G_e} = \frac{1}{1 + (a/\omega)^b} \tag{8}$$

G_e and G_d are the equilibrium and glassy moduli respectively. Log G_e is 6.39 and curve fitting yielded the constants 0.5948 for b, 9.1796 for

log a , and 10.3 for log G_d . The advantage of having an analytic expression is that the exact spectrum can be calculated. The approximations can then be compared to it without error due to data analysis. The exact spectrum was found by Tschoegl to be

$$H'(\tau) = \frac{2}{\pi} (G_d - G_e) \frac{(a\omega)^b \sin \pi b/2}{a^{2b} + 2(a\omega)^b \cos \pi b/2 + \omega^{2b}} \Bigg| \omega = 1/\tau \qquad (9)$$

Dependence of the Approximation on the Slope of the Spectrum

As mentioned previously, if the intensity function is replaced by a delta function, an exact relationship results. In Fig. 2 is a plot of a portion of the log of the relaxation spectrum directly above a plot of an intensity function of exaggerated skewness. When $H(\theta) \cdot I(\theta/\tau)$ is integrated from $\theta = 0$ to $\theta = \infty$ for the parameter $\tau = \tau_o$, parts of the spectrum adjacent to τ_o contribute to the integral. If the skew is to the right as pictured in Fig. 2 , $H(\tau)$ to the right of τ_o will be weighted more heavily than that to the left of τ_o . But $H(\theta)$ is a rapidly decreasing function at this point (log $H(\theta)$ is plotted) and the product $H(\theta) \cdot I(\theta/\tau)$ may approach zero as rapidly on the right side as on the left.

Similarly, we would expect an intensity function skewed to the left to provide a poor approximation resulting in an integral which would be too high. Deriving the spectrum at τ_o from $G'(\omega)$ with a left skewed intensity function, therefore, would require a shift of greater magnitude than that indicated by inspection of the intensity function alone.

By the same argument, one would expect the symmetric intensity functions to also give approximations that are too high in any area where the spectrum is changing rapidly. Of course the symmetric case would provide a better overall approximation for both positive and negative slopes of the spectrum than the skewed case.

The accuracy of the approximation (or the shift in τ_o required) is not dependent directly on the slope of $H'(\tau)$ vs. log τ, however. The integral is over the product of the intensity function and $H(\tau)$; and therefore one is interested in the relative change in $H(\tau)$ as one moves away from log τ_o. Thus we can say that the necessary shift will be dependent on the slope of log $H(\tau)$ vs. log τ evaluated at log τ_o.

Using the expression for the modulus of polyisobutylene determined by Tschoegl (Eq. (8)), the second order approximations for the spectrum were evaluated along with the exact spectrum. The calculations were done with the aid of Citran on the Caltech computer time-sharing program, and are shown in Table I. The second and fifth columns show the left and right approximations with no shift in the intensity function. The third and sixth columns show them with a shift of the peak of the intensity function to the point of interest. The fourth and seventh columns give these approximations with a shift of the median of the intensity function to the point of interest. Column eight contains the exact spectrum as calculated from Eq. (9).

In Fig. 3 is plotted log $H_1'(\tau)$ and log $H_3'(\tau)$, the spectrum derived from symmetric intensity functions, along with the log of the exact spectrum $H(\tau)$. Where the slope of log $H'(\tau)$ is steep, the approximations are high as expected. Also they are in error by a

constant amount where the slope is constant.

In Fig. 4 log $H_{2R}'(\tau)$ and log $H_{2L}'(\tau)$ are plotted with the log of the exact spectrum. We see that $H_{2R}'(\sqrt{2}\tau)$ works very well where the slope of log $H(\tau)$ is negative and $H_{2L}'(\tau/\sqrt{2})$ is most appropriate for a positive slope. The fine accuracy of the approximations in certain areas is partly coincidental, however, since a steeper or shallower slope of the log of the spectrum would shift the approximation above or below the exact values respectively. This becomes well apparent near the peak of the spectrum. Of course, at the peak, any approximation will give a low value. One way to counteract the effect of a changing slope might lie in modifying the shift factor. For instance, we have essentially been shifting log τ by log $\sqrt{2}$ in calculating the second order approximations $H_{2R}'(\tau)$ and $H_{2L}'(\tau)$. For mild slopes, this shift is too much and should be decreased. Thus the shift can be made arbitrary and it would merely be coincidence if a shift to the peak or to the median of the intensity function was used. These points would still be useful, however, in understanding the mathematics involved in the approximation. This immediately brings to mind an iterative correction procedure to yield an accurate approximation. For a particular approximation, the best shift factor for the slope of log $H'(\tau)$ vs. log τ could be tabulated and used in a recalculation. The proper intensity function should be chosen, however, to keep the shift to a minimum. One would always like most of the contribution to the approximation to come from the area directly around the point of interest. That is, one should keep the peak of the intensity function as close to the parameter τ_o as possible.

Conclusion

In practice one would be working with experimental data rather than an analytic function. First and second derivatives can usually be obtained, but the error increases rapidly with the order of the derivative. Therefore, as noted by Tschoegl, either a second order approximation or a third order approximation in which the third order term makes a small contribution would be most useful in calculating a relaxation spectrum from modulus data. In comparing Eqs. (8), one sees that the asymmetric approximations would be most desirable; and it has been shown that a right or left approximation should be carefully chosen with regard to the relaxation spectrum being calculated. In fact, a skewed approximation should be chosen over a symmetric one for regions of steep slope.

It should also be remembered that the function used for testing the approximations was a very simple one. If there were fluctuations in the data over an order of log τ that was smaller than the order of the intensity function (approximately one decade), they would be smoothed out. Even fluctuations over a band of log τ greater than the spread of the intensity function may be considerably smoothed. One therefore should choose an intensity function which gives the closest approximation with the least amount of shift, keeping in mind the general slope of the relaxation spectrum in the area of interest as well as the order and relative contribution of the derivatives involved in the approximation.

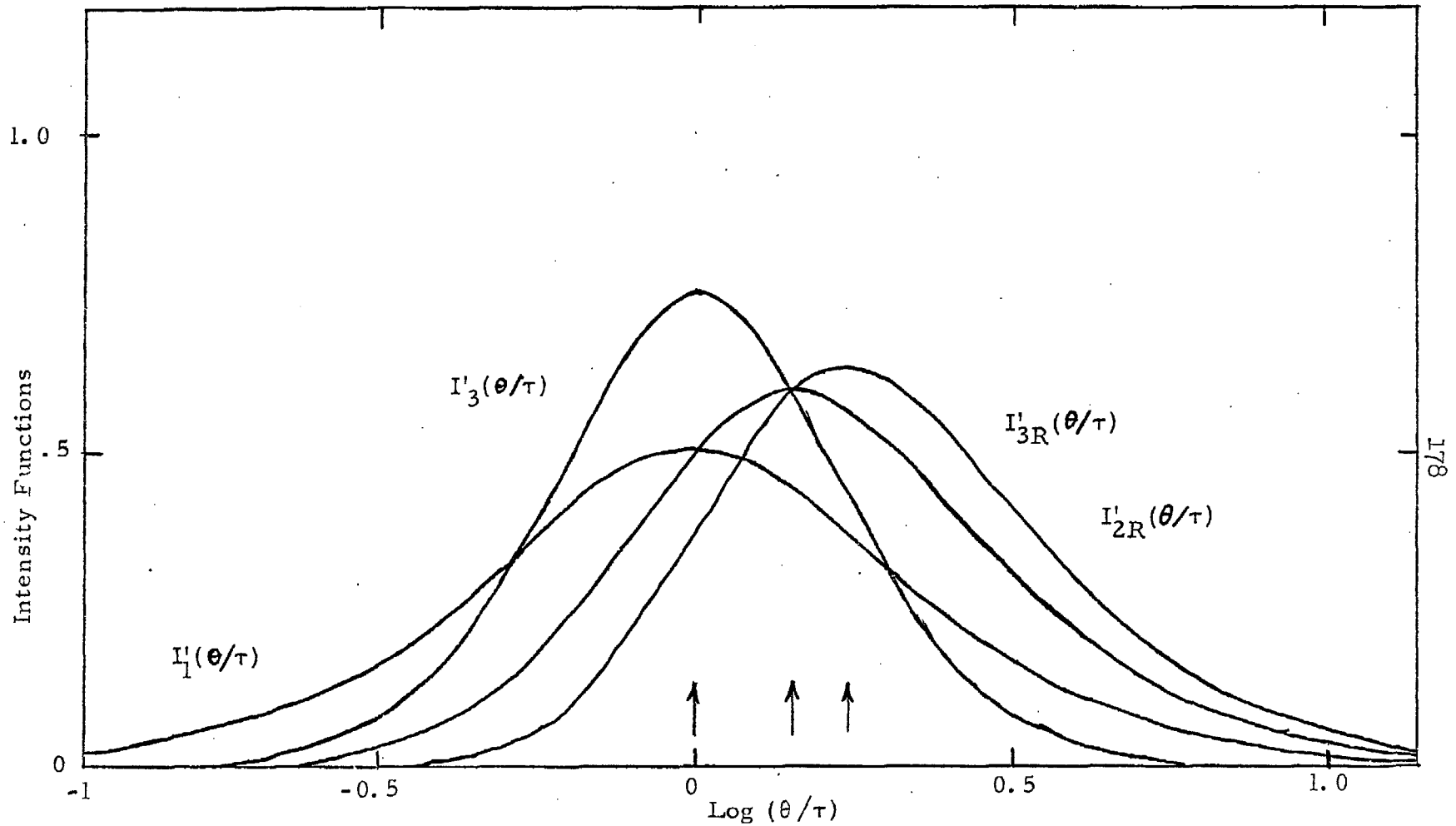

Fig. 1 Intensity Functions for Various Approximations

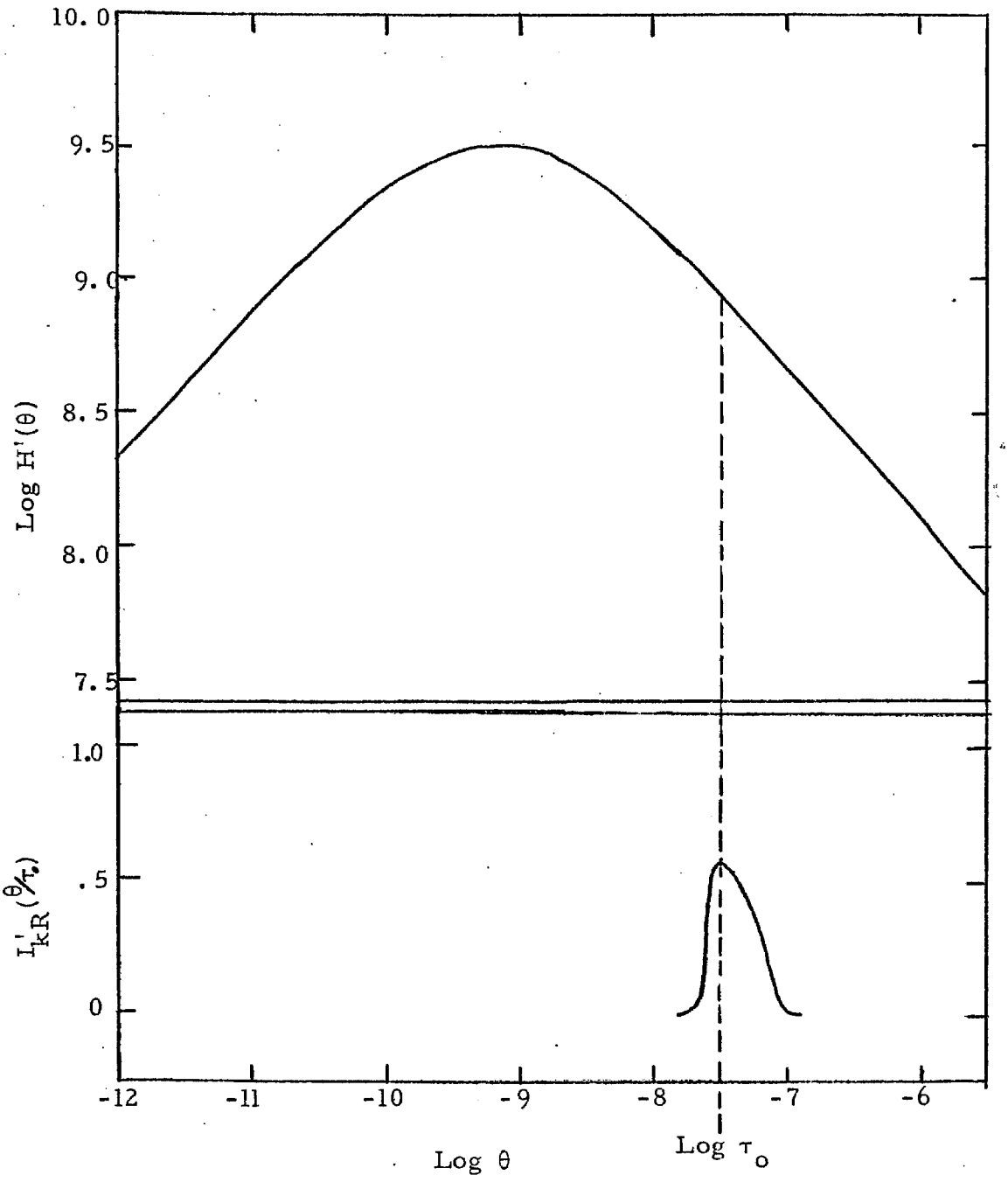

Fig. 2 Log H'(θ) and Skewed Intensity Function $I'_{kR}(\theta/\tau_o)$ as Functions of Log θ

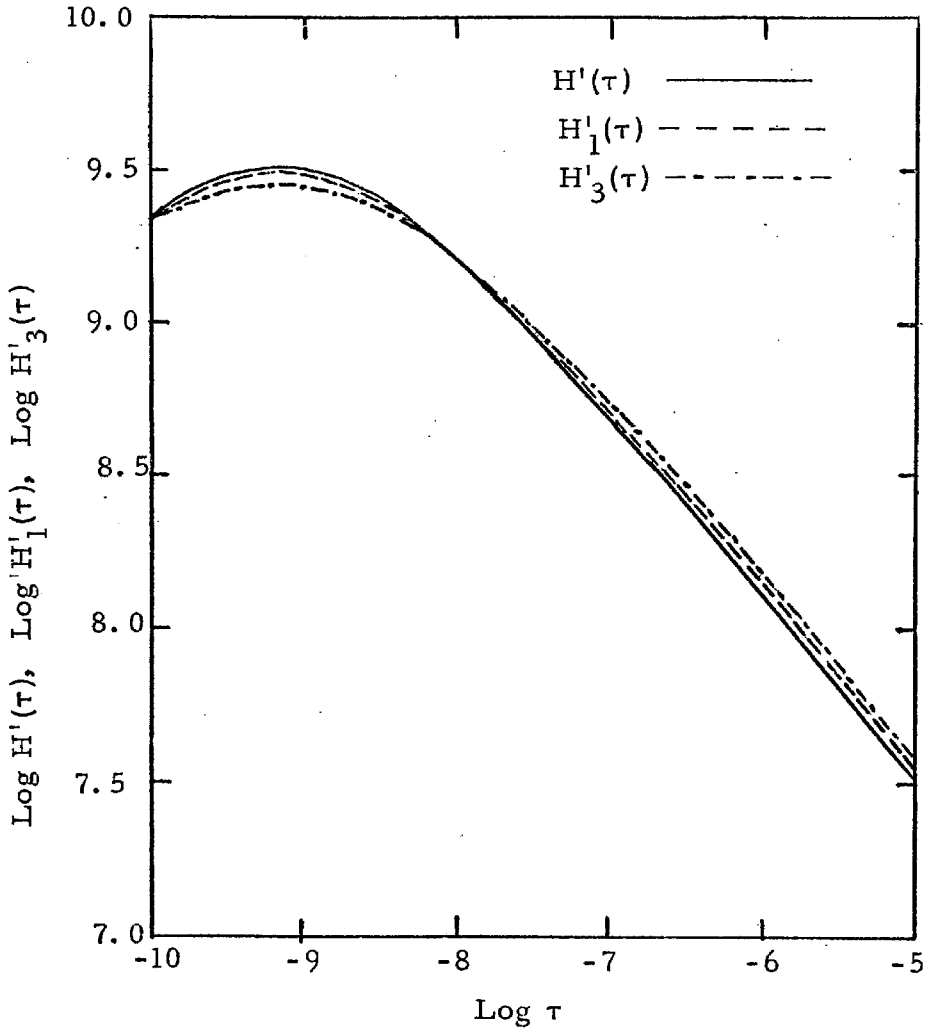

Fig. 3 Log $H'(\tau)$, Log $H'_1(\tau)$, Log $H'_3(\tau)$ as Functions of Log τ.

TABLE I

Approximations to the Relaxation Spectrum from the Storage Modulus of Polyisobutylene

Log τ	Log $H'_{2R}(\tau)$	Log $H'_{2R}(\sqrt{2}\tau)$	Log $H'_{2R}(1.553\tau)$	Log $H'_{2L}(\tau)$	Log $H'_{2L}(\tau\sqrt{2})$	Log $H'_{2L}(\frac{\tau}{1.553})$	Log $H'(\tau)$
-12.00	8.488	8.402	8.379	8.233	8.320	8.343	8.321
-11.80	8.600	8.516	8.493	8.349	8.435	8.458	8.436
-11.60	8.710	8.627	8.605	8.463	8.548	8.571	8.551
-11.40	8.817	8.737	8.714	8.576	8.660	8.683	8.664
-11.20	8.921	8.843	8.822	8.688	8.770	8.792	8.775
-11.00	9.020	8.946	8.925	8.796	8.876	8.898	8.883
-10.80	9.114	9.044	9.024	8.902	8.979	8.999	8.988
-10.60	9.201	9.136	9.118	9.004	9.077	9.096	9.089
-10.40	9.279	9.221	9.205	9.100	9.168	9.186	9.183
-10.20	9.347	9.297	9.282	9.190	9.251	9.267	9.270
-10.00	9.403	9.362	9.350	9.271	9.325	9.338	9.347
-9.80	9.445	9.415	9.405	9.341	9.386	9.397	9.412
-9.60	9.472	9.453	9.447	9.399	9.433	9.441	9.461
-9.40	9.481	9.476	9.472	9.443	9.465	9.469	9.493
-9.20	9.474	9.481	9.481	9.470	9.480	9.481	9.505
-9.00	9.450	9.470	9.473	9.481	9.478	9.476	9.497
-8.80	9.409	9.441	9.448	9.475	9.459	9.453	9.469
-8.60	9.354	9.397	9.407	9.452	9.424	9.415	9.425
-8.40	9.286	9.338	9.351	9.413	9.374	9.362	9.362
-8.20	9.207	9.267	9.283	9.360	9.311	9.297	9.287
-8.00	9.119	9.186	9.203	9.294	9.237	9.221	9.202
-7.80	9.024	9.096	9.115	9.218	9.154	9.136	9.109
-7.60	8.923	9.000	9.020	9.132	9.063	9.044	9.009
-7.40	8.818	8.898	8.919	9.040	8.966	8.946	8.905
-7.20	8.710	8.792	8.814	8.941	8.864	8.843	8.797
-7.00	8.599	8.683	8.705	8.838	8.759	8.737	8.686
-6.80	8.486	8.571	8.594	8.732	8.650	8.627	8.574
-6.60	8.372	8.458	8.481	8.622	8.538	8.516	8.460
-6.40	8.257	8.344	8.367	8.511	8.425	8.402	8.344
-6.20	8.140	8.228	8.251	8.397	8.311	8.288	8.228
-6.00	8.023	8.111	8.135	8.283	8.196	8.172	8.111
-5.80	7.906	7.994	8.018	8.167	8.079	8.056	7.994
-5.60	7.788	7.877	7.901	8.050	7.962	7.938	7.876
-5.40	7.670	7.759	7.783	7.933	7.845	7.821	7.758
-5.20	7.552	7.641	7.665	7.816	7.727	7.703	7.640
-5.00	7.433	7.523	7.547	7.698	7.609	7.585	7.521
-4.80	7.315	7.404	7.428	7.580	7.491	7.467	7.403
-4.60	7.196	7.285	7.310	7.461	7.372	7.348	7.284
-4.40	7.077	7.167	7.191	7.343	7.254	7.230	7.166
-4.20	6.959	7.048	7.072	7.224	7.135	7.111	7.047
-4.00	6.840	6.929	6.953	7.106	7.016	6.992	6.928
-3.80	6.721	6.810	6.835	6.987	6.898	6.873	6.809
-3.60	6.602	6.692	6.716	6.868	6.779	6.755	6.690
-3.40	6.483	6.573	6.597	6.749	6.660	6.636	6.571
-3.20	6.364	6.454	6.478	6.630	6.541	6.517	6.452
-3.00	6.245	6.335	6.359	6.512	6.422	6.398	6.333

References

1. Tschoegl, N. W., "Approximation Methods for the Determination of the Relaxation Spectrum from the Storage Modulus," in "A Research Program on Solid Propellant Physical Behavior," Part III, Third Annual Report, Contract No. AF 04(611)-9572, MATSCIT PS 67-1, June 1967. AFRPL-TR-67-193.

2. Ferry, J. D., Viscoelastic Properties of Polymers, John Wiley, New York (1961).

PROPOSITION III

THE ROLE OF COMPUTATIONAL ERRORS IN THE COMPUTER SIMULATED PACKING OF CIRCLES

Abstract

A computer program to simulate the random close packing of circles was prepared by H. Kausch and modified by the author (1). It is proposed that computational errors play an important role when the circles pack in an hexagonal close packed lattice. By modifying the computations and by working in double precision, this is shown to be the case. Interestingly, computational errors play a desirable role in the investigation of random circle packing.

Introduction

The principle employed in constructing the computer program for the simulation of the random packing of circles in a plane under the influence of a weak centripetal force is indicated in Fig. 1. At the start a circle is placed at the origin. Under the action of the postulated weak central force, any circle approaching the center circle, or an aggregate of circles already placed, will follow a straight line until it encounters the first circle in its way. The direction, θ_j, of the incoming circle is randomly selected, using a computer subroutine for the selection of random numbers, x_1, between zero and 2π.

In a typical placement, a circle approaches the origin along the direction, θ_j, as shown in the figure. It encounters the first circle in its path, that at i_1, in position j_1. Upon contact, the circle is made to roll around i_1 so that it always approaches the origin.

If the circle hits another during this rolling procedure, its packing may be ended. The program takes care of the fact, however, that under the action of a weak central force, and with no adhesion between the circles, the rolling motion would turn into a direct approach toward the center again once the circle had reached a position such as j_2, where it breaks contact with circle i_1. In this case the circle then adopts the appropriate new angle which it follows until it contacts a new circle, i_2. It now rolls on circle i_2 until it contacts a new circle again. If the polar angle of the rolling circle is between that of i_2 and the new circle, the rolling is terminated. Otherwise, the rolling procedure continues until a stable position is

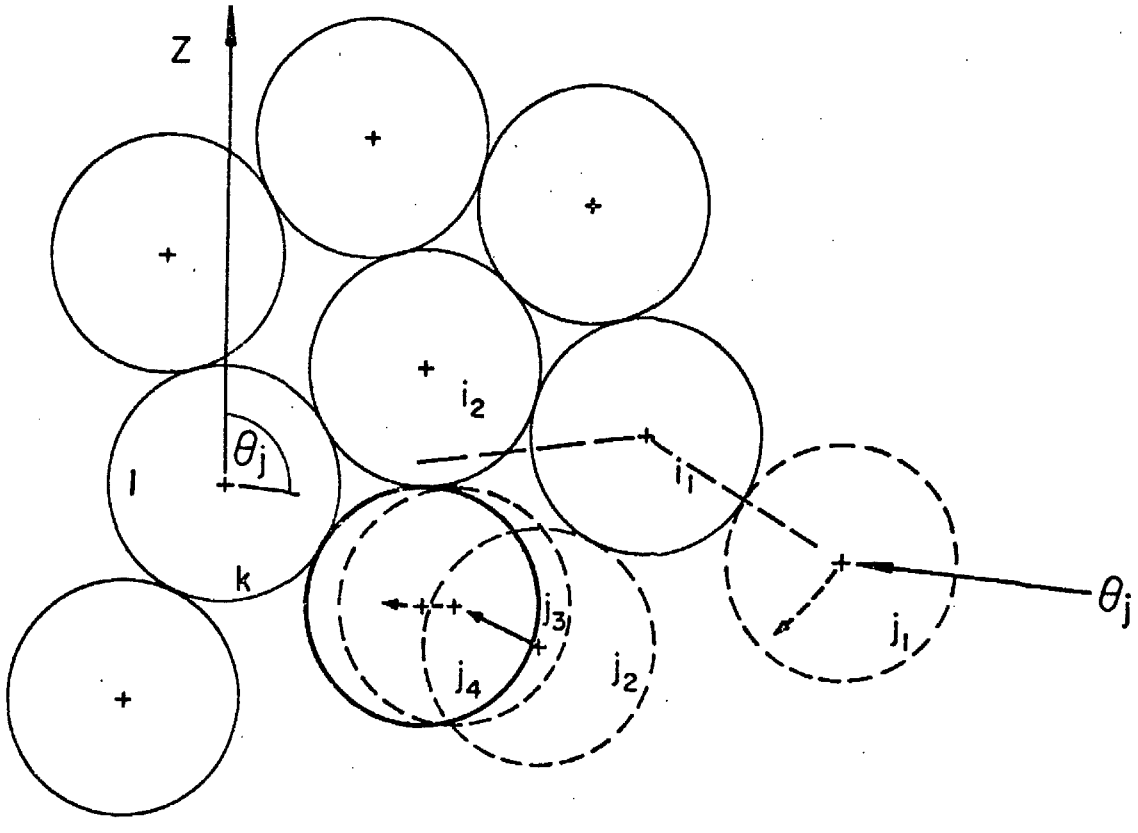

Figure 1. Random Packing Process for Uniform Circles: $j_1, \ldots j_4$, successive positions of incoming circle beginning at angle θ_j; i_1, i_2, indices of circles met in first encounters; k, index of circle met in stable position.

reached. In Fig. 1 the circle has reached a stable position when it contacted circle k. The only exception is made with the circles which encounter the first circle, whereupon the rolling ceases.

The packing fraction of a given area A is defined as the fraction of the area which is covered by circles. For any given aggregate of randomly packed circles, the packing fraction, ϕ, depends upon the choice of the area to be inspected, and on its size. It will be independent of these only in the limit of a large A.

The polygon which offers itself naturally for the determination of the packing fraction in random packing is that formed by the centers of the peripheral circles on the boundary of the aggregate. The peripheral circles are all those circles which can be connected with a point outside the aggregate by a line which does not cut or touch a circle of the aggregate. Such a polygon will be called a boundary polygon. An example is shown in Fig. 2.

The packing fraction in the area enclosed by the boundary polygon is

$$\phi = (A_c - A_s)/A_p \qquad (1)$$

where A_c is the area of all circles enclosed or cut by the polygon, A_s is the area of those portions of cut circles which fall outside of the polygon, and A_p is the area of the polygon itself. Equation (1) is exact only for cases of simple regular lattices where unit cells are formed by connecting the centers of adjacent circles. For random packing or complex lattices, where the unit cells are not defined in this manner, Eq. (1) approaches the correct value in the limit of a

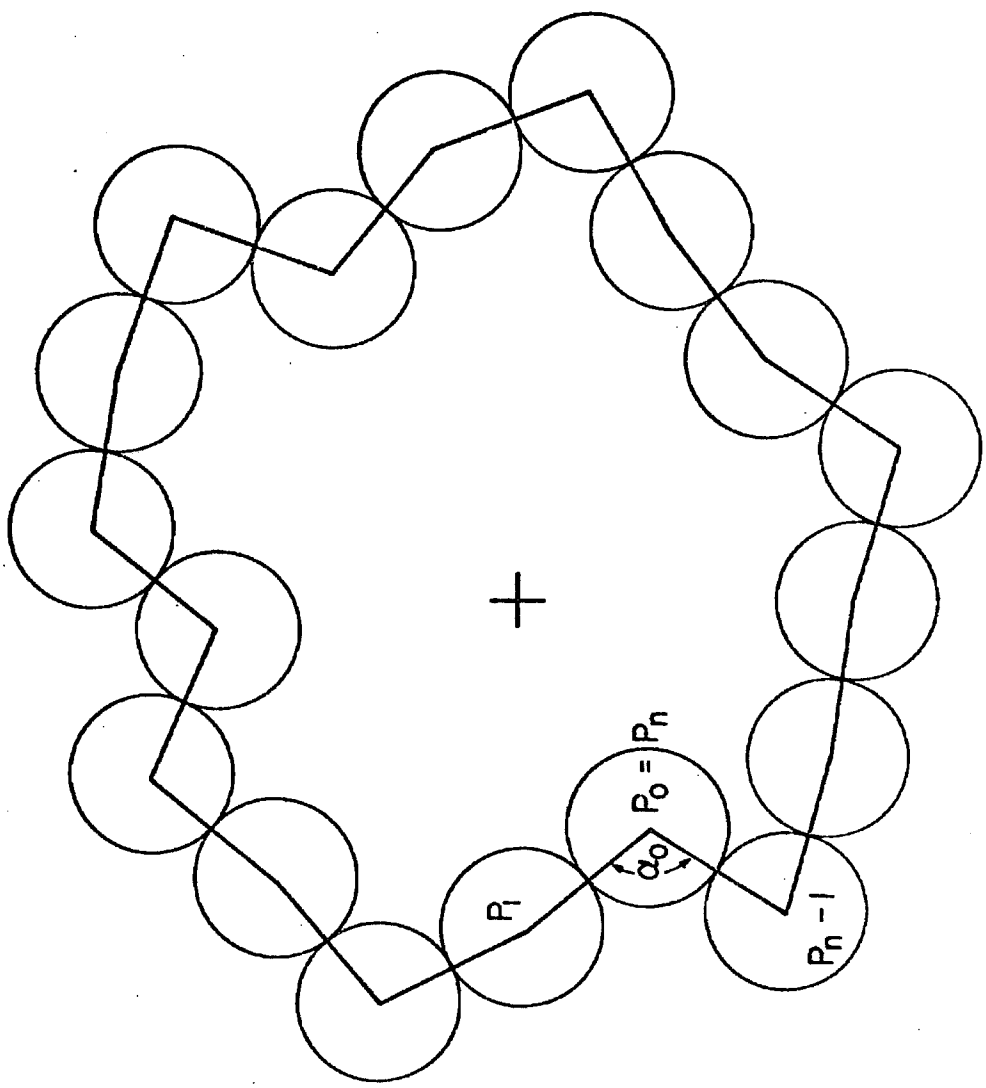

Figure 2. Boundary Polygon through Centers of Peripheral Circles.

large number of circles. A_c is obtained by adding the area of any new circle to the sum of the areas of the previously placed ones. To calculate A_s and A_p it is necessary to keep a tally of the coordinates of the outermost circles by continuous scanning. The scan starts with the circle placed last (P_o), and continues clockwise to the next circle in contact with the preceding one (P_1,P_2, etc.), until the coordinates of P_o ($= P_n$) reappear.

The area of the polygon, A_p, is calculated as the sum of the triangular areas formed by successive corner points and the origin. A_s is given by

$$A_s = \sum_{i=1}^{n} r_i^2 \alpha_i/2 \qquad (2)$$

where α_i is the outside angle of the polygon corner at the center of circle i. This is shown in Fig. 2 for P_o.

Uniform circles were studied to determine the packing fraction in random packing and the number of circles which had to be placed to obtain a statistically meaningful value. The program determined the integral packing fractions anew after the placement of every fiftieth circle, up to a maximum number of 1600 circles. Simultaneously, differential packing fractions, defined by

$$\varphi_{n-k}(n) = \frac{A_{p,n}\varphi(n) - A_{p,k}\phi(k)}{A_{p,n} - A_{p,k}} \qquad (3)$$

were computed. In Eq. (3) n is the current number of circles and k is a specified number of circles less than n. Thus $\phi_{200}(n)$ is the packing fraction of the last 200 circles preceding and including n.

Computational Errors in Circle Packing

It is apparent that the placement of the first few circles will affect the subsequent placement of additional circles. The computer program was modified to allow nonrandom placement of the first seven circles in order to investigate this effect at least superficially. If this nucleus is very irregular, with substantial voids generated by the random placement of the first several circles, effects of the nucleus die out rapidly with the further addition of circles. Particularly interesting, however, is the case where the in initial circle is surrounded by six hexagonally close packed (HCP) circles. All circles impinging on an HCP lattice should propagate that lattice. Symmetric and partially HCP nuclei also have long range effects, but are not considered here.

Figure 3 shows the packing fraction for 200 circles, $\phi_{200}(n)$, vs. n, the total number of circles (the first three circles are accumulated packing fractions). The initial test, shown by the open circles, gave, instead of the propagation of the HCP structure with a packing fraction of 0.9068 as expected, a very rapid fall-off after approximately two hundred circles; and the packing fractions appeared to level off near the value of 0.82 determined for random packing (1). Examination of a plot of the coordinates of the circles showed the appearance of an occasional void outside the first two hundred circles, and circles placed afterward in the vicinity of these voids showed irregular packing.

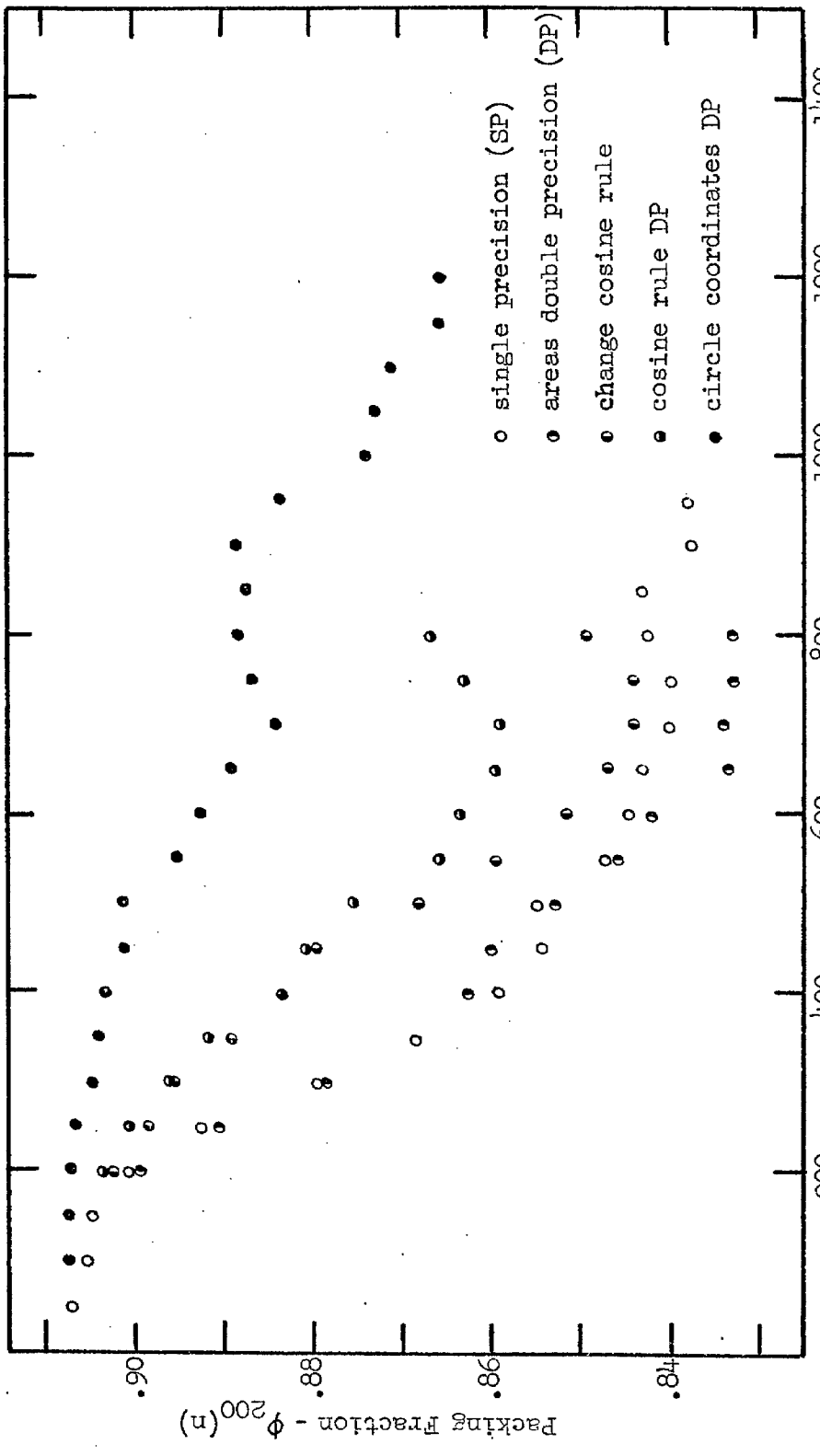

Figure 3 . Change in Packing Fraction Due to Improvements in Computational Precision.

It was felt that the formation of these voids could only be due to computational errors, eg. round-off and truncation, and not due to the packing scheme of the program. An effort was made to improve the computations.

First, it was observed that a more accurate calculation was needed to determine reliable packing fractions. As previously described, the evaluation of the areas used in calculating the packing fraction in Eq (1) involves considerable summation. A_c often involves about 1000 such summations and A_s and A_p involve about 200. Since single precision accuracy on the IBM System/360 is only 1 part in $10^{6.3}$ before round-off, and since the areas may be two or three orders of magnitude larger than the individual terms being summed, an accuracy of only 1 part in 10^3 or 10^4 is seen for each term. With accumulating round-off error, one can only expect an accuracy of two or three digits at best. This summation was improved by making the area totals double precision so that each single precision term is added to a double precision total. The difference is shown in Fig. 3 where the right-filled symbols, ◑, represent the improved calculation. The actual packing is not affected, but the reliability of the packing fractions in representing the packing is significantly improved.

Anyone carrying out numerical calculations must be aware of the dangers involved in subtracting numbers that are close in magnitude. The difference often has considerably less accuracy than the minuend and subtrahend. In program Circlepack, taking differences is unavoidable. The angle between adjacent circles (referred to the origin) must be determined by subtraction, and subtraction is used in

the cosine rule for the triangle formed by adjacent circles and the origin. The latter case is particularly insidious since squaring is involved before subtraction. Of course, the whole problem becomes more pronounced for circles far from the origin since the central angle becomes smaller. It was found that certain forms of the cosine rule were more suitable than others. For instance, in replacing

$$a^2 = b^2 - 2 \cdot b \cdot c \cdot \cos\theta + c^2 \tag{4}$$

by

$$a^2 = b \cdot (b - 2 \cdot c \cdot \cos\theta) + c^2 \tag{5}$$

by carrying out subtraction before a multiplication instead of after, improvement could be obtained as shown in Fig. 3 by the left-filled symbols, ◐. In this case, only one usage of the cosine rule was modified in this way; and this was in a loop searching for the proper circles hit, and not in the actual computation of the coordinates of the new circle. Thus, the improvement seen in Fig. 3 came about because Eq. (5) resulted in a more accurate selection of the circles touched by the incoming circles.

This success prompted trying double precision calculations within this selection process only, without extending double precision to the coordinates of the circles. The results are shown in Fig. 3 by the bottom-filled symbols, ◒. Finally, double precision was used also in the calculation of the coordinates of each new circle (essentially extending double precision throughout the calculations). The result is shown by the completely filled circles. Voids still form, but they must be small as they do not initiate catastrophic breakdown of the

regular lattice. The packing fractions remain high out to large numbers of circles and decrease only very gradually from the theoretical value.

Discussion

As shown above, computational errors initiate voids which rapidly propagate a disordered growth. Therefore, the "computer circles" are uniform only within a certain tolerance established by the closeness with which the computer can compare two numbers. In this sense, the computer experiments can be likened to real experiments involving disks with a dimensional tolerance. If desired, this error can be reduced by working in double precision arithmetic.

An interesting phenomenon arises in the random packing experiments which is related to this error question. A typical computation of the random packing of uniform circles is illustrated in Fig. 4, showing also the boundary polygons obtained after the placement of 50, 200, 450, and 800 circles. For simplicity, the outlines of the circles were drawn only in the representative area shown in the lower right corner. The formation of voids is clearly visible.

The cross-hatched areas in Fig. 4 indicate "crystalline" regions with hexagonal close packing. Such regions develop whenever an hexagonally close packed nucleus is formed through the vagaries of random packing, and tend to propagate before the packing becomes random again. The formation and development of the regions depends on the mode of action of the ordering force. This can be seen in Fig. 4 in the areas where two large "crystallites" lie close to each other.

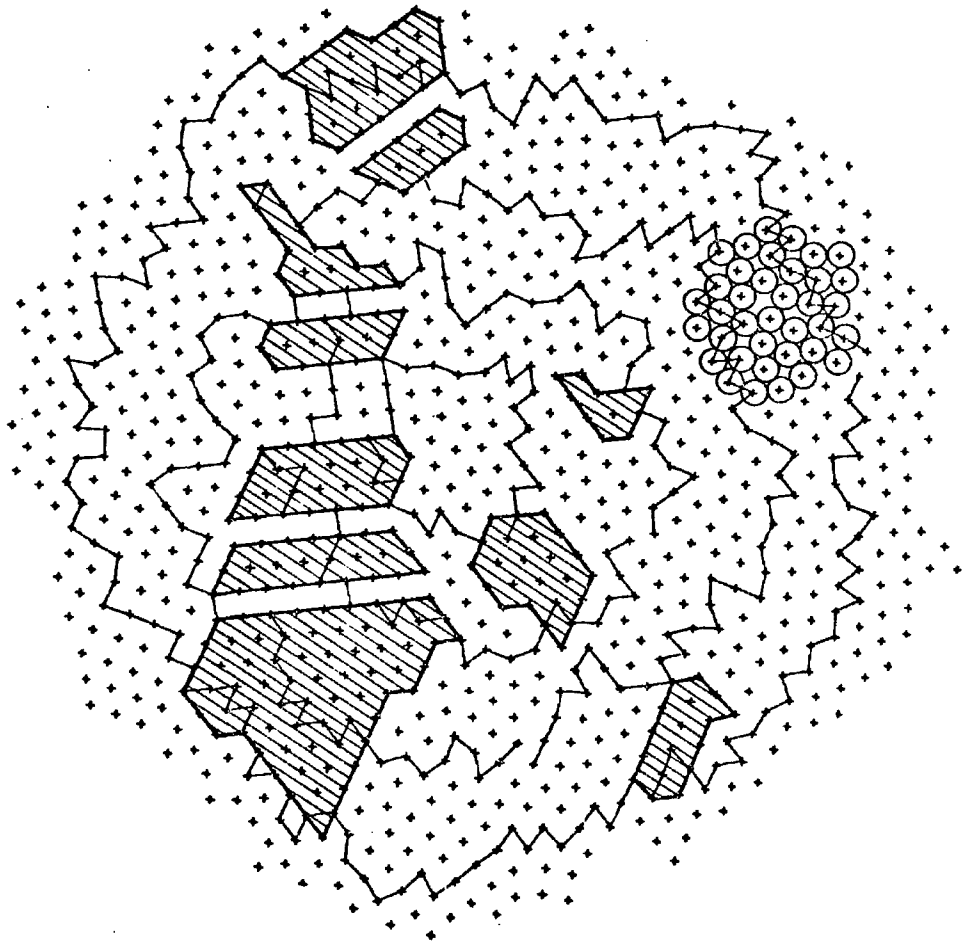

Figure 4. Random Packing of Uniform Circles.

Such crystallites are separated by "slip lines" along which the packing is between cubic and HCP. The slip lines arise here because the central force disrupts the growth of the crystallites when they become too wide. Under the influence of a gravitational field rather than a centripetal force, one would expect the crystalline regions to be more extensive.

Since we are most interested in random packing free of the influence of an ordering force, the data were corrected by the tedious process of identifying, calculating, and subtracting the crystalline areas.

It is now obvious that computational errors must play a significant role in disrupting these crystalline regions just as they did in disrupting the ideal lattice. The errors strongly affect circle placement in the regular hexagonal lattice where very close tolerances must be preserved in order to propagate the lattice. However, the calculations in a random structure should not be nearly as sensitive. Thus, the errors work in one's favor to minimize these crystalline regions without significantly upsetting the random packing behavior.

Reference

1. H. H. Kausch, D. G. Fesko, and N. W. Tschoegl, J. Coll. and Interface Sci., (in press).